# Numerical optimization of isolation systems for reciprocating engines



PUBLISHER

© Dimitris Papadakis

# NUMERICAL OPTIMIZATION OF ISOLATION SYSTEMS FOR RECIPROCATING ENGINES

by

DIMITRIS PAPADAKIS

A Master's Thesis
submitted in partial fulfilment of the requirements for
the award of
Master of Philosophy
of the Loughborough University of Technology

October 1986

# STATEMENT OF ORIGINALITY

The author hereby takes full responsibility for the work submitted in this thesis and claims originality for all the work contained herein except where due acknowledgement is given or specific reference is made.

CONTENTS

# ABSTRACT

The use of numerical optimization methods to select reciprocating engine anti-vibration characteristics is investigated. A rigid body power train model coupled through an arbitrary array of vibration isolators to a rigid supporting structure forms the basis of the dynamic model. By calculating the forced response of the power train to its internally generated excitation, the strain energy summed over the isolators may be determined. This energy, which is indicative of the efficiency of the vibration isolative mounts, is used as the objective function in the optimization procedure. The method is expected to be useful in preliminary design studies of front wheel drive vehicles where traditional methods of mounting automotive engines are not necessarily applicable.

Each isolator is approximated by a set of massless linear springs acting along and about its elastic axes and the engine as a rigid body described by its inertia properties with respect to a reference frame fixed to its centre of mass. The undamped eigen solution for the system is found, it being assumed that these modes can be used to uncouple the damped equation of forced vibration. The excitation due to unbalanced inertial and combustion forces are approximated by Fourier series. The response to each excitation harmonic is computed by modal superposition with damping being introduced on a modal basis. The mean square response and the maximum strain energy summed over all harmonics is then determined.

For any specific engine speed the system strain energy can be expressed as a single function of the isolator design variables, viz stiffness, position and orientation and hence minimized by a numerical algorithm. The optimal values of the design variables are computed by a NAG FORTRAN routine within the feasible region defined by bounds on design variables and by other constraints. Two such constraints are of practical importance: (a) static deflection at the isolator, and (b) engine static rotations. This new approach has the advantage of directly linking the numerical process of finding the optimum isolator configuration simultaneously with both the static and the dynamic forced response of the engine.

The method has been extensively tested numerically on a contemporary four cylinder diesel engined car with promising results. It is clear, however, that final modifications might be necessary at the final design stage to account for road input excitation.

## ACKNOWLEDGEMENTS

The author would like to take this opportunity to acknowledge the contribution made by the following individuals at various stages of the project.

Dr M G Milsted, for his supervision and guidance given throughout the course of this research project.

T S Bharj and A V Phillips of the Ford Motor Company for their advice on the acceptability of the modelling principles and the donation of technical data.

J Ogendo for his advice on various mathematical and software problems.

Last, but not least, the reception staff of the Computer Centre for their service.

# PRINCIPAL NOTATION

A list of the most commonly used symbols is given below, where bold-type characters indicate either a vector or a matrix.

## a) Scalars

| | |
|---|---|
| $a_k$, $b_k$ | Fourier coefficients |
| $a_r$ | Modal mass for the $r^{th}$ mode of vibration |
| $b_o$ | Frequency independent Fourier coefficient |
| $c_r$ | Modal stiffness of the $i^{th}$ mode of vibration |
| $\hat{c}_r$ | Modal complex stiffness |
| $c_i(x)$ | The $i^{th}$ constraint function |
| $d_i$ | Distance of the $i^{th}$ cylinder centre from the crankshaft centre |
| $d_{ij}$ | Elements of direction cosine matrix |
| e | Basis of the natural logarithm |
| $f_i$ | Internally generated engine force in the $i^{th}$ direction |
| $\hat{f}^{(r)}$ | The complex genralized force for the $r^{th}$ mode of vibration |
| $f_i^{(s)}$ | The $i^{th}$ element of the static force vector |
| $F(\mathbf{X})$ | Optimization objective function |
| g | Acceleration of gravity |
| $I_{ij}$ | Moments and products of inertia |
| j | -1 |
| $k_{ij}$ | Elements of the global stiffness matrix |
| $k_p$,$k_r$,$k_s$ | Isolator stiffness in the p,r,s local direction respectively |
| L | Load on the isolators |
| m | Power train mass |
| $m_{rec}$ | Reciprocating mass |
| $m_{rot}$ | Rotating mass |
| n | Number of engine cylinders |
| $p_r$ | The $r^{th}$ principal coordinate |
| $q_i$ | Internally generated engine moments in the $i^{th}$ direction; generalized coordinates |

| | |
|---|---|
| $q_x'$ | Final drive torque |
| $r$ | Crank radius |
| $r_x^{(n)}, r_y^{(n)}, r_z^{(n)}$ | Position coordinates of the $n^{th}$ isolator |
| $t$ | Time |
| $V_{jk}$ | The $k^{th}$ element of the eigenvector corresponding to the $j^{th}$ natural frequency |
| $w_i$ | Weighting factor for the $i^{th}$ constrain function |
| $\overline{x_i^2}$ | Mean square response for the $i^{th}$ generalized coordinate |
| $x, y, z$ | Global translational coordinates: |
| $x_c, y_c, z_c$ | Crankshaft centre coordinates |
| $y$ | Transformed optimization variable |
| $\hat{\alpha}_r$ | Modal complex receptance |
| $\alpha_N$ | Polynomial coefficients |
| $\alpha, \beta, \gamma$ | Eulerian angles |
| $\eta_r$ | Modal loss factor |
| $\theta_i$ | Angle between the $i^{th}$ and the No 1 cylinder crank |
| $\lambda$ | Ratio of the crank radius to the conrod length |
| $\rho$ | Penalty parameter |
| $\phi, \theta, \psi$ | Global rotational displacements |
| $\omega$ | Engine speed |
| $\omega_r$ | The $r^{th}$ modal frequency |

Vectors and Matrices

| | |
|---|---|
| A | Direction cosine matrix; Modal mass matrix; Matrix whose $i^{th}$ row contains the coefficients of the $i^{th}$ constraint; The Jacobian matrix of the constraints |
| B | Approximation to the Hessian matrix G |
| C | Direction cosine matrix; Modal stiffness matrix |
| f | Complex vector of the generalized forces |
| G | Hessian matrix with elements; the second partial derivatives of f(x) |
| I | Global inertia matrix |
| $I_p$ | Principal inertia matrix |

l.c.
l.c.
l.c.

| | |
|---|---|
| $K$ | Global stiffness matrix |
| $K_p^{(n)}$ | Principal axis translational stiffness matrix for the $n^{th}$ isolator |
| $K_\lambda^{(n)}$ | Principal axis rotational stiffness matrix for the $n^{th}$ isolator |
| $K_{xx}$ | Translational stiffness submatrix |
| $K_x$ | Translational-rotational submatrix |
| $K$ | Rotational-rotational submatrix |
| $M$ | Mass matrix |
| $p$ | Vector of principal coordinates/ the n-dimensional vector of search |
| $R$ | Position matrix |
| $T$ | Transformation matrix |
| $U$ | Transformation matrix |
| $u$ | Translational subvector of $x$ |
| $v$ | Eigenvector. Rotational subvector of $x$ |
| $V$ | Modal matrix |
| $x$ | General displacement vector with respect to the global axes. Vector of optimization variables |
| $x_p$ | General displacement vector with respect to the principal axes |
| $Z$ | Matrix the columns of which form the basis for the feasible subspace |
| $W$ | The Hessian matrix of the Lagrangian function |
| $\lambda$ | The vector of the Lagrange multipliers |
| $\Omega$ | Spectral matrix |
| $\delta_v$ | Virtual displacement vector |
| $\theta$ | Gradient vector with elements, the first partial derivatives of $f(x)$ |

# CHAPTER 1

## INTRODUCTION

During the early years of the motor vehicle it was customary to securely bolt the engine into the vehicle chassis. Engine vibration spl inf. was a minor problem compared with the severe shake caused by the solid rubber tyres on the primitive vehicle body. Further the solid engine structure provided a very stiff cross member for the chassis. In fact the first attempts to isolate the engine can be attributed to crankcase failures induced by chassis distortion on the rigidly bolted power train. As road noise was filtered with rapidly increasing improvements on the vehicle such as the introduction of pneumatic tyres, improved suspensions, quieter body construction etc, engine induced vibration became disturbing. Subsequently efforts were made to make engines quieter using existing theoretical knowledge of engine dynamics.

The introduction of well balanced configurations, such as the in-line six cylinder engine, improved matters considerably. Compared with the four cylinder engine's inherent 2nd (and also 4th, 6th ...) order force and moment unbalance, the six cylinder engine's 6th (and also 12th, 18th ...) order force unbalance and 3rd (and also 6th, 9th ...) torque unbalance impose a lower degree of interaction between the idling speed excitation spectrum and the rigid engine isolator spectrum, thus reducing engine vibration considerably. However, even a perfectly balanced reciprocating engine will require some degree of isolation as uneven firing gives rise to half order torque harmonics which can cause considerable vibration at engine idle due to their low frequency. Despite the dynamic advantages of the six cylinder engine, the four cylinder engine has continued to play a dominating role in the future of the motor car, providing a sensible compromise for size, dynamic balance, power, manufacturing cost and reliability. Ingenious mechanisms developed to improve the balance of the four cylinder engine have proved too expensive for large scale production and as a result solutions of the engine vibration problem by engine isolation have continued to be investigated.

Lack of powerful numerical algorithms on fast digital computers left engineers with no alternative but the development of easy to use methods for engine vibration isolation. Such methods were extensively used for the design of isolation systems for front engine-rear wheel drive (North-South) arrangements with impressive results. However, the increasing trend for smaller vehicles and front engine-front wheel drive (East-West) arrangements introduced new problems in the design of isolation systems, mainly due to space restrictions and the increased reaction torque on the power train imposed by the integral engine-gearbox-final drive designs. Motivated by this new class of problems and by the availability of reliable numerical optimization routines, some different approaches to the design of power train isolation systems have evolved.

The main principles of traditional methods for isolating engine vibration will now be briefly outlined along with their numerical implementation. The merits and weaknesses of the methods will be described and a new approach based on a somewhat different view of engine isolation system design will be outlined.

## 1.1 BACKGROUND

The methods used for the investigation of engine isolation systems were based on the well established vibration theory that a body supported on resilient supports possesses a number of natural frequencies (often referred to as eigensolutions) depending on the number of degrees of freedom considered in the vibration model. Investigation of the eigensolution (usually in the range of 5-20 Hz) for a rigid engine-isolator system revealed that by careful design of the isolation system the modes of vibration could be decoupled and hence the rigid engine-isolator spectrum could be controlled. The main requirement for complete decoupling is that the elastic centre of the dynamic system must coincide with the centre of mass. Partial decoupling can be achieved in a number of ways depending on the relative position of the elastic centre from the centre of mass, known to be a function of the isolator position, orientation and stiffness properties. Engine vibration isolation based on this principle was discussed by Crede [1] in 1957 and conditions for decoupling four modes were derived. Investigators such as Horovitz [2], Wilson [3] and Bolton-Knight [4], to name but three, developed conditions for decoupling the modes of vibration for a six degrees-of-freedom engine model by considering isolators inclined in different planes. Their work is discussed by Lee [5] in his attempt to investigate the decoupling of the engine modes of vibration for a six degrees-of-freedom model allowing complete freedom on the isolator orientation and extending his analysis to deriving conditions for total decoupling.

Whatever the approach to modal decoupling there are two main points to be made. Firstly, that by decoupling the modes of vibration the frequency spectrum is narrowed, and secondly that with decoupled modes the interaction between engine vibration and engine shake can be controlled or even avoided. It should be noted, however, that all the investigators mentioned earlier were concerned with the isolation of the traditional 'North-South' engine arrangement, and that direct application of such methods to 'East-West' engines has not yet been recorded.

Efforts have been made, in recent years, to design isolation systems for 'East-West' engines using numerical optimization methods. The main requirement with such methods is that a function which is believed to describe the dynamic response of the system is defined and is then numerically minimized subject to a number of conditions. Literature research revealed that the earliest attempt to investigate optimum isolation systems using such methods dates back to 1971. D. Zibello [6] developed a numerical procedure to establish the optimum stiffness and damping characteristics for an established isolation system, using a numerical technique which required data from vehicle ride evaluations. This particular approach to engine vibration isolation is most appropriate for final 'tuning' purposes and offers no assistance at the preliminary design stage.

In 1979 S.R. Johnson [7] produced a numerical algorithm based on a grounded rigid engine-isolator model but the orientation of the isolators is not included in the optimization procedure and static requirements had to be separately satisfied. His objectives were to decouple all the modes of vibration, using kinetic energy modal distributions, place the rigid body spectrum below the excitation spectrum and finally constrain the modal frequencies within specified frequency bands. Although his work provides a useful tool for investigating optimal isolation systems, it lacks generality since optimal isolator orientation cannot be investigated and static analysis is not integrated into the optimization procedure. An even more constrained approach was presented by J.E. Bernard and J.M. Starkey [8] in 1983. Their objective was to keep the modal spectrum of the grounded engine rigid body away from a specified frequency band by assigning weighted penalties to solutions that allowed modal frequencies into that band. Additional penalties were assigned to solutions that required large changes of design variables as such solutions were considered uneconomical. Apart from the unrealistic approach to engine vibration isolation, the surprising feature of this work is the mathematical complexity it introduces to predict changes in the eigenvalues of the system caused by changes in the design variables. Such procedures are useful for systems with large numbers of degrees of freedom but seem unjustifiable for a six degree of freedom model.

Finally in 1984 P.E. Geck and R.D. Patton [9] produced an optimization algorithm for isolating a grounded rigid model based on a method that statically decouples the roll mode. Other objectives were to place the bounce mode high and the roll mode low in the frequency spectrum. Their work included the isolator orientation in the optimization procedure but again the static analysis is kept separate. Complete vehicle-power train mode shapes are presented in their paper which clearly demonstrates the interaction of engine vibration and engine shake thus supporting the use of modal decoupling as an optimization objective. Further their experience with complete vehicle optimization methods and the failure of such algorithms to cope with the complexity of such models is discussed in their paper as a supporting argument for subsystem optimization.

It seems that in an effort to investigate optimum isolation systems for reciprocating engines, traditional practices based on the rigid engine-isolator spectrum have been conveniently formulated for the purpose of utilizing modern numerical optimization algorithms. However, none of the methods, discussed earlier, include the static analysis into the optimization procedure. Although the application of modal decoupling successfully provided isolation systems for 'North-South' engine arrangements there is no evidence that such isolation systems were optimum. If modal decoupling is used as the optimization objective for the investigation of optimum isolation systems for 'East-West' engine arrangements then there is no guarantee that the solution will be other than an optimum decoupled isolation system. Finally, if powerful numerical algorithms are used in such a way to solve the complex engine isolation problem, then their potential is underrated. A new approach to optimum engine isolation design is adopted here. The optimization objective is defined in terms of the forced response of the engine to its internally generated forces while the static requirements are incorporated into the optimization procedure in terms of constraints.

A brief discussion of this new approach will now be presented during an introductory description of the contents of this thesis.

## 1.2 A NEW APPROACH

At the very early stage, the question that had to be answered was whether the six degree of freedom, grounded, rigid engine model is an adequate one, although such a model is widely used. Discussions with a motor car manufacturer [10] confirmed the view that models of low dimensionality had an important role to play in preliminary design calculations. For reasons of simplicity the six degree of freedom rigid engine isolator model is used, but the investigation of optimum isolation systems is based on the principle of minimizing the forces generated at the isolators. The FORTRAN-coded procedure that investigates optimum isolation systems is developed on this principle and it will be presented in the following stages. which calculates

First, a rigid body power train model coupled through an arbitrary array of isolators to a rigid supporting structure is analysed for dynamic response. The rigid body power train is described by the inertia properties of the power train and each isolator is approximated by a set of linear springs acting along and about its elastic axes. The position and orientation of each isolator with respect to the power train centre of mass is described by three Cartesian coordinates and three Euler angles respectively. The dynamic system is excited by the internally generated engine forces and the response of the system to the resulting series of harmonic excitations is computed. Graphical presentation of both the response and the mode shapes of the system are presented.

Next, a brief introduction to the development of numerical optimization methods is followed by the definition of the general optimization problem. The objective optimization function is then defined in terms of the maximum strain energy of the system, which is indicative of the efficiency of the vibration isolative mounts, and is optimized with respect to the isolator position, orientation and stiffness-properties. The optimization design space is defined by bounds on the optimization variables and constraints on the isolator static displacement, power train static rotations and the rigid body frequency spectrum. It is the constraints on the isolator static displacements and the power train static rotations that take care of the static requirements while constraints on the rigid engine isolator spectrum allows some control on the separation of engine vibrations and engine shake. The NAG FORTRAN routine used to perform the optimization, transforms the original constrained problem into a series of unconstrained subproblems by an augmented Lagrangian function transformation and each subproblem is minimized by a quasi-Newton method. The main steps of the algorithm are explained with the aid of a flowchart diagram and the various numerical requirements such as scaling, constraint weighting and the importance of the optimization monitoring information is explained on practical grounds.

Finally, the optimum solution obtained from the computer program, starting from the isolation system of an existing production engine, is presented and the feasibility of the optimum isolation system is discussed. Through this discussion it will become evident that by allowing freedom on the elastic coupling of the vibration system and minimizing force transmission, better isolation systems can be established. It is recognised, however, that to be genuinely useful spl inf.? in industry the exhaust system must be included in the model, due to its importance on the East-West engine vibration characteristics and that engine shake must be incorporated. The exhaust system can be included to a first approximation if an equivalent stiffness element, in the form of an additional isolator, can be provided and the inertia properties of the power train with the exhaust can be measured. Likewise, rubber hoses or other linkages between the power train and the vehicle structure can be included in the model with no further modification to the code. Engine shake, however, cannot be included without modification of the model unless an equivalent excitation vector at the power train centre of mass can be computed.

Finally an area of concern with the algorithm developed here is its current inability to include non-linear isolator characteristics. The effect of this limitation on the static analysis section of the problem is discussed to the extent of suggesting a way to remove such limitations from the program.

# CHAPTER 2

## ENGINE VIBRATION

The response of a four cycle reciprocating engine excited by its internally generated forces and isolated from a rigid foundation by a set of isolators, as shown in Figure 2.1, is investigated in this chapter.

The power train (engine-gearbox assembly) will generally be subjected to a number of different types of forces generated by driving conditions, engine power and gravity. For the purpose of the following analysis it is convenient to distinguish between static and dynamic forces applied to the frame of the power train.

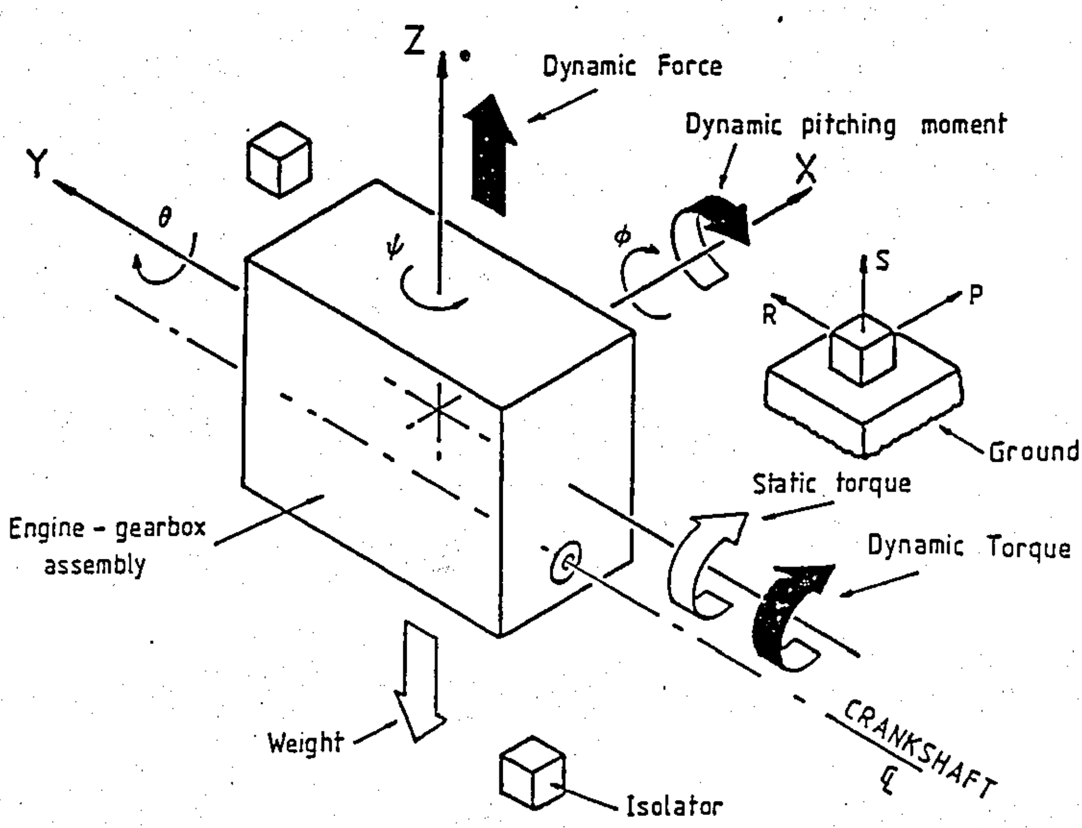


FIGURE 2.1: ARRANGEMENT OF THE POWER TRAIN AND ISOLATORS

The static forces of primary concern are the engine weight force and the zero frequency component of the engine torque reaction. Also of concern are forces resulting from the motion of the vehicle such as braking and cornering. Strictly speaking, these are dynamic forces, but for the purpose of this analysis they will be regarded as static since, for normal driving conditions, variations in them are very slow compared to the engine forces. The importance of the quasi-static forces is that they can cause large engine displacements and consequently possible interaction of moving and stationary parts, which is undesirable.

Dynamic forces on the other hand are responsible for shaking the engine and are generated by combustion gas pressure variations and by unbalanced reciprocating or rotating inertias. For modern reciprocating engines where balance of rotating inertias can be well established, the dynamic forces can be generally represented, as in Figure 2.1, by a vertical unbalance force due to the reciprocating parts, a pitching moment resulting either from a non-symmetric crank arrangement, or by an offset vertical force and finally a rolling torque caused by the vertical unbalance force and gas pressure fluctuations.

The isolators must, therefore, be designed and positioned in such a way so that they will support the power train under the worst possible static conditions, prohibiting large engine displacements and simultaneously attenuating the transmission of engine vibration to the supporting structure. The following dynamic analysis, which is developed with respect to a Cartesian reference frame fixed at the power train centre of mass, with the Z axis vertical positive upwards, the Y axis horizontal, positive towards the front of the engine and the X axis lateral to form a right handed system, will set the foundations for the discussion of engine vibration attenuation which will be presented in the next chapter.

## 2.1 THE VIBRATION MODEL

In deriving the equations of motion the physical system shown in Figure 2.1 is represented by discrete elements possessing either stiffness or inertia as shown in Figure 2.2. The underlying assumptions embodied in this model are the following:

1. The structure supporting the isolators is rigid
2. The engine structure is rigid
3. The mass of the vibration isolators can be neglected
4. Dynamic displacements are small.

As each of these assumptions imply that certain approximations can be made to the physical system, the validity of these approximations will now be discussed.

With a rigid supporting structure, there are two defects introduced into the mathematical model. One is that road inputs, which are known to be important cannot be included in the following analysis and the

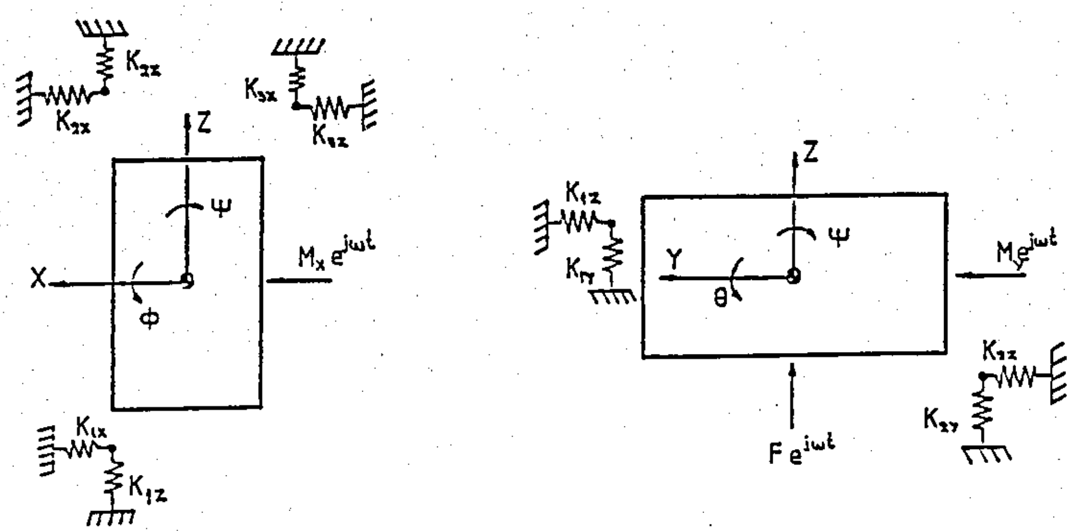


FIGURE 2.2: DISCRETE-ELEMENT MODEL LAYOUT

second is that consideration of vibration transmission to the chassis is prevented. The first defect could be removed by modifying the model to include a rigid body representation of the chassis connected to the road surface by a simple suspension model, thus allowing consideration of engine shake. Consideration of vibration transmission to the chassis, however, requires finite element models of the chassis which are too complicated for preliminary design studies, and further such models are known to be extremely difficult to use in numerical optimization algorithms due to the number of variables involved and the time required for system changes during optimization as a result of the finite element software procedures.

The approximation of the power train by a rigid body is by no means unreasonable as the frequencies of the structural modes of the power train are well above those involving what are effectively rigid body motions of the power train unit on its isolators. Similarly the approximation of the isolators by massless springs is no cause for alarm. Whilst wave propagation in vibration isolators has been observed, the frequency range where it might be of concern is well above the rigid body frequency range of the engine on its isolators.

The assumption of small dynamic displacements, however, allows the approximation of the isolators as linear springs. Since the dynamic deflections are known to be small it is appropriate to treat this part of the problem within the framework of linear small amplitude vibration theory, although the force deflection characteristics of rubber are notoriously nonlinear. The isolator nonlinearity is, however, important in calculating the deflection of the system under conditions of high static engine torques. This aspect of the problem will be discussed at the end of this chapter with the aid of numerical results from the computer program.

Equations of motion: The equations of free-undamped vibrations are formulated first. The resulting eigensolution is then used to find a modal solution to the damped forced vibration problem resulting from the application of internally generated engine forces.

The undamped equations of motion are of the form:

$$\mathbf{M}\,\ddot{\mathbf{x}} + \mathbf{K}\,\mathbf{x} = 0 \tag{2.1}$$

where **M** and **K** are the mass and stiffness matrices of the system expressed in the global X,Y,Z coordinates located at the power train mass centre. The vector **x** is of order six being comprised of three translations and three rotations, i.e. consisting

$$\mathbf{x}^T = [x,\ y,\ z,\ \phi,\ \theta,\ \psi] \tag{2.2}$$

The mass matrix has the form

$$\mathbf{M} = \left[\begin{array}{ccc|ccc} m & 0 & 0 & 0 & 0 & 0 \\ 0 & m & 0 & 0 & 0 & 0 \\ 0 & 0 & m & 0 & 0 & 0 \\ \hline 0 & 0 & 0 & I_{xx} & -I_{xy} & -I_{xz} \\ 0 & 0 & 0 & -I_{yx} & I_{yy} & I_{yz} \\ 0 & 0 & 0 & -I_{zx} & -I_{zy} & I_{zz} \end{array}\right] \tag{2.3}$$

and is assembled by direct application of Newton's second law of motion to the power train rigid body. A slight problem might arise when assembling the rotational inertia submatrix as the power train inertia properties are usually given with respect to its principal inertial axes. Greenwood [11], however, shows that by equating the rotational kinetic energy of the body in the two coordinate systems the rotational inertia properties of the body can be transformed from one axis set to another. Let **C** denote the direction cosine matrix such that

$$\mathbf{x}_p = \mathbf{C}\,\mathbf{x} \tag{2.4}$$

where $x_p$, x represent a vector in the principal axis and the global axis respectively. Then, if $I_p$ and I denote the rotational inertia matrices in two such axis systems, respectively, it can be shown that:

$$I = C^T I_p C \tag{2.5}$$

The stiffness matrix has the form

$$K = \left[\begin{array}{c|c} K_{xx} & K_{x\theta} \\ \hline K_{\theta x} & K_{\theta\theta} \end{array}\right] \tag{2.6}$$

and by virtue of the reciprocal properties of mechanical systems the stiffness matrix will be symmetric. Subsequently it holds that $K_{x\theta} = K_{\theta x}^T$. Each submatrix in (2.6) can be assembled by considering the contribution of each isolator separately and then summing over all the isolators. Let P, R, S denote the local elastic axes of the $n^{th}$ isolator in Figure 2.1 and $A^{(n)}$ the direction cosine matrix so that Consequently

$$x^{(n)} = A^{(n)} p^{(n)} \tag{2.7}$$

where $x^{(n)}$ denotes a translational displacement with respect to the global axes and $p^{(n)}$ the equivalent displacement with respect to the $n^{th}$ isolator elastic axes.

Smollen [12] shows that by considering the forces generated at the $n^{th}$ isolator due to a translation of the suspended body and then transforming these forces back to the global axes, the translational-translational stiffness submatrix due to the $n^{th}$ isolator is given by

$$K_{xx}^{(n)} = A^{(n)}\ K_{p}^{(n)}\ A^{T(n)} \tag{2.8}$$

Similarly by considering the moments about the body axes due to the forces generated at the $n^{th}$ isolator by a translation of the body, the rotational-translational stiffness submatrix is given by

$$K_{\theta x}^{(n)} = R^{(n)}\ K_{xx}^{(n)} \tag{2.9}$$

where $R^{(n)}$ is the skew-symmetric position matrix for the $n^{th}$ isolator,

$$R^{(n)} = \begin{bmatrix} 0 & -r_z^{(n)} & r_y^{(n)} \\ r_z^{(n)} & 0 & -r_x^{(n)} \\ -r_y^{(n)} & r_x^{(n)} & 0 \end{bmatrix}$$

The skew symmetric form is explained by examining the vector expression **r x f**. The zeros on the leading diagonal of its matrix equivalent are simply an expression of the fact that forces cannot generate moments about their line of action and vice versa.

Finally the rotational-rotational stiffness submatrix is assembled by considering the moments which will result on the body due to forces and moments generated on the $n^{th}$ isolator by a general body rotation with the result

$$K_{\theta\theta}^{(n)} = R^{(n)} K_{xx}^{(n)}\ R^{T(n)} + A^{(n)}\ K_{\lambda}^{(n)}\ A^{T(n)} \tag{2.10}$$

Summing over the isolators gives the total stiffness matrix for the system as

$$K = \left[\begin{array}{c|c} \sum_{n=1}^{s} K_{xx}^{(n)} & \sum_{n=1}^{s} K_{xx}^{(n)} R^{T(n)} \\ \hline \sum_{n=1}^{s} R^{(n)} K_{xx}^{(n)} & \sum_{n=1}^{s} R^{(n)} K_{xx}^{(n)} R^{T(n)} + \sum_{n=1}^{s} A^{(n)} K_{\lambda}^{(n)} A^{T(n)} \end{array}\right]$$

Isolator orientation: Whilst providing the simplest representation of finite rotations, the six fold redundancies among the nine direction cosines make them unsuitable for use in an optimization algorithm. The reason for this is that each redundancy can only be removed by an equality constraint viz the sum of squares of the elements in any row or column of the direction cosine matrix $A^{(n)}$ must equal to unity. This problem is overcome when the orientation of the $n^{th}$ isolator with respect to the engine axes is specified by three ordered rotations about the isolator elastic axes. The angles of the ordered rotations are the Euler angles and the order of rotation which will be employed here is the "Yaw-Pitch-Roll" order as follows.

First the isolator is rotated through an angle $\alpha$ about the S elastic axis

Second the isolator is rotated through an angle $\beta$ about the P elastic axis

and finally, the isolator is rotated through an angle $\gamma$ about the R elastic axis.

Following this method as illustrated by Synge and Griffith [13], the transformation matrix $A^{(n)}$ can be derived as

$$A^{(n)} = \begin{bmatrix} d_{11} & d_{12} & d_{13} \\ d_{21} & d_{22} & d_{23} \\ d_{31} & d_{32} & d_{33} \end{bmatrix}$$

where $d_{11} = \cos\gamma \cos\alpha - \sin\gamma \sin\beta \sin\alpha$

$$
\begin{aligned}
d_{21} &= \cos\gamma \sin\alpha + \sin\gamma \sin\beta \cos\alpha \\
d_{31} &= -\sin\gamma \cos\beta \\
d_{12} &= -\cos\beta \sin\alpha \\
d_{22} &= \cos\beta \cos\alpha \\
d_{32} &= \sin\beta \\
d_{13} &= \sin\gamma \cos\alpha + \cos\alpha \sin\beta \sin\alpha \\
d_{23} &= \sin\gamma \sin\alpha - \cos\gamma \sin\beta \cos\alpha \\
d_{33} &= \cos\gamma \cos\beta
\end{aligned}
\tag{2.11}
$$

and

$$
\begin{aligned}
0 &\leqslant \alpha \leqslant 2\pi \\
-\pi/2 &\leqslant \beta \leqslant \pi/2 \\
0 &\leqslant \gamma \leqslant 2\pi
\end{aligned}
\tag{2.12}
$$

<u>Natural frequencies and mode shapes</u>: These are found by seeking solutions of the form $x = v\, e^{j\omega t}$ to equation (2.1). The non-trivial solutions resulting from such trial solutions satisfy

$$(K - \omega^2 M)\ v = 0 \tag{2.13}$$

thereby giving the six natural frequencies and mode shapes of the engine on its mounts. The natural frequencies can be assembled in a diagonal spectral matrix $\Omega$, and the six mode shapes corresponding to the natural frequencies form the columns of the modal matrix V of the system.

Graphical presentation of mode shapes is conveniently performed if the general body motion of a mode of vibration is expressed as a screw displacement. The basic theory involved together with the FORTRAN-code translation of the screw-displacement analysis is presented in Appendix B. Figure 2.3 shows one such presentation of the mode shapes for the Ford 1.6 litre engine which is used throughout the thesis as a practical example. ???

T

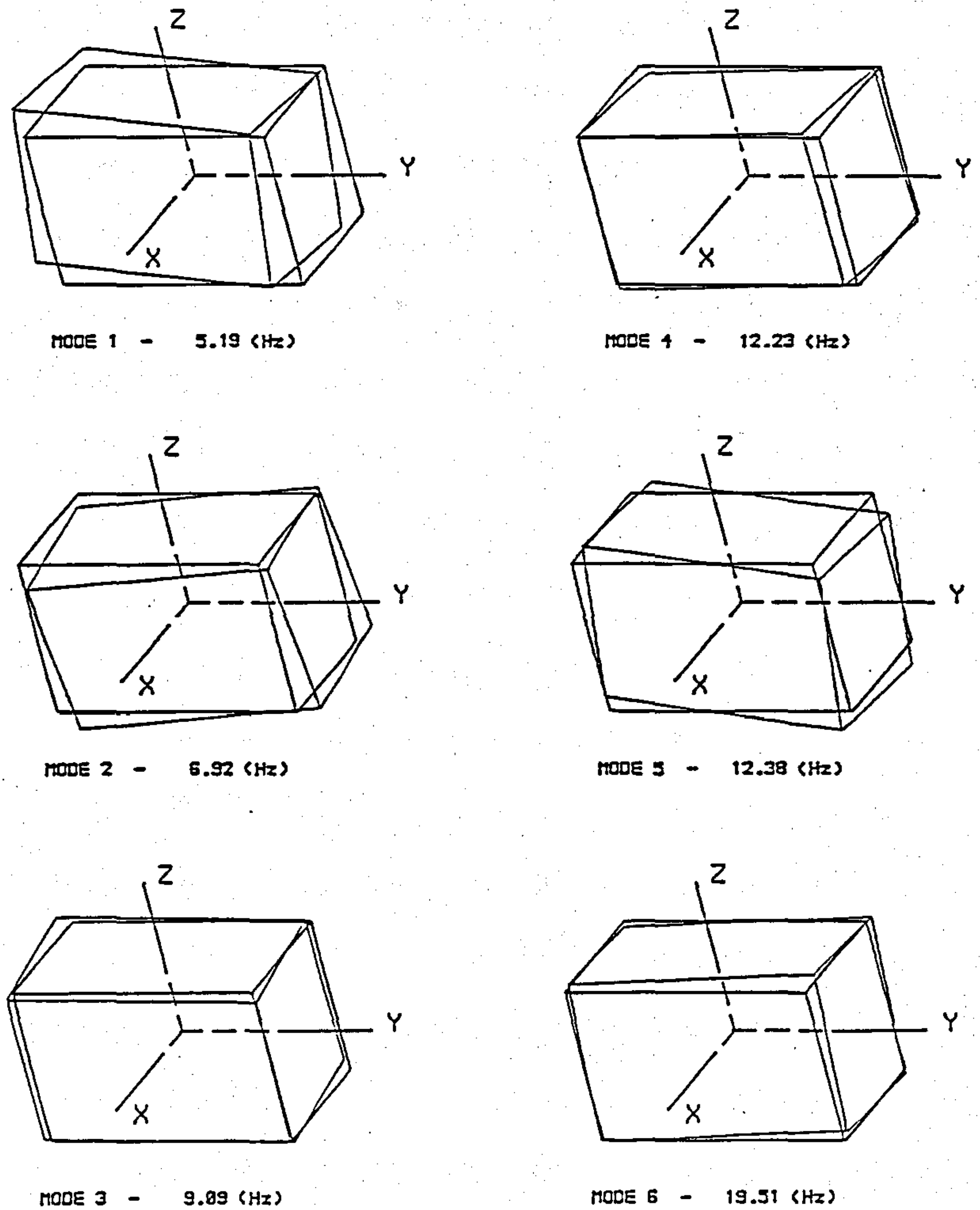


Fig. 2. 3 Mode shapes (Ford diesel 1.6 litre engine)

## 2.2 INTERNALLY GENERATED FORCES

The matrix equation of motion (2.1) is now completed with the addition of an external force vector, thus

$$M\ddot{x} + Kx = \hat{f}\,e^{j\omega t} \tag{2.14}$$

where $\hat{f}$ is the complex vector of the generalized forces of the power train centre of mass containing both magnitudes and phase angles. The derivation of the components of $\hat{f}$ for reciprocating engines is discussed, in varying detail, by a number of authors including Biezeno [14], Taylor [15], Shigley [16] and a brief outline of their results appropriately formulated for this work is presented in Appendix A. What is required for the forced response analysis are analytical expressions for the components of $\hat{f}$ in equation (2.14). By approximating the mass properties of the piston, con-rod and crank, for each cylinder of an n-cylinder in-line reciprocating engine, by a rotating mass ($m_{rot}$) concentrated at the crank pin and a reciprocating mass ($m_{rec}$) concentrated at the gudgeon pin and the gas pressure torque by a Fourier series (i.e. $T = -nb_o - \sum_{k=1}^{\infty} a_k \sin k\omega t - \sum_{k=1}^{\infty} b_k \cos k\omega t$) the forces and moments generated by each cylinder summed with respect to a Cartesian reference frame fixed at the centre of the crankshaft (see Appendix A) are given by equations (2.15) to (2.20). The other parameters involved in these equations are the crank radius r, the engine speed $\omega$, the angle between the $i^{th}$ cylinder crank and the No 1 cylinder crank $\theta_i$, the distance $d_i$ of the $i^{th}$ cylinder centre from the crankshaft centre and the ratio of the crank radius to the con-rod length $\lambda$.

$$f_x = m_{rot}\, r\omega^2\, \mathrm{Im}\left[\sum_{i=1}^{n} e^{j(\omega t+\theta_i)}\right] \tag{2.15}$$

$$f_y = 0 \tag{2.16}$$

$$f_z = (m_{rot} + m_{rec})\ r\omega^2\ \mathrm{Re}\ [\ \sum_{i=1}^{n} e^{j(\omega t+\theta_i)}] +$$

$$+\ m_{rec}\ r\omega^2\ \mathrm{Re}\ [\lambda \sum_{i=1}^{n} e^{j2(\omega t+\theta_i)}] \qquad (2.17)$$

$$q_x = -(m_{rot} + m_{rec})\ r\omega^2\ \mathrm{Re}\ [\ \sum_{i=1}^{n} d_i e^{j(\omega t+\theta_i)}] -$$

$$-\ m_{rec}\ r\omega^2\ \mathrm{Re}\ [\lambda \sum_{i=1}^{n} d_i e^{j2(\omega t+\theta_i)}] \qquad (2.18)$$

$$q_y = m_{rot}\ r\omega^2\ \mathrm{Im}\ [\ \sum_{i=1}^{n} d_i e^{j(\omega t+\theta_i)}] \qquad (2.19)$$

$$q_2 = -m_{rec}\ r^2\omega^2\ \mathrm{Im}\ [\ \sum_{i=1}^{n} (\frac{\lambda}{4} e^{j(\omega t+\theta_i)} -$$

$$- \frac{1}{2} e^{j2(\omega t+\theta_i)} - \frac{3\lambda}{4} e^{j3(\omega t+\theta_i)})] -$$

$$- \sum_{k=1}^{\infty} a_k\ \mathrm{Im}\ [\ \sum_{i=1}^{n} e^{jk(\omega t+\theta_i)}] -$$

$$- \sum_{k=1}^{\infty} b_k\ \mathrm{Re}\ [\ \sum_{i=1}^{n} e^{jk(\omega t+\theta_i)}] \qquad (2.20)$$

However, equations (2.15) to (2.20) give the components of the vector $\hat{f}$ in equation (2.14) if, and only if, the crankshaft centre coincides with the power train centre of mass and the crankshaft and cylinder centre lines are parallel to the global axes. Generally, the crankshaft centre does not coincide with the power train centre of mass, and it is possible that both the crankshaft and cylinder centre lines will be skewed with respect to the global axis. If $\hat{f}'$ represents the force vector at the centre of the crankshaft with components given by equations (2.15) to (2.20), then a transformation might be required on $\hat{f}'$ to yield the global force vector $f$ of equation (2.14).

For the general case, where none of the conditions mentioned above is satisfied, the required transformation matrix will be derived on the principle that the virtual work done on the power train by each of the two force vectors is the same i.e.

$$\hat{f}' \, \delta \hat{v}' = \hat{f} \, \delta v \qquad (2.21)$$

where $\delta v'$, $\delta v$ are the virtual displacement vector in the crankshaft local axes and the global axes respectively. With reference to Figure 2.4, let $U$ denote the transformation matrix such that

$$x'' = U \, x'$$

Then if $\delta x$, $\delta\phi$ are the translational and rotational subvectors of $\delta v$ and $\delta x''$, $\delta\phi'$ the equivalent subvectors of $v'$ and $R_c$ is the position matrix for the crankshaft centre with respect to the global axes, assembled from the coordinates $x_c$, $y_c$, $z_c$ shown in Figure 2.4, then it follows that

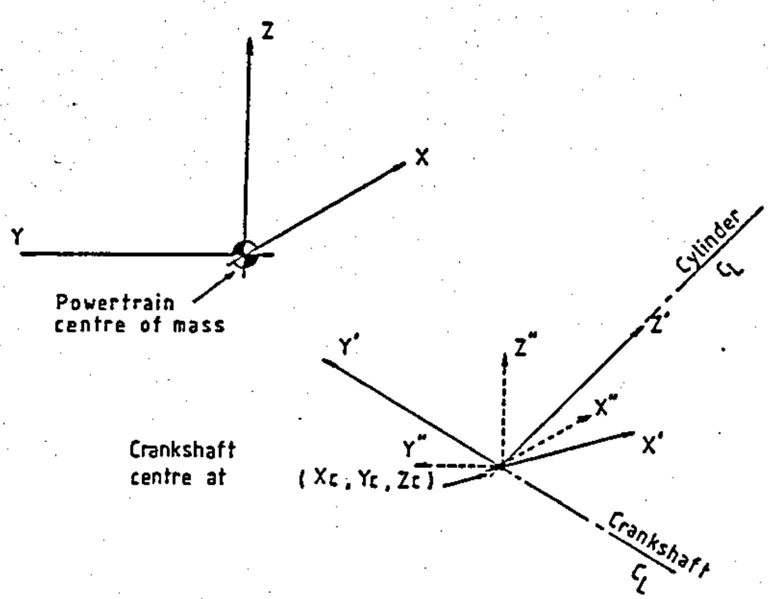


FIGURE 2.4: GLOBAL AND CRANKSHAFT REFERENCE FRAMES

$$\delta \mathbf{x}' = U^T \, \delta\mathbf{x} + U^T R_c^T \, \delta\phi$$

$$\delta\phi' = U^T \, \delta\phi$$

or
$$\delta \mathbf{v}' = T \, \delta\mathbf{v} \tag{2.22}$$

where
$$T = \left[\begin{array}{c|c} U^T & U^T R_c^T \\ \hline 0 & U^T \end{array}\right]$$

Substituting for $\delta \mathbf{v}'$ into equation (2.21) the following relationship between $\hat{\mathbf{f}}$ and $\hat{\mathbf{f}}'$ is obtained

$$\hat{\mathbf{f}} = T^T \hat{\mathbf{f}}' \tag{2.23}$$

## 2.3 CALCULATION OF FORCED RESPONSE

As the mode shapes span the frequency spectrum of the system they can be used as basis vectors to describe the response of the system to a harmonic excitation i.e. the response of the system at any other frequency can be expressed as a linear combination of the modal vectors. The equation of motion (2.14) can be decoupled by a linear transformation utilising the orthogonality properties of the modal vectors with respect to the mass and stiffness matrices of the system shown for example by Bishop, Gladwell and Michaelson [17]. The coordinates which decouple the equations of motion, referred to as the principal coordinates, are related to the generalized coordinates by the linear transformation ???

$$\mathbf{x} = V \, \mathbf{p} \tag{2.24}$$

where $\mathbf{p}$ is the vector of the principal coordinates. When the system is vibrating in a natural mode the only non-zero element in $\mathbf{p}$ is the one corresponding to that mode. Applying the above transformation to equation (2.14) and premultiplying by $\mathbf{V}^T$ yields

$$\mathbf{V}^T \mathbf{M} \mathbf{V} \ddot{\mathbf{p}} + \mathbf{V}^T \mathbf{K} \mathbf{V} \mathbf{p} = \mathbf{V}^T \hat{\mathbf{f}} e^{j\omega t}$$

which in view of the orthogonality properties of the eigenvectors reduces to

$$\mathbf{A} \ddot{\mathbf{p}} + \mathbf{C} \mathbf{p} = \mathbf{V}^T \hat{\mathbf{f}} e^{j\omega t}$$

or in component form:

$$a_r \ddot{p} + c_r p_r = \hat{f}^{(r)} e^{j\omega t} \qquad (2.25)$$

where $a_r$ and $c_r$ are the modal mass and stiffness coefficients and $\hat{f}^{(r)}$ is the complex generalized force for the $r^{th}$ mode of vibration.

Stiffness proportional damping is introduced by a modal loss factor $\eta_r$ (equal to the cyclic energy loss divided by the maximum strain energy of the mode), by making the modal stiffness complex i.e. by replacing $c_r$ with

$$\hat{c}_r = c_r (1 + j \eta_r) \qquad (2.26)$$

Substituting $\hat{c}_r$ for $c_r$ in equation (2.25) and solving for $p_r$ gives the response in the principal coordinates as

$$p_r = \hat{\alpha}_r \hat{f}^{(r)} e^{j\omega t} \tag{2.27}$$

where $\hat{\alpha}_r$ is the complex receptance

$$\hat{\alpha}_r = \frac{(\omega_r^2 - \omega^2) - j \eta_r \omega_r^2}{a_r[(\omega_r^2 - \omega^2)^2 + (\eta_r \omega_r^2)^2]} \tag{2.28}$$

The complex amplitude of the generalized coordinates $\hat{x}_i$ is then computed by substituting equation (2.27) into (2.24) giving

$$\begin{aligned} \hat{x}_i &= \sum_{j=1}^{n} [\sum_{r=1}^{n} v_i^{(r)} \hat{\alpha}_r v_j^{(r)}] \hat{f}_j \\ &= \sum_{j=1}^{n} \hat{\alpha}_{ij} \hat{f}_j \end{aligned} \tag{2.29}$$

where $\hat{\alpha}_{ij} = \sum_{r=1}^{n} \alpha_r v_i^{(r)} v_j^{(r)}$ is the receptance linking the response of the $i^{th}$ coordinate to an excitation in the $j^{th}$ coordinate. The solution in the time domain, to agree with equation (2.14) is given as

$$x_i(t) = (x_i' + j x_i'')e^{j\omega t} \tag{2.30}$$

<u>Multi-frequency excitation</u>: As noted above, equations (2.15) to (2.20) express the excitation as a series of harmonics of the engine speed $\omega$. Since our interest is mainly in the magnitude of the response, a measure of the total response of the system for a particular engine speed is given by the sum of the mean square values of the responses to the individual excitation harmonics.

For the $m^{th}$ harmonic of excitation the response for the $i^{th}$ generalized coordinate is computed from equation (2.29) by substituting $\hat{\alpha}_r^{(m)}$ for $\hat{\alpha}_r$ and $\hat{f}_j^{(m)}$ for $\hat{f}_j$. The receptance for the $m^{th}$ harmonic is calculated from equation (2.28) by replacing $\omega$ with $m\omega$ and equation (2.30) is now modified as

$$x_i^{(m)}(t) = (x_i'^{(m)} + j\, x_i''^{(m)})e^{jm\omega t} \tag{2.31}$$

The mean square response is then computed by direct application of Parseval's formula to equation (2.31) giving the mean square response for the $i^{th}$ generalized coordinate as:

$$\overline{x_i^2} = \frac{1}{2} \sum_{m=1}^{n} [(x_i'^{(m)})^2 + (x_i''^{(m)})^2] \tag{2.32}$$

So far we have considered the dynamic characteristics of engine isolation systems and developed analytical expressions for the forced response of the power train to its internally generated forces. These expressions will be used in the following chapter for the formulation of the optimum system isolation problem. However, the feasibility of such systems will depend on their ability to satisfy the static requirements mentioned at the beginning of this chapter and consequently analytical expressions are required to implement these requirements into the optimization procedure.

Analytical expressions for the power train centre of mass displacement and the isolators deflection will now be derived from a static analysis of the engine-isolator system.

## 2.4 STATIC ANALYSIS

As was mentioned in the introductory part of this chapter, the static forces experienced by the engine frame are primarily the engine weight and the static torque (i.e. output torque at the drive line). The static torque on the engine frame is of great importance as, under maximum-torque engine speed with first gear engaged and sudden release of the clutch, it can reach extremely high values. Forces arising from vehicle driving conditions will not be included in the following analysis as they cannot possibly arise at the same time with the maximum static torque on the engine frame and consequently if they are included the calculated static displacements will be overestimated, and when used as feasibility criteria in the optimization procedure the result will be a statically overdesigned and dynamically less efficient isolation system.

The following static analysis will be developed with respect to the engine global axis coordinates shown in Figure 2.1 and the assumption made in that the isolators possess linear load-deflection characteristics. However the possibility of implementing nonlinear characteristics by an iterative numerical procedure is also discussed in the following sections of this chapter.

For static equilibrium of the engine-isolator system the following matrix equation must be satisfied:

$$f^{(s)} = K\, x^{(s)} \tag{2.33}$$

where $f^{(s)}$ is the static force vector at the power train mass centre

$$f^{T(s)} = [f_x^{(s)},\ f_y^{(s)},\ f_z^{(s)},\ q_x^{(s)},\ q_y^{(s)},\ q_z^{(s)}]$$

and is assembled from the engine weight and the final drive torque as follows.

Let $q'_x$ denote the final drive torque and $\mathbf{R}'$, $\mathbf{U}'$ denote the position and direction cosine matrices of the final drive axis, with respect to the global axes. The static force vector at the power train mass centre due to $q'_x$ is given by

$$\mathbf{f}_t^{(s)} = \mathbf{T}^T \mathbf{f}'$$

where $\mathbf{f}'^T = [0, 0, 0, 0, q'_x, 0]$ and $\mathbf{T}$ is the transformation matrix relating drive train and global coordinates. The total static force vector is then computed by adding the engine weight to the appropriate element of $\mathbf{f}_t^{(s)}$ i.e.

$$\mathbf{f}^{(s)} = \mathbf{f}_t^{(s)} + [0, 0, -mg, 0, 0, 0]^T \qquad (2.34)$$

Finally the stiffness matrix $\mathbf{K}$ is that derived by equations (2.8) to (2.10) and $\mathbf{x}^{(s)}$ is the static displacement vector at the power train mass centre i.e.

$$\mathbf{x}^{T(s)} = [x^{(s)}, y^{(s)}, z^{(s)}, \phi^{(s)}, \theta^{(s)}, \psi^{(s)}]$$

Solving equation (2.33) for $\mathbf{x}^{(s)}$ gives the displacements of the power train mass centre as

$$\mathbf{x}^{(s)} = \mathbf{K}^{-1} \mathbf{f}^{(s)} \qquad (2.35)$$

The deflections at each isolator can now be derived by considering the displacements along each isolator's local axes due to the translations and rotations of the power train.

If $R^{(n)}$, $A^{(n)}$ are the position and direction cosine matrices of the $n^{th}$ isolator local axes with respect to the global axes and $u^{(s)}$, $v^{(s)}$ are the translational, rotational subvectors of $x^{(s)}$ respectively, it can be shown that the translations at the $n^{th}$ isolator with respect to its local axes are given by

$$u_n^{(s)} = A^{(n)}\, u^{(s)} + A^{(n)}\, R^{T(n)}\, v^{(s)} \qquad (2.36)$$

By placing constraints on the values of the elements of $x^{(s)}$ and $u_n^{(s)}$, computed by equations (2.35) and (2.36), static stability of the engine isolator system can be maintained and isolator stress levels can be kept within acceptable limits as will be discussed in the following chapter.

The implementation of both the static and the forced response analysis into a FORTRAN computer program will now be briefly discussed and pre-optimization computer results will be presented and discussed.

## 2.5 NUMERICAL RESULTS

The selected NAG optimization routine (EO4UAF), which will be discussed in the next chapter requires two user supplied subroutines. EO4UAF calls FUNCT1 to compute the value of the optimization function and then CON1 to compute the value of each constraint function. The basic computational steps involved in these subroutines are outlined in the flow charts presented in Figures D2 and D3 of Appendix D. The flow charts illustrate that the dynamic response and the static displacements of the power train are computed within these subroutines and that FUNCT1 can also be used, outside the optimization loop, to

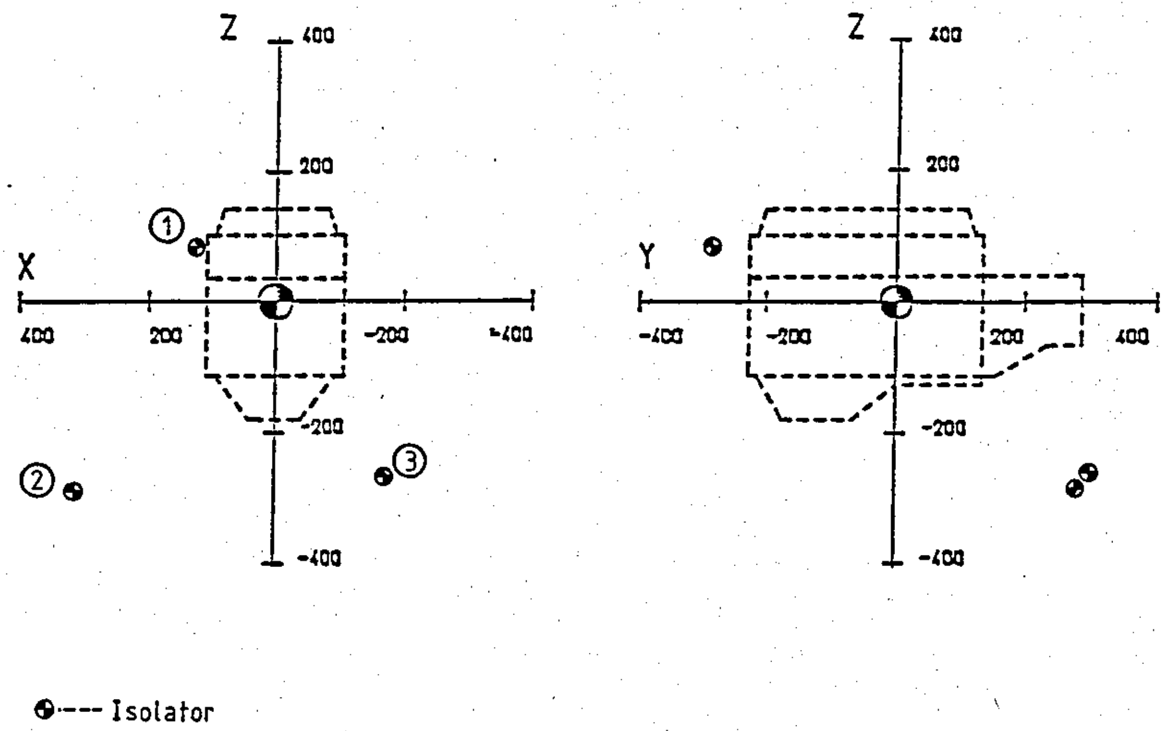


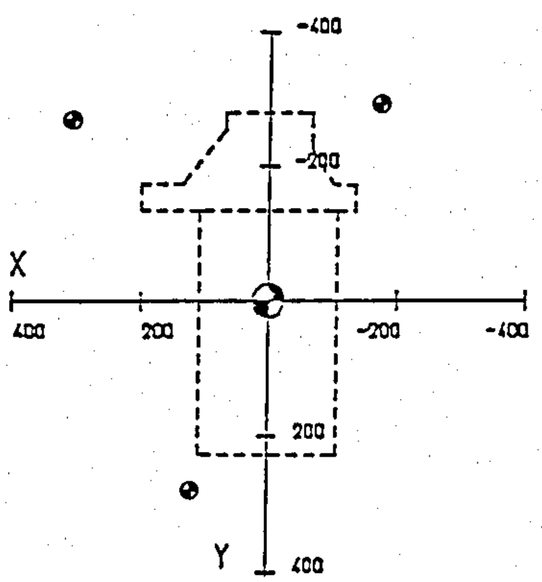


**ENGINE DATA**

| | | |
|---|---|---|
| TYPE | : | Ford four cylinder Diesel |
| Capacity | : | 1606 cc |
| Power | : | 40 KW |
| Maximum speed reduction of final drive | : | 12.827 |
| Mass | : | 197 Kg |

Inertia matrix .
$$\begin{bmatrix} 13.2 & 1.41 & 0.259 \\ 1.41 & 7.02 & -2.03 \\ 0.259 & -2.03 & 10.7 \end{bmatrix}$$

Fig. 2.5 Engine - isolator Layout

compute the dynamic response of the power train for a specified range of engine speeds. Using this facility a test run was made to check the code for possible "bugs" and the programming errors found were corrected. The presentation of the results and the following discussion aim to explain what exactly is being computed under the general term 'dynamic response', and to point out any sensitive areas that could be important in a numerical optimization procedure. The limitations of the static analysis imposed by the linearity of the model will be demonstrated by numerical results and the possibility of modifying the program to include non-linear load-deflection characteristics for the isolators will be discussed. The results which will be presented were obtained using the necessary data for the power train-isolator arrangement shown in Figure 2.5. The legend gives a brief description of the power train while the complete set of the data used can be found in Appendix C.

The dynamic response of the power train to its internally generated forces over a range of engine speeds is presented in Figures 2.6 to 2.11. Each of the Figures 2.6 to 2.10 show the six dynamic displacements of the power train mass centre as a function of engine speed for various harmonics of the excitation. Theoretically, the 1/2 and the odd number harmonics should not exist with a 0-180-180-0 crank arrangement. The presence of these harmonics is due to the fact that the torque excitation vector is computed using the measured torque spectrum which was supplied with the other engine data listed in Appendix C. In contrast to mathematical models, the half order and odd order harmonics are always present in real engines as a result of cylinder-to-cylinder combustion irregularities. As can be seen from Figure 2.6. the 1/2 order harmonic excites the rigid power train modes well within the engine operating speed although its effect to the overall vibration level is not considerable as it can be observed from the mean square displacement graph in Figure 2.11. However, its presence becomes increasingly important as the cylinder-to-cylinder combustion irregularities become more and more uneven for reasons such as bad carburation, bad timing or misfiring to name but three. Although the dynamic response to the 1/2 order excitation harmonic is not expected to play a significant role in the optimization procedure, it will give a point of comparison between the initial and the final optimum isolation systems.

It should be mentioned at this point that the torque spectrum which was used, was obtained from measurements at an engine speed of 800 rpm and zero engine load. In order to avoid unnecessary programming complications, the same spectrum was used for the computation of the dynamic displacements at all engine speeds. Apart from the already mentioned simplification the most unrealistic part of these plots is the lower limit of the engine speed range which was set to 50 rpm and which is too far below the lowest possible idling speed for any real engine. However, setting the bottom limit to such a low value allows all the resonant peaks to appear on the plots. Unfortunately the level of these peaks is highly affected by the constant torque spectrum and consequently it is not possible to use the peak level for mode shape identification. Nevertheless the magnitude of the response can be used to assess the contribution of the individual harmonics of the excitation to the overall response of the system.

One way of checking the program is by examining whether the peaks of the response curves occur at the computed eigenvalues. For the system of Figure 2.5 the eigenvalues were found to be as follows

| n | Hertz | rpm |
|---|---|---|
| 1 | 5.19 | 311.69 |
| 2 | 6.92 | 415.07 |
| 3 | 9.09 | 545.2 |
| 4 | 12.23 | 733.58 |
| 5 | 12.38 | 742.62 |
| 6 | 19.51 | 1170.58 |

From Figure 2.7, which gives the response to the first order excitation harmonic, it can be seen that the peaks occur at the frequencies listed above. Further, the peaks in the response curves, for the other excitation harmonics, occur at 1/n times these ???

frequencies. The missing sixth peak on the response plot is due to the numerical closeness of the fourth and fifth modal frequencies.

A quick comparison of the magnitude of the harmonic responses will reveal that the second excitation harmonic plays a dominant role. This domination is reflected in the mean square displacement plots of Figure 2.11 where the contribution of the other excitation harmonics, to the overal response, does not appear to be substantial.

The question that arises now is whether there exists a dominant mode shape. This kind of information will be of good value at a later stage when trying to understand, in physical terms, how the optimum isolation system was obtained by the numerical optimization algorithm. Mode shape identification was attempted using the pictorial representation of the mode shapes presented earlier in Figure 2.3 and the two dimensional views shown in Figures 2.12-2.14 were produced to aid such an attempt. However it was found impossible to succeed due to the urelated scaling among translations and rotations. Time did not permit further investigations to be carried out on the scaling of the translations and the rotations that result from the screw displacement of the body (Appendix B). An alternative was to use the modal kinetic energy distribution.

Johnson and Subhedar [18] give the modal kinetic energy distribution as

$$KE_{kl} = \frac{1}{2} m_{kl} \, v_{jk} \, v_{jl} \, \omega_j^2 \tag{2.37}$$

where $m_{kl}$ is the k,l element of the mass matrix

$v_{jk}$ is the $k^{th}$ element of the eigenvector corresponding to the $j^{th}$ natural frequency

$\omega_j$ is the $j^{th}$ natural frequency

It is further stated in their paper that the summation of the energies due to the off-diagonal terms in the mass matrix is termed the coupling energy of the system. However it is not clear to the author what exactly is meant by this term especially when it can be associated with a negative sign. However using this method the following kinetic energy distributions were obtained for the system shown in Figure 2.5:

Using Table 2.1, the peaks on the dynamic response plots can now be related to the rigid power train mode shapes. The roll mode seems to play a key role in the dynamic behaviour of the dynamic model. The dynamic response to the second excitation harmonic indicates that the roll displacement almost dominates the dynamic response. Further from Table 2.1 it is obvious that the roll mode is excited at the top of the modal spectrum and well within the engine operating speed range, and what is more important is that the second excitation harmonic excites this mode at an engine speed which is fairly close to the engine idling speed. These observations indicate that the isolation system is designed to be fairly stiff in roll. It is beyond doubt that the stiffness of an East-West engine isolator system in roll is a critical design factor.

| Modal Frequency | X | Y | Z | $\phi$ | $\theta$ | $\psi$ | COUPL. |
|---|---|---|---|---|---|---|---|
| 5.19 | 2.26 | 64.83 | 14.30 | 8.20 | 5.63 | 5.0 | -0.22 |
| 6.92 | 8.32 | 32.95 | 40.6 | 5.24 | 9.94 | 3.35 | -0.4 |
| 9.08 | 48.25 | 0.01 | 19.64 | 11.37 | 21.03 | 12.26 | -12.56 |
| 12.23 | 23.0 | 0.0 | 3.66 | 33.4 | 9.95 | 47.23 | -17.24 |
| 12.38 | 8.97 | 2.12 | 21.34 | 42.64 | 4.56 | 19.44 | 0.93 |
| 19.51 | 9.3 | 0.06 | 0.42 | 1.98 | 57.1 | 18.7 | 12.44 |

TABLE 2.1: PERCENTAGE MODAL KINETIC ENERGY DISTRIBUTION

As mentioned earlier, the engine isolation system is also responsible for reacting the maximum final drive torque. For the power train described in Figure 2.5 this is about 12.8 times the maximum engine output torque and up to double that value for the case of sudden release of the clutch in first gear. The question that remains to be answered is whether the given isolation system is statically over-designed and consequently dynamically less efficient.

Subroutine CON1 computes the static displacements of the power train and the deflections of the isolators using the linear analysis described in Section 2.4. However, the load-deflection characteristics of the commonly used isolators (rubber-mounts) are notoriously nonlinear. This nonlinearity is demonstrated in Figure 2.15 which is the x-direction load-deflection characteristics for the left-hand upper and lower mounts of the Escort 1.6 Diesel [10]. It can be appreciated from these graphs that linearity is maintained only in the low load region (approximately 2 kN for the isolators shown) and that linear aproximations to the isolator deflection, under high loading conditions, will be overestimated to say the least. In order to demonstrate the magnitude of the error induced by the linear analysis the relevant numerical information was selected from the computer results of the test run and will now be presented.

| Isolator No | Translational Stiffnesses (kN/m) | | |
|---|---|---|---|
| | $k_p$ | $k_r$ | $k_s$ |
| 1 | 418 | 132 | 165 |
| 2 | 288 | 77 | 226 |
| 3 | 288 | 77 | 226 |

TABLE 2.2: ISOLATOR STIFFNESSES

The dynamic translational stiffnesses used for each isolator along each of its elastic axes are given in Table 2.2 above. Although the static rates of rubber isolators are generally lower than the dynamic rates, it was decided to use the dynamic rates for the static analysis since computing and updating a second stiffness matrix during optimization would increase considerably the computation time consumption without any significant gain. Using the dynamic stiffness matrix, which is computed in FUNCT1, the static deflections of the isolators due to the engine weight and the maximum final drive torque were computed by CON1 as shown below in Table 2.3.

Assume, for sake of argument, that the load-deflection characteristics presented in Figure 2.15 also apply for the Z-direction of isolators 2 and 3; the isolators are oriented so that the p, r, s directions coincide with x, y, z respectively. Using the computed deflections from Table 2.3 and the appropriate stiffness rates from Table 2.2, in the linear relationship F = ke, the forces on the second and third isolators are given as $F_z^{(2)} = 4.7$ kN and $F_z^{(3)} = 3.54$ kN and the corresponding deflections suggested by the load-deflection-characteristics are $Z_2 = 15.8$ mm and $Z_3 = 11.6$ mm. The numerical difference between the computed and the interpolated deflections might not seem considerable at first. However, had the constraint on that deflection been 15 mm, then the corresponding stiffness rate would

| Isolator No. | Deflection in mm | | |
|---|---|---|---|
| | X | Y | Z |
| 1 | 1.63 | 0.562 | 4.7 |
| 2 | 2.43 | 9.74 | 20.8 |
| 3 | 0.061 | 10.71 | 15.65 |

TABLE 2.3: COMPUTED ISOLATOR DEFLECTIONS

have been increased, by the linear model, from 226 kN/m to at least 315 kN/m in order to avoid constraint violation. It can be appreciated that such changes, apart from being unnecessary, are generally speaking, undesirable.

One way to improve the linear model, is to introduce the isolator load-deflection characteristics into the computations, by the iteration loop suggested by the modified flow chart of CON1 presented in Figure 2.16. First a polynomial is fitted to each load-deflection curve (using a NAG routine such as E02AFF) so that the deflection $X_{ij}$ for the $i^{th}$ isolator in the $j^{th}$ direction is expressed as a function of the applied load i.e.

$$X_{ij}(L) = \alpha_o + \alpha_1 L + \alpha_2 L^2 + \alpha_3 L^3 + \ldots + \alpha_N L^N \qquad (2.38)$$

where L is the load and $\alpha_N$ are the polynomial coefficents. Next the first linear approximation to the static displacements is computed using the linear analysis of Section 2.4 and the forces on each isolator are estimated. Using these forces in equation (2.38) an interpolated value for each deflection is calculated and compared with that previously computed. If the difference between these two values exceeds a specified tolerance, then the corresponding stiffness rate is updated using the relationship:

$$K_{ij} = F_{ij}/X_{ij}(L) \qquad (2.39)$$

The static stiffness matrix (now separate from the dynamic stiffness matrix) is recomputed and the isolator deflections are re-evaluated according to Section 2.4. This method is demonstrated graphically in Figure 2.17 and was also successfully tested manually for convergence on a single isolator.

Unfortunately the effect of the linear model on the optimization constraints was discovered at a stage when time limitations did not permit the author to carry out the necessary modifications to the program, test it and optimize all over again.

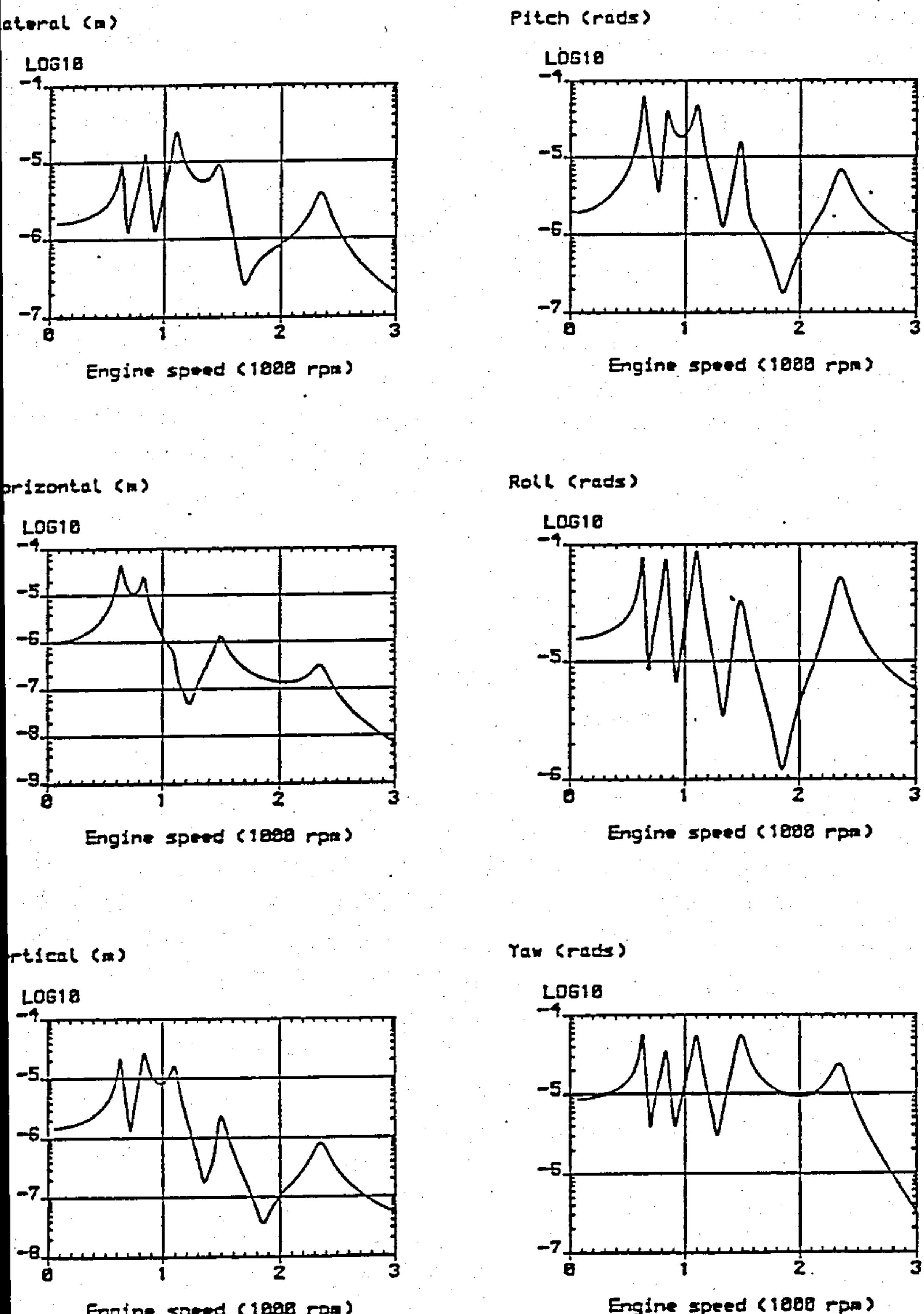


Fig. 2.6: Dynamic response of power train mass-centre due to the ½ order excitation harmonic

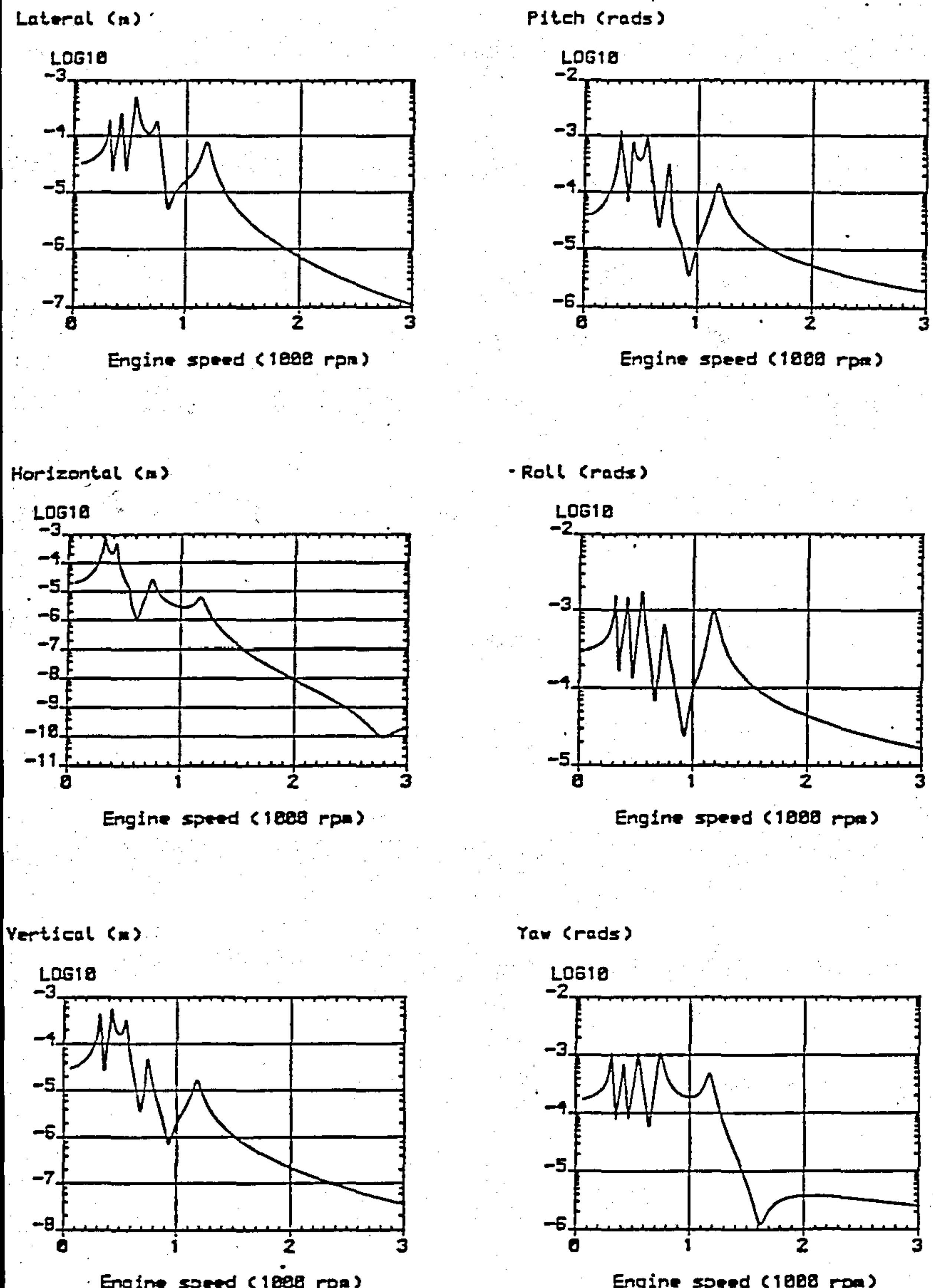


Fig. 2.7: Dynamic response of power train mass-centre due to the first order excitation harmonic

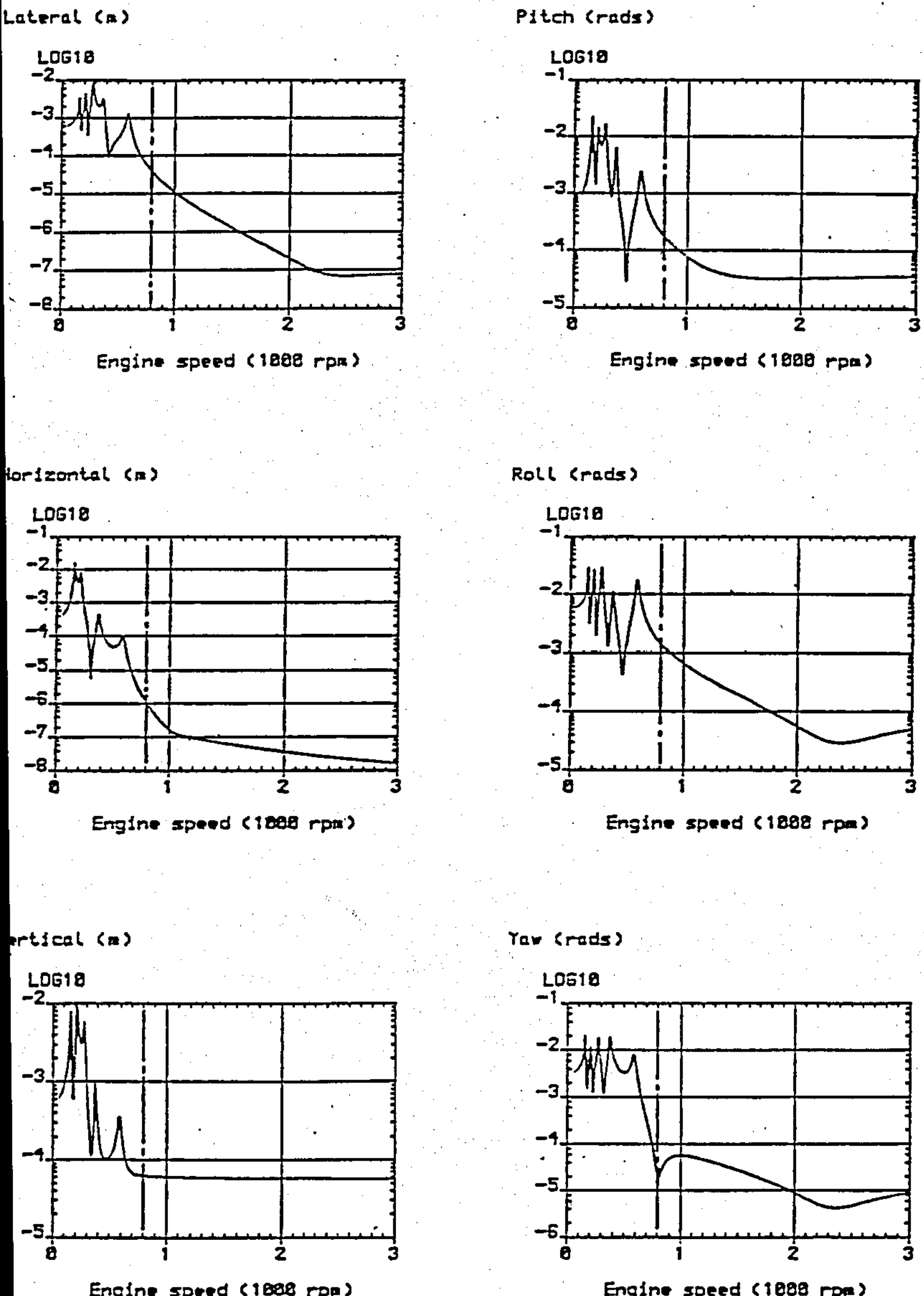


Fig. 2.8 : Dynamic response of power train mass-centre due to the 2nd order excitation harmonic

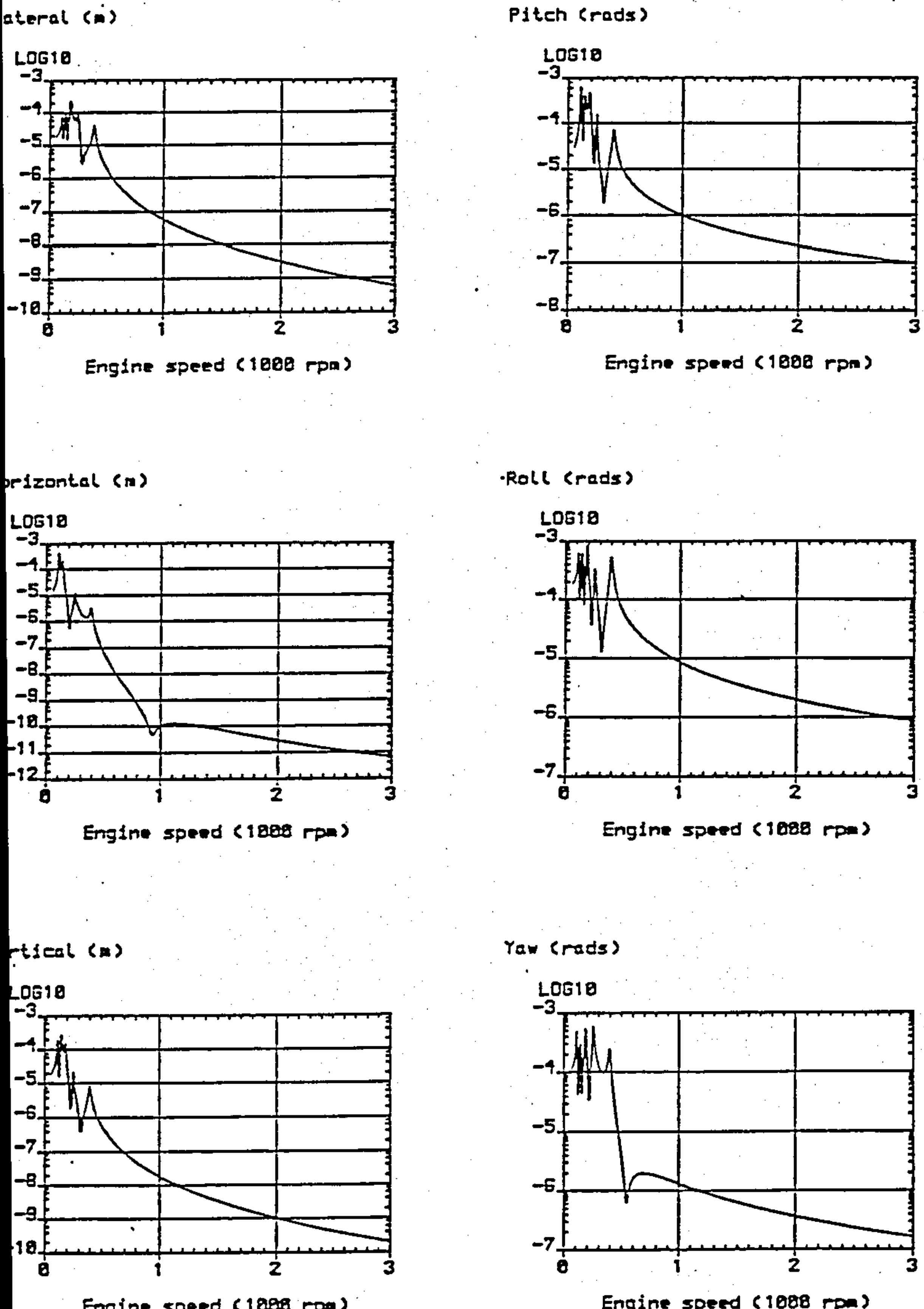


Fig. 2.9 : Dynamic response of power train mass-centre due to the third order excitation harmonic

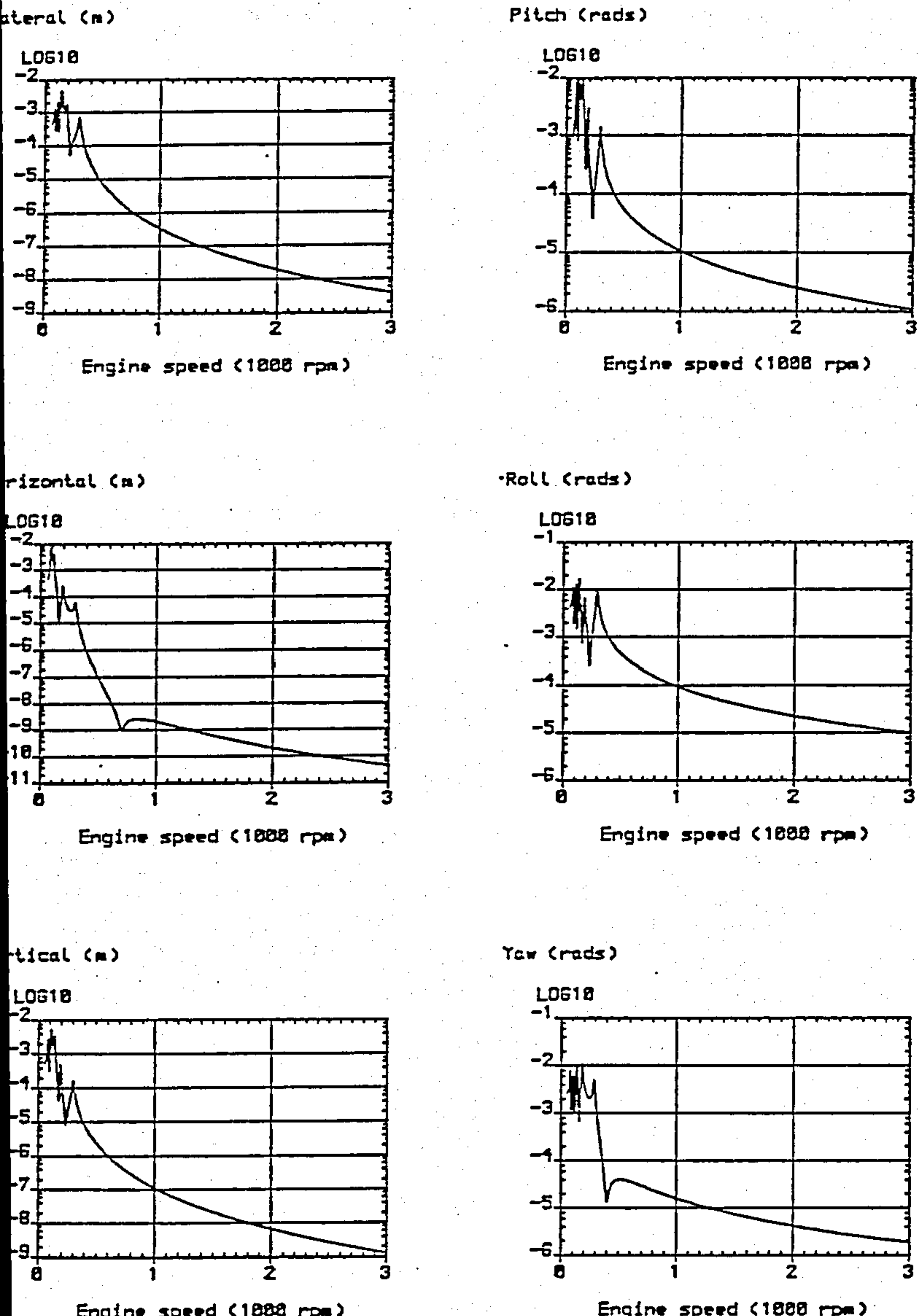


Fig. 2.10: Dynamic response of power train mass-centre due to the fourth order excitation harmonic

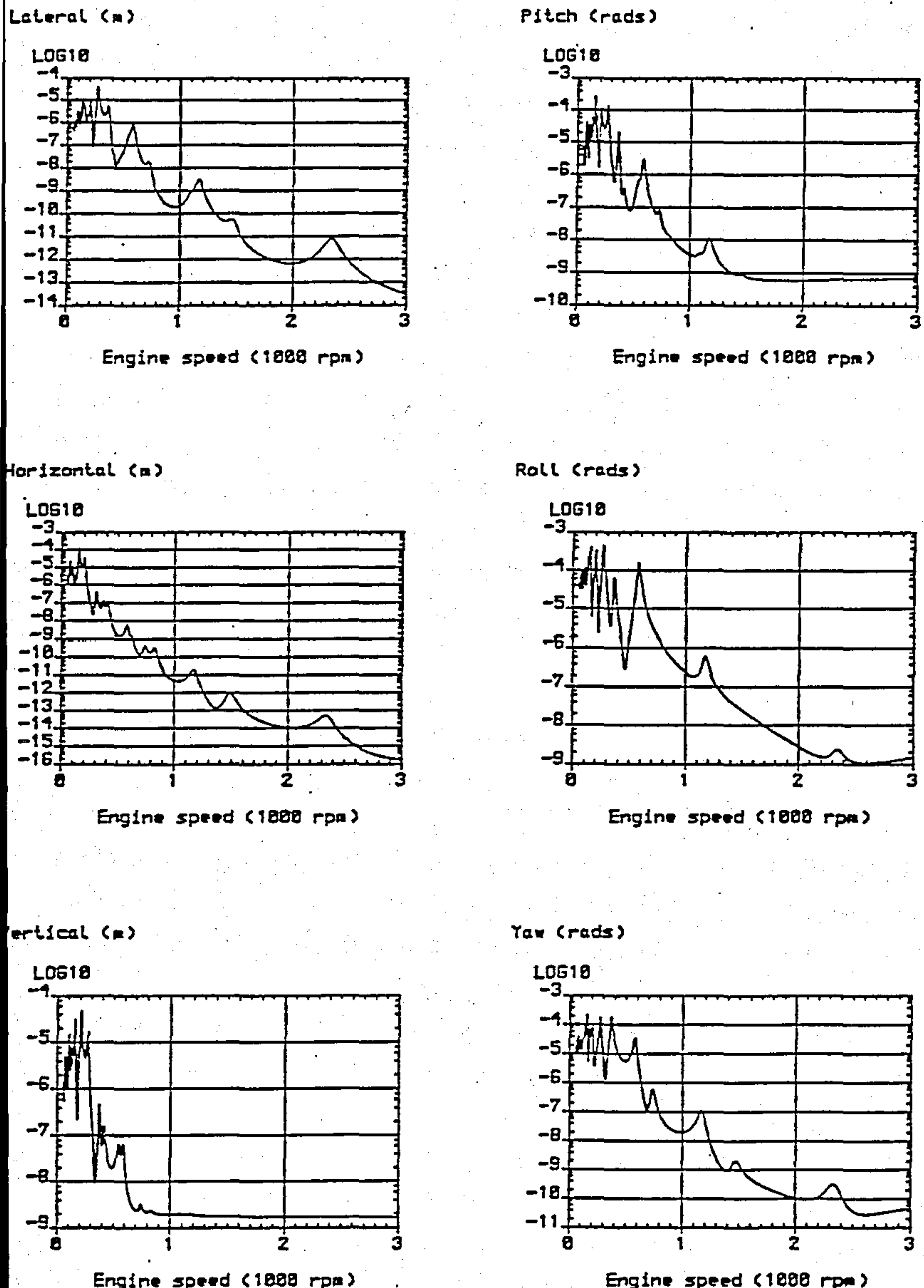


Fig. 2.11: Mean square response of power train mass-centre engine speed

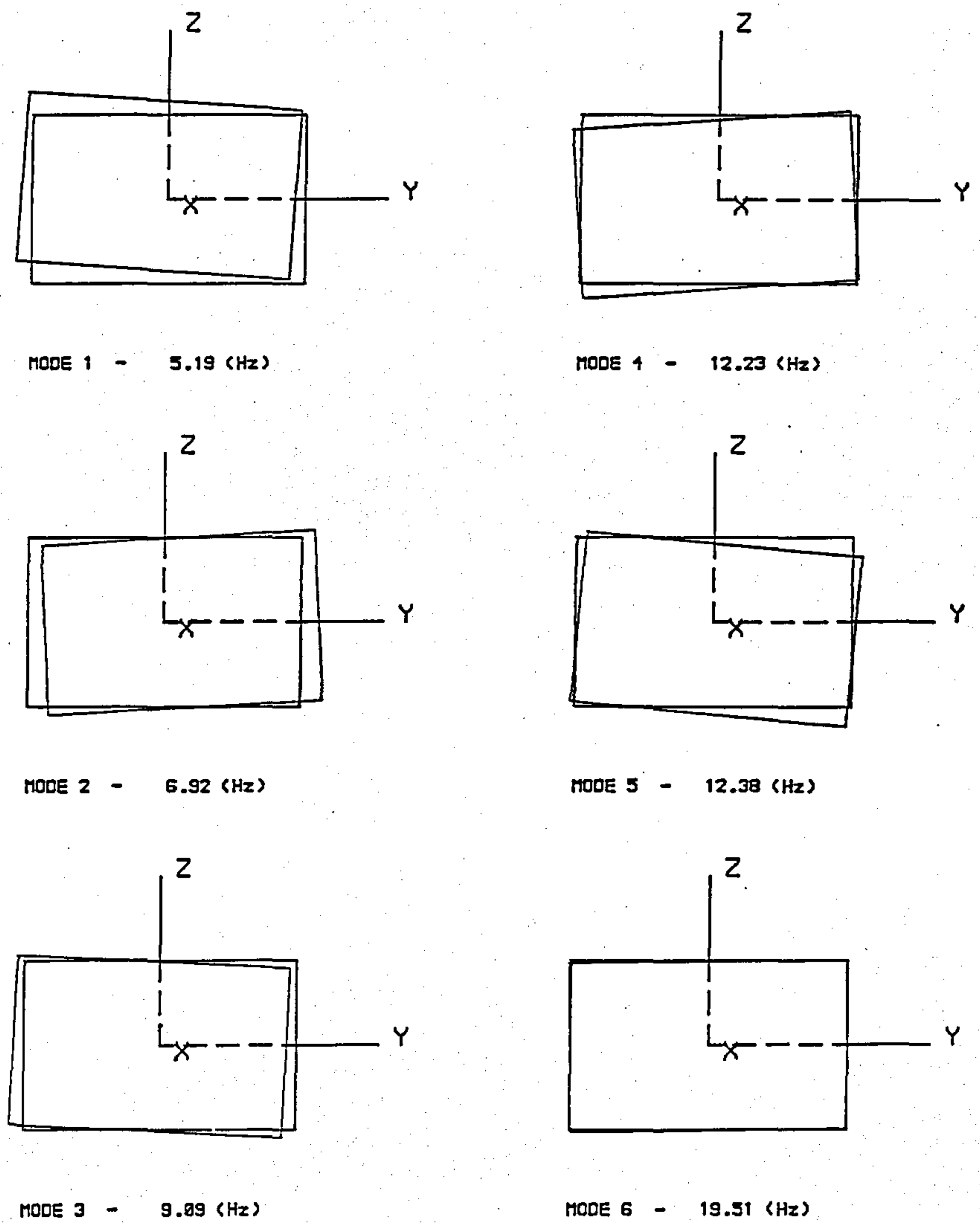


Fig. 2.12 Mode shapes (Ford diesel 1.6 litre engine)

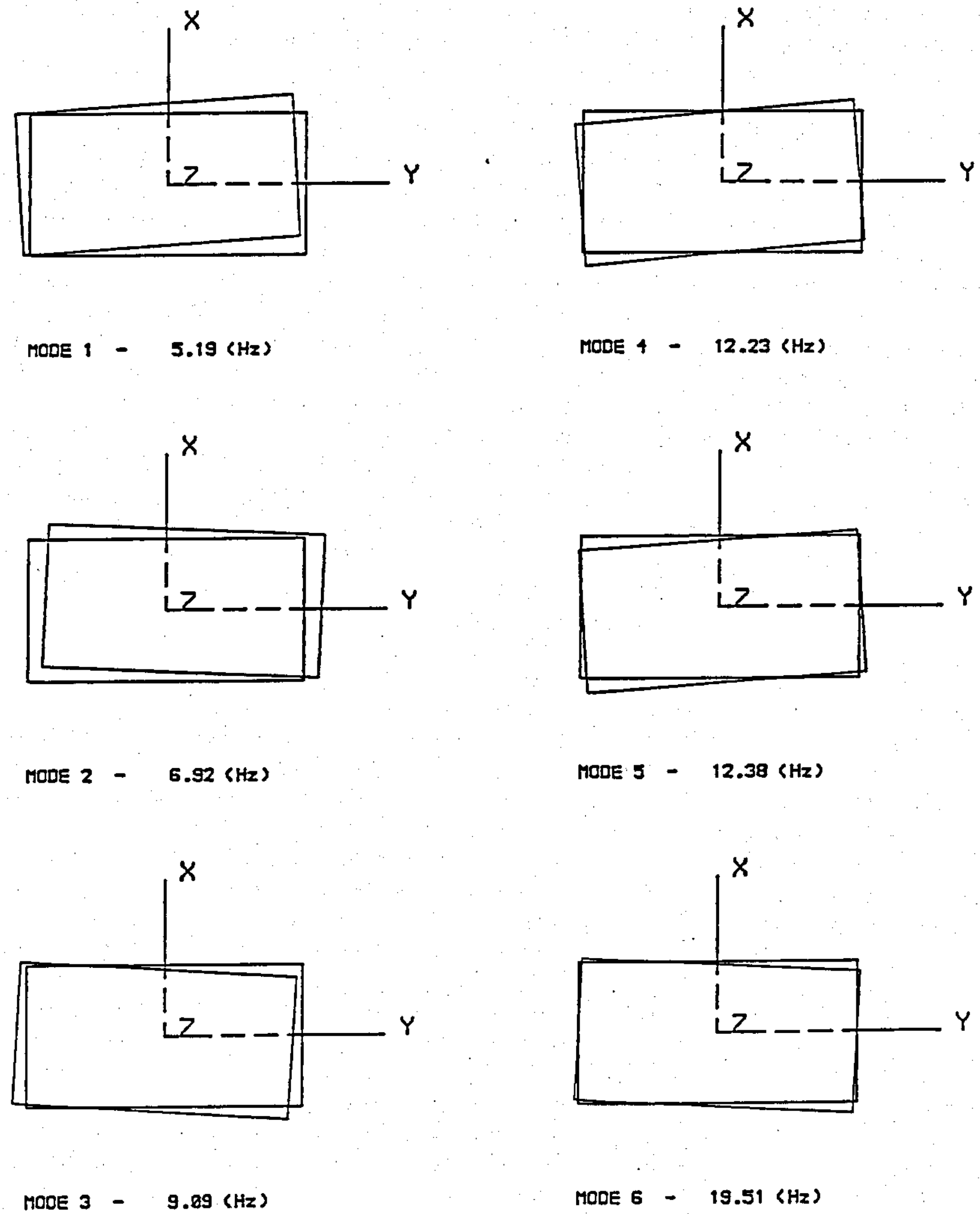


Fig. 2.13 : Mode shapes (Ford diesel 1.6 litre engine)

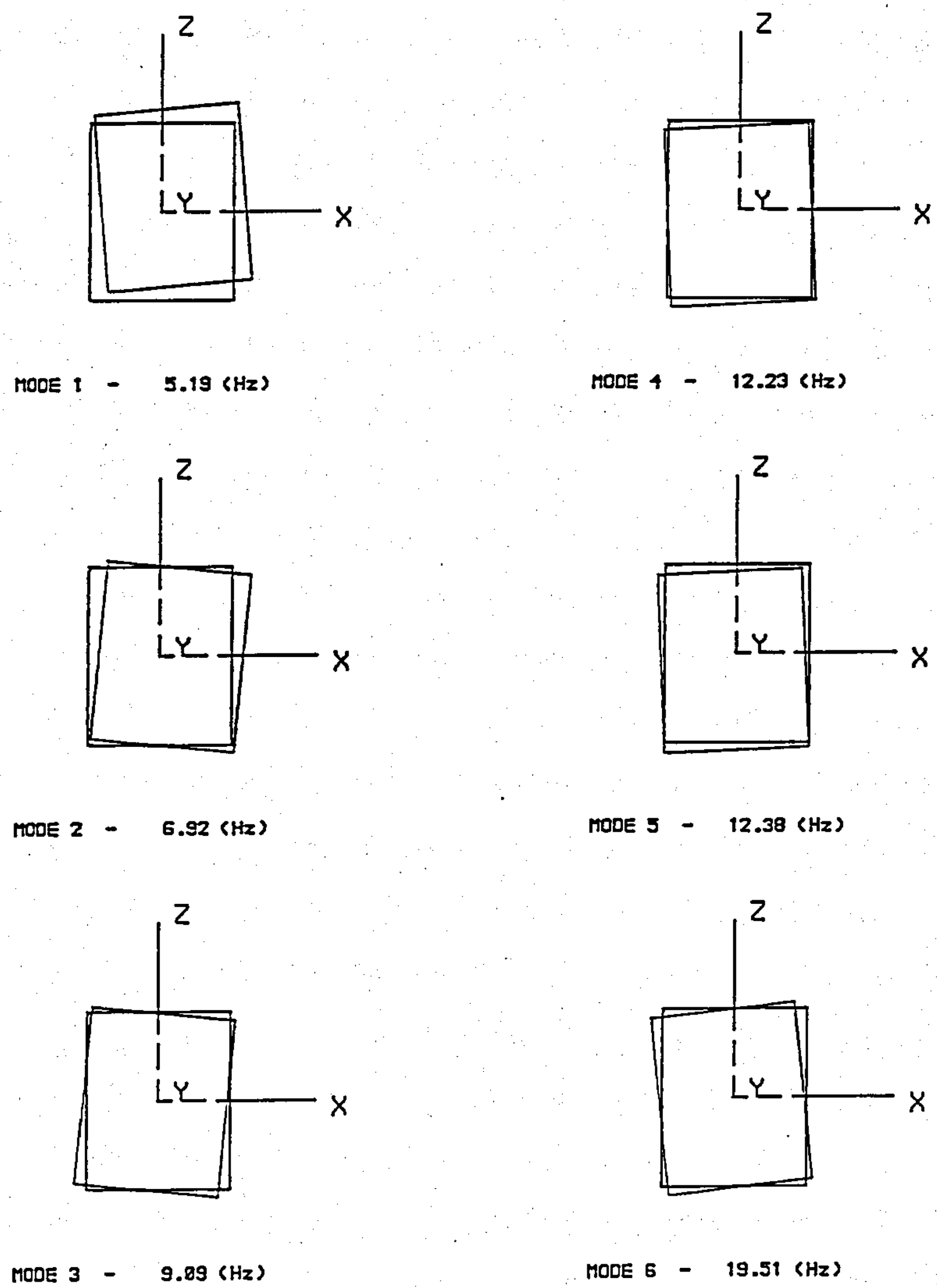


Fig. 2.14: Mode shapes (Ford diesel 1.6 litre engine)

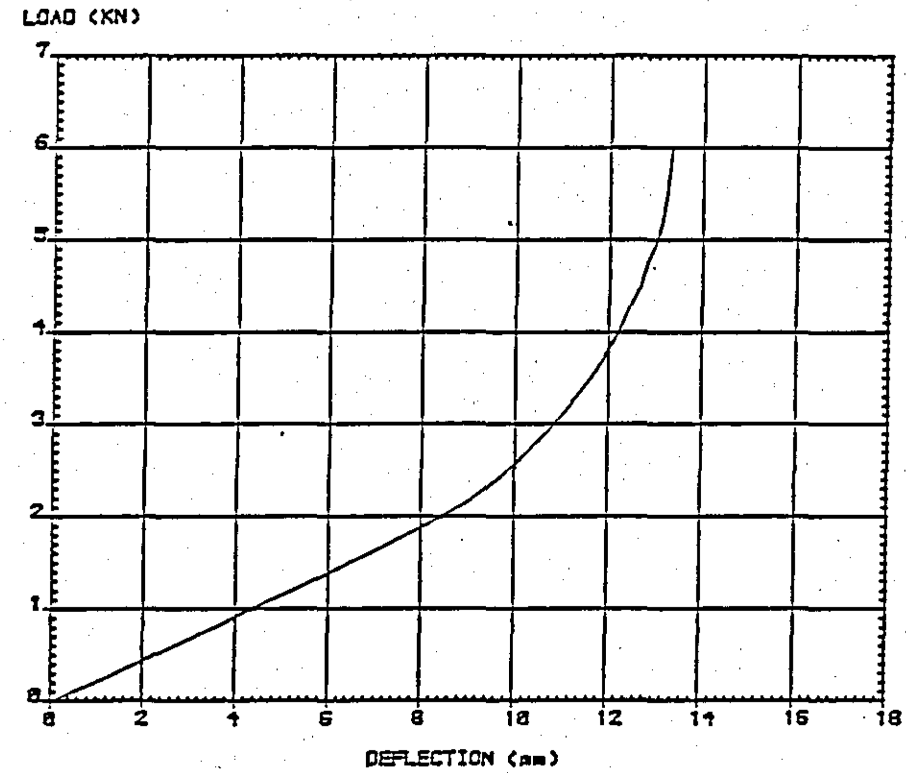


(a)

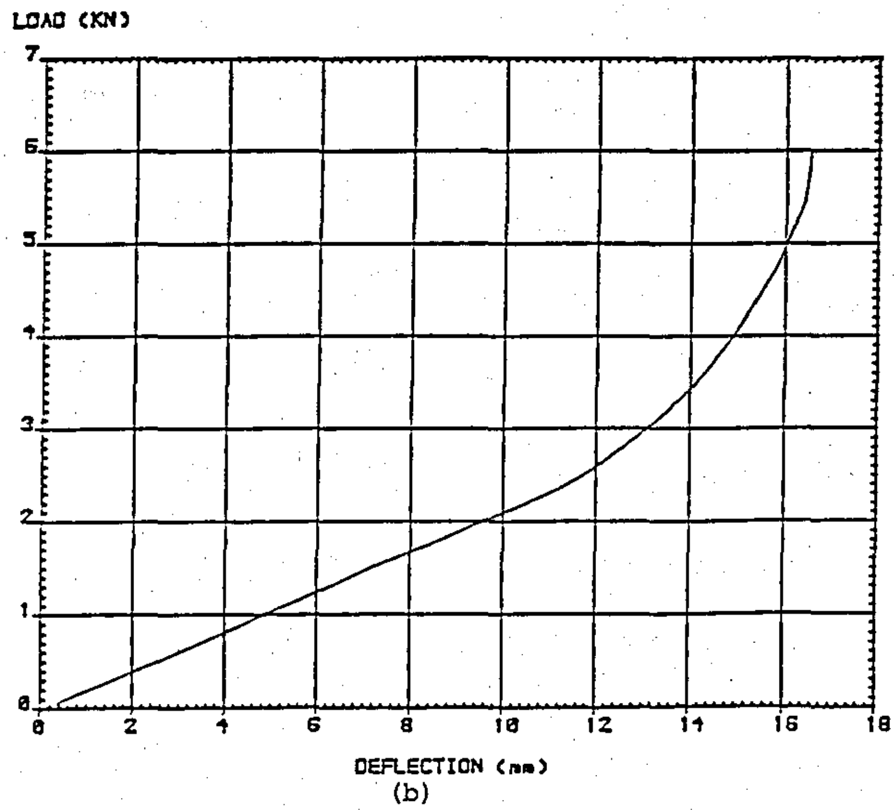


(b)

FIGURE 2.15: ISOLATOR LOAD-DEFLECTION CHARACTERISTICS FOR (a) ISOLATOR NO 2 IN THE X-DIRECTION AND (b) ISOLATOR NO 3 in the X-DIRECTION (see Figure 2.5)

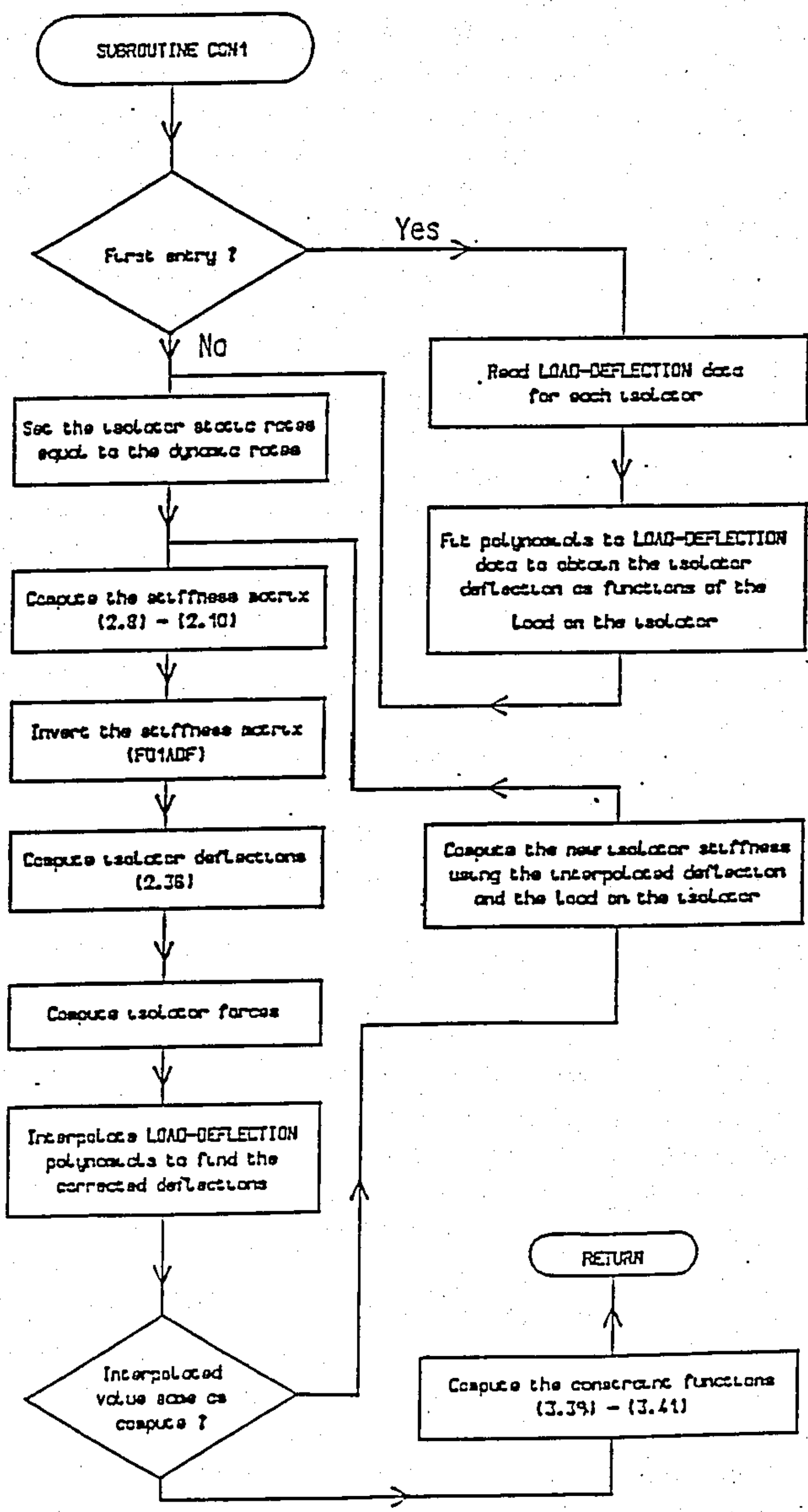


Fig. 2.16: Possible modification of subroutine CON1 to incorporate nonlinear Load-Deflection characteristics

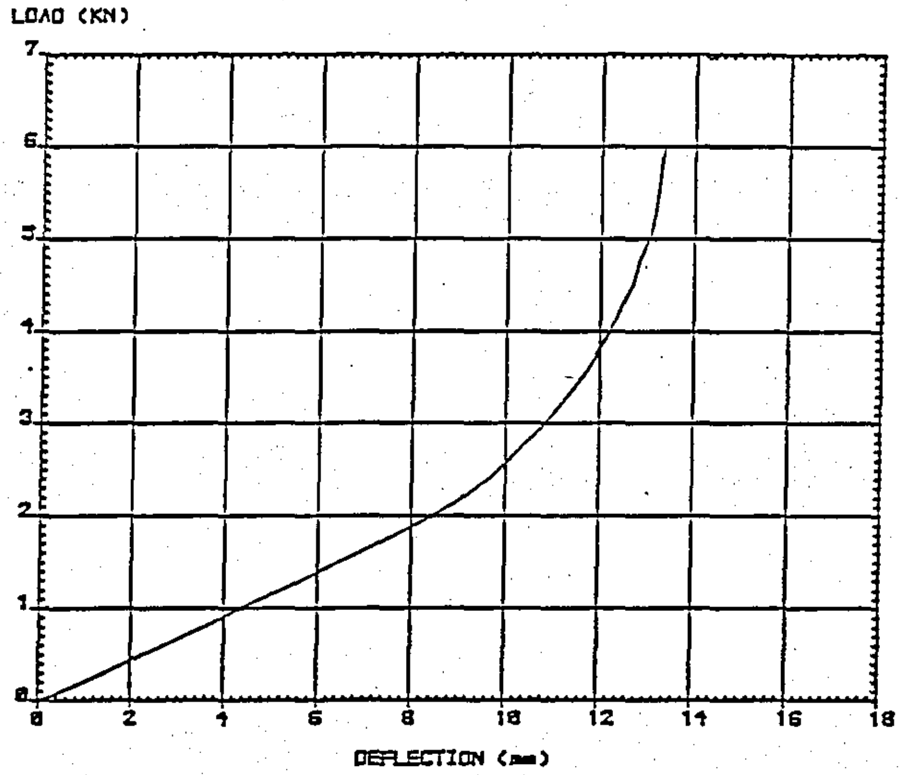


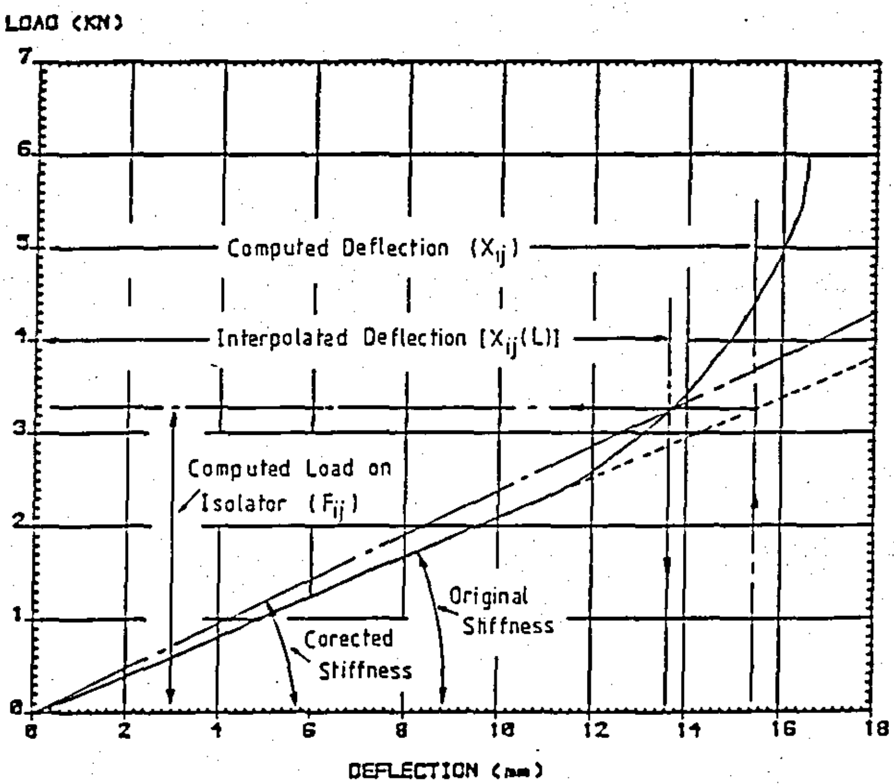


FIGURE 2.17: GRAPHICAL INTERPRETATION OF THE PROPOSED MODIFICATION TO SUBROUTINE CON1 (shown in Figure 2.16)

# CHAPTER 3

## NUMERICAL OPTIMIZATION

Numerical optimization can be "loosely" defined as that numerical procedure that seeks optimal values of design variables which minimize or maximize a specific quantity termed the objective function while satisfying a variety of conditions that define acceptable values of the variables, termed constraints. Numerical optimization methods are reported by Ragsdell [19] to have been born of the logistical needs of World War II and the work of George Dantzig on linear programming. Early numerical optimization methods, such as the well known simplex method, could only address problems where all the functions involved were linear combinations of the design variables and consequently could not satisfy all demands as most problems are nonlinear and many of these cannot be accurately approximated by linear functions. Numerical algorithms that can deal with nonlinear problems have been developed since the late 1950's and have been used in numerous industrial applications ranging from structural designs to economics. Recent developments and applications of numerical optimization algorithms, including numerous references, have been edited by Lev [20] and cover the period 1972-1980.

Background reading by the author of this thesis on optimization literature has created the impression that modern numerical optimization algorithms are either developed on the principle that the design space is searched for the optimum solution by some directed search method or on the principle that the design space is searched in a random way (Monte Carlo method). It has been argued [9] that the main advantage of optimization algorithms developed on the latter principle is that there is less chance of missing the global minimum, due to the random search process. However, methods based on "search directions" have been found to be more widely used both in Europe and in the United States. Such methods can be classified into two groups, namely transformation methods, which transform the nonlinear constrained problem into a series of nonlinear unconstrained subproblems and linearization methods which solve a linear approximation of the nonlinear constrained problem.

In the following sections of this chapter a brief explanation of the general optimization problem will be presented and the objectives for the investigation of optimum isolation systems for reciprocating engines will be developed. Finally the transformation type numerical algorithm, used to perform the optimization and troublesome numerical areas associated with it, will be discussed.

## 3.1 THE GENERAL OPTIMIZATION PROBLEM

In mathematical terms the general constrained optimization problem can be stated as follows:

$$\begin{aligned}
&\text{minimize} && f(x),\ X^T = [x_1, x_2, \ldots, x_N] \varepsilon R^N \\
&\text{subject to:} && l_i \leqslant x_i \leqslant u_i, \quad i = 1, 2, \ldots, N \\
& && c_j(x) \geqslant 0, \quad j = 1, 2, \ldots, J \\
& && h_k(x) \equiv 0, \quad k = 1, 2, \ldots, K
\end{aligned} \tag{3.1}$$

where $f(x)$ is the objective, a function of the design variables $x_i$; $c_j(x)$, $h_k(x)$ are the inequality and equality constraint functions respectively and $l_i$, $u_i$ are the lower and upper bounds respectively on the design variables.

The n-dimensional space $R^N$, formed by the set of all vectors X closed with respect to linear combination, is divided into two subspaces which constitute the feasible and infeasible regions of the design space. Within the feasible subspace of $R^N$, all vectors X satisfy the constraints and consequently such vectors are feasible solutions to

(3.1). However, if $X^*$ is an optimum solution then it can be shown that in addition to (3.1) $X^*$ must satisfy various other conditions known as optimality conditions.

Sufficient conditions for $x^*$ to be a strong local minimum of the general constrained problem will next be discussed during an introduction to optimality conditions for multivariate functions. The derivation of these conditions is extensively discussed by various authors such as Gill, Murray and Wright [21] and Luenberger [22] to name but two articles and involves complicated mathematical analysis which is beyond the scope of this work. However, for the purpose of this thesis, a greatly condensed explanation of the theory will suffice, and what is presented here is drawn mainly from [21].

Consider first the unconstrained minimization problem of a multivariate function defined as:

$$\text{Minimize} \qquad f(x), \quad x \in R^N \tag{3.2}$$

Since there are no constraints, then the entire design space $R^N$ is feasible. If $x^*$ is a local minimum of $f(x)$ then the function must be stationary at $x^*$ and must also display positive curvature. Following reference [21], $f(x)$ is assumed to be twice continuously differentiable and consequently it can be approximated by a Taylor expansion about $x^*$ given as:

$$f(x^* + \varepsilon p) = f(x^*) + \varepsilon p^T g(x^*) + \frac{1}{2}\varepsilon^2 p^T G(x^* + \varepsilon\theta p)p \tag{3.3}$$

where $\theta$ satisfies $0 \leq \theta \leq 1$, $\varepsilon$ is a positive scalar and p is an n-dimensional vector ($p \varepsilon R^N$). The vector $g(x^*)$ is the vector of first partial derivatives of the function at the point $x^*$ given as

$$g(x^*)^T = [\frac{\partial f}{\partial x_1}, \frac{\partial f}{\partial x_2}, \ldots, \frac{\partial f}{\partial x_n}](x^*) \tag{3.4}$$

and $G(x^*)$ is the nxn Hessian matrix of $f(x^*)$ composed of the second partial derivatives of $f(x^*)$ as:

$$G(x^*) = \begin{bmatrix} \frac{\partial^2 f}{\partial x_1^2} & \frac{\partial^2 f}{\partial x_1 \partial x_2} & \cdots & \frac{\partial^2 f}{\partial x_1 \partial x_n} \\ \vdots & & & \vdots \\ \frac{\partial^2 f}{\partial x_1 \partial x_n} & \frac{\partial^2 f}{\partial x_2 \partial x_n} & \cdots & \frac{\partial^2 f}{\partial x_n^2} \end{bmatrix} \tag{3.5}$$

reductio ad absurdum

Using equation (3.3) and a series of contradictory arguments, it is shown in [21] that the sufficient conditions for $x^*$ to be a strong local optimum of f are:

$$\begin{gathered} ||g(x^*)|| = 0 \\ G(x^*) \text{ is positive definite} \end{gathered} \tag{3.6}$$

where $||\cdot||$ denotes a vector norm. If the first condition of (3.6) is satisfied then by definition of a vector norm, $g(x^*)$ must be the zero vector and hence $x^*$ is a stationary point. However, if the Hessian matrix is positive definite then for any n-dimensional vector p it holds that $p^T G p > 0$ and consequently $x^*$ is a local optimum as it can be deduced from equation (3.3). From equations (3.6) and (3.2) it follows that the optimum can be any point x, $x \in R^N$ which satisfies equations (3.6).

If constraints are introduced so that the optimization problem becomes that defined by equations (3.1) then it can be shown that there exists x, $x \in R^N$, which satisfies equations (3.6) but does not satisfy the constraint functions.

The set of all vectors $\mathbf{x}$, $\mathbf{x} \epsilon R^N$ which satisfy the constraints, define~~s~~ the subspace of feasible solutions to equations (3.1). For the derivation of the optimality conditions for the general optimization problem it is necessary to consider means for characterizing the set of feasible points in a neighbourhood of a feasible point i.e. a point $\mathbf{x} \epsilon R^N$ that satisfies all the functional constraints. Luenberger [22] argues that a fundamental concept that simplifies the required theoretical development is that of an active constraint. An inequality constraint $C_j(\mathbf{x}) \geqslant 0$ is said to be active at a feasible point $\mathbf{x}$ if $C_j(\mathbf{x}) = 0$ and inactive at $\mathbf{x}$ if $C_j(\mathbf{x}) > 0$. By convention then, any equality constraint $h_k(\mathbf{x})$ is active at any feasible point. The significance of the active constraints is that their presence restricts feasible perturbations about a feasible point. This is graphically illustrated in Figure 3.1 where $C_1(\mathbf{x})$, $C_2(\mathbf{x})$ and $C_3(\mathbf{x})$ are inequality constraints and the feasible region is that enclosed by the curves $C_i(\mathbf{x}) = 0$, $i = 1, 2, 3$. If $\mathbf{x}^*$ is a local optimum, it is obvious from Figure 3.1 that local properties satisfied at $\mathbf{x}^*$ do not depend on the inactive constraints $C_2$, $C_3$.

Following ~~the~~ reference [21], consider first the case when all the constraints are linear functions of the design variables and let $\hat{A}$ denote the matrix, whose $i^{th}$ row contains the coefficients of the $i^{th}$ active constraint at the feasible point $\hat{\mathbf{x}}$. Due to the linearity of the constraints, the properties of linear subspaces can be used to define all feasible directions of search from a feasible point. It can be shown that the sufficient condition for $\mathbf{p}$ to be a step from any feasible point to any other feasible point can be expressed as:

$$\hat{A}\,\mathbf{p} = 0 \tag{3.7}$$

It will later be illustrated that even if only one of the constraints is nonlinear, then it is more complicated to characterize feasible perturbations and that in fact there is no feasible direction $\mathbf{p}$ along which feasibility can be retained.

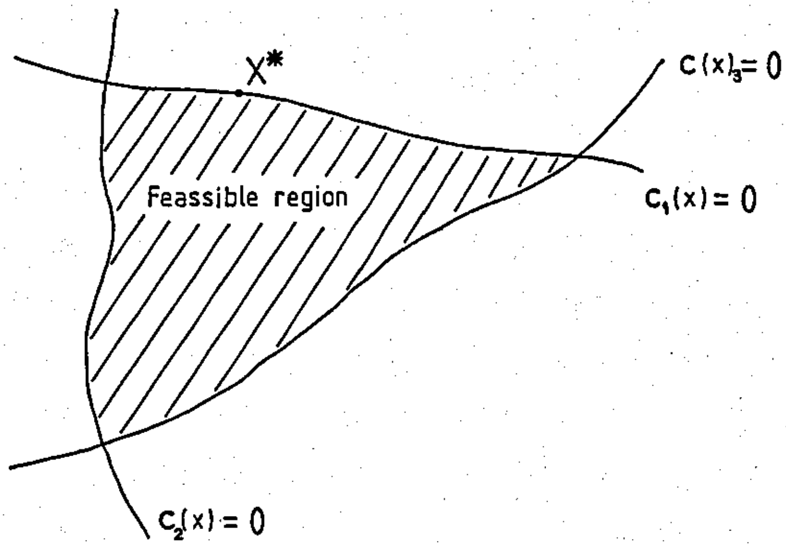


FIGURE 3.1: EXAMPLE OF ACTIVE AND INACTIVE CONSTRAINTS

Continuing the discussion on linear constraints, if **Z** denotes the matrix, the columns of which form the basis for the subspace of all feasible vectors **p** defined by equation (3.7) then any vector **p** satisfying it can be written as a linear combination of the columns of Z i.e. $\mathbf{p} = Z\,\mathbf{p}_Z$ for some vector $\mathbf{p}_Z$. If $\mathbf{x}^*$ is a feasible point then the Taylor expansion of $f(\mathbf{x})$ about $\mathbf{x}^*$ along such direction is given as:

? which is feasible

$$f(\mathbf{x}^* + \varepsilon Z\,\mathbf{p}_Z) = f(\mathbf{x}^*) + \varepsilon \mathbf{p}_Z^T Z^T g(\mathbf{x}^*) + \frac{1}{2}\varepsilon^2 \mathbf{p}_Z^T Z^T G(\mathbf{x}^* + \varepsilon\theta\,\mathbf{p}) z\,\mathbf{p}_Z \qquad (3.8)$$

where $\varepsilon$, $\theta$ are defined as before. The vector $Z^T g(\mathbf{x}^*)$ is termed the projected gradient of $f(\mathbf{x})$ at $\mathbf{x}^*$ and the matrix $Z^T G\, Z$ the projected Hessian of $f(\mathbf{x})$ at $\mathbf{x}^*$.

If $\mathbf{x}^*$ is a local minimum of $f(\mathbf{x})$ then it follows from equation (3.8) that $\mathbf{p}_Z^T Z^T g(\mathbf{x}^*)$ must vanish for every $\mathbf{p}_Z$ and that the projected Hessian must be positive definite (i.e. $f(\mathbf{x}^*)$ must display positive curvature at $\mathbf{x}^*$). The first condition implies that

$$Z^T g(x^*) = 0 \qquad (3.9)$$

which further implies that $g(x^*)$ must be a linear combination of the rows of **A** i.e.

$$g(x^*) = \hat{A}^T \lambda^* \qquad (3.10)$$

for some vector $\lambda^*$, termed the vector of Lagrange multipliers and which is unique only if the rows of $\hat{A}$ are linearly independent. The $j^{th}$ Lagrange multiplier ($\lambda_j$) is a first order indication of the change in $f(x)$ which would result from a positive step along a perturbation **p** such that:

$$\hat{a}^T p > 0$$

$$\hat{a}_i^T p = 0 \;\forall\; i \neq j$$

where $\hat{a}_i^T$ is the $i^{th}$ row of the matrix $\hat{A}$ (see equation (3.7)).

The sufficient optimality conditions for the linearly constrained problem can be expressed as:

$$C(x^*) \geqslant 0 \quad \text{and} \quad \hat{A}\, x^* = 0$$

$$Z^T g(x^*) = 0 \quad \text{or equivalently } g(x^*) = \hat{A}^T \lambda^*$$

$$\lambda_i^* > 0, \; i = 1, 2, \ldots, t$$

(where t is the number of active constraints) and $$Z^TG(x^*)Z \text{ is positive definite.}$$

If the $j^{th}$ Lagrange multiplier is negative, then it means that a positive step along a non-binding perturbation (i.e. $\hat{\underline{a}}_j^T\, p > 0$) with respect to the $j^{th}$ active constraint will reduce the objective function and hence $x^*$ cannot be optimum. However, if $\lambda_j = 0$ then no indication is given about the change in f(x) which will result by such perturbation and consequently extra restrictions are required on the Hessian matrix to ensure that f(x) displays positive curvature along such perturbations.

Consider now the case when one or all of the constraints are nonlinear. The problem that arises is that in general there is no feasible direction p such that $\hat{C}_i(\hat{x} + \alpha\; p) = 0$ holds for all sufficiently small$|\alpha|$. If feasibility is to be retained with respect to $\hat{C}_i = 0$ then it will be necessary to move along a feasible arc with origin at $x^*$. Further if $\hat{C}_i$ is to remain identically zero for all points on the arc then the rate of change of $\hat{C}_i$ along the arc must be zero at $x^*$. If p is a tangent to a feasible arc for all constraints, then it can be shown that

$$\hat{A}(x^*)p = 0 \tag{3.12}$$

where $\hat{A}(x^*)$ is the Jacobian matrix of the constraints i.e. the matrix whose $i^{th}$ row is the gradient vector of the $i^{th}$ constraint. However, if equation (3.12) holds, it does not follow that p is a tangent to a feasible arc and it can be shown that the condition of equation (3.12) is sufficient only if the matrix $\hat{A}(x^*)$ possesses full row rank, i.e. when the gradients of the active constraints at $x^*$ are linearly independent.

Due to the fact that the matrix $A(x^*)$ is not constant, a constant basis for the feasible subspace cannot be defined. The matrix Z is now defined as the matrix whose columns form a basis for the set of vectors orthogonal to the rows of $\hat{A}(x^*)$ at $x^*$ and is denoted $Z(x^*)$. Although first order optimality conditions can be easily derived by arguing that the function must be stationary at $x^*$ along any feasible arc, giving the necessary condition as

$$g(x^*)p = 0 \tag{3.13}$$

where $p$ satisfies equation (3.12), the derivation of second order optimality conditions is more complicated as it requires information about the constraint curvature at $x^*$. However, if equation (3.13) holds for every $p$ that satisfies equation (3.12) then it follows that

$$Z(x^*)\ g(x^*) = 0 \tag{3.14}$$

must be true, or equivalently

$$g(x^*) = \hat{A}(x^*)^T \lambda^* \tag{3.15}$$

for some vector $\lambda^*$ of Lagrange multipliers. Again following [21] consider now the Lagrangian function defined as

$$L(x, \lambda) = f(x) - \lambda^T \hat{C}(x) \tag{3.16}$$

Equation (3.15) states that $x^*$ is a stationary point of the Lagrangian when $\lambda = \lambda^*$. Based on this property and for reasons of convenience, the second order optimality conditions can be derived by analysing the Lagrangian function and seeking conditions for $f(x^*)$ to display non-negative curvature at $x^*$ along any feasible arc. If $W(x, \lambda)$ denotes the Hessian of the Lagrangian function then the sufficient optimality conditions for the nonlinear constraint problem are:

$$C(x^*) \geqslant 0 \text{ with } \hat{C}(x^*) = 0$$

$$Z(x^*)^T g(x^*) = 0 \quad \text{or equivalently } g(x^*) = \hat{A}(x^*)^T \lambda^*$$

$$\lambda_i^* > 0 \quad i = 1, 2, \ldots, t \quad \text{and}$$

$$Z(x^*)^T W(x^*, \lambda^*) Z(x^*) \text{ is positive definite.}$$

Again if any Lagrange multiplier is zero then extra restrictions must be applied to the Hessian to ensure that $f(x)$ displays positive curvature along any feasible arc $p$, for which equation (3.12) holds for all constraints associated with positive Lagrange multipliers but not necessarily so for constraints associated with zero Lagrange multipliers.

Although this brief presentation has by no means covered all aspects of the derivation of optimality conditions for the general optimization problem, it is believed that the main concepts involved have been introduced sufficiently for the purpose of this work. What will follow is a short explanation of a method which attempts to compute the optimum solution to the general optimization problem of equation (3.1) when nonlinear constraints are present. In general optimization methods are iterative and involve the solution of two main subproblems, namely the computation of a feasible direction of search from a current estimate of the optimum and the computation of the step length along such direction that will give a "better" approximation of the optimum. A model algorithm is shown in the flow diagram of Figure 3.2.

However, as was previously discussed when nonlinear constraints are present, the computation of a feasible search direction is in general an impossible task, and consequently a method based on feasible directions cannot be directly employed.

Transformation Methods: One approach to solving the nonlinear constrained problem is to construct a function whose unconstrained minimum is either $x^*$ or is related to $x^*$ is a known way. The original problem can then be solved by formulating a sequence of unconstrained subproblems. Such a function can be constructed by augmenting the Lagrangian function defined earlier by equation (3.16).

Gill, Murray and Wright [21] argue that the most popular augmented Lagrangian function is given by

$$L(x, \lambda, \rho) = f(x) - \rho^T \hat{C}(x) + \frac{1}{2} \rho \hat{C}(x)^T \hat{C}(x) \qquad (3.18)$$

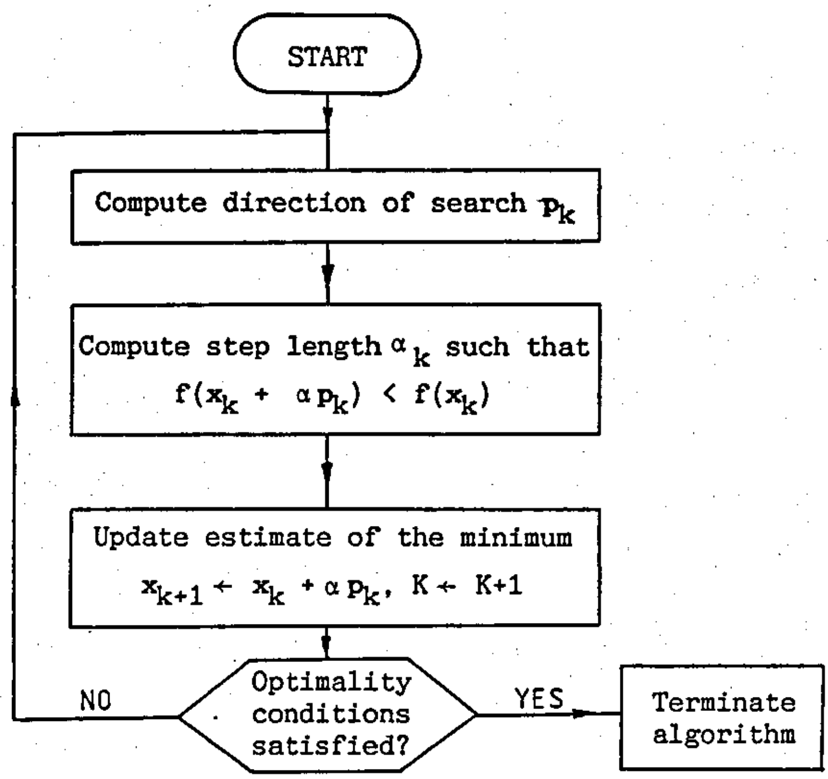


FIGURE 3.2: MODEL OPTIMIZATION ALGORITHM

where $\rho$ is a positive penalty parameter. It can be shown that if $\lambda = \lambda^*$ then $x^*$ is a stationary point of $L(x, \lambda, \rho)$ and that there exists a finite $\bar{\rho}$ such that $x^*$ is an unconstrained minimum of $L(x, \overset{*}{\lambda}, \rho) \forall \rho > \bar{\rho}$. The theory of augmented Lagrangian methods is beyond the scope of this work and it will not be further discussed. However, practical experience with this particular function will be discussed later in an attempt to give an interpretation of the various terms involved in equation (3.18).

Having defined the unconstrained subproblem a direction of search method, such as the one which will now be discussed, can be used to obtain the unconstrained minimum.

<u>Newton's Method</u>: This is an iterative procedure that attempts to which converge to the local minimum of the unconstrained problem defined earlier by equation (3.2), and is based on a local quadratic approximation of the objective function about the current approximation of the minimum. Assuming that the function is twice continuously differentiable then a Taylor expansion about the current point $x_k$ is given as:

$$f(x_k + p) \approx f(x_k) + g(x_k)^T p + \frac{1}{2} p^T G(x_k) p \tag{3.19}$$

The computation of the search direction p is implemented by seeking a vector p which minimizes the right hand side of equation (3.19) i.e. by finding the stationary point of

$$\phi(p) = g(x_k)^T p + \frac{1}{2} p^T G(x_k) p \tag{3.20}$$

This requires the solution of the linear system of equation

$$G(x_k)\ p_k = -\ g(x_k) \tag{3.21}$$

According to reference [21] equation (3.21) defines the Newton method and the vector p so computed is termed Newton's direction. If $G(x_k)$ in equation (3.20) is positive definite and consequently the quadratic model has a unique minimum, then equation (3.21) guarantees that $p_k$ is a descent direction since

$$g(x_k)^T p_k = -g(x_k)^T \; G^{-1}(x_k) \; g(x_k) < 0.$$

Further if the condition number of $G(x_k)$ $(\mathrm{cond}(G(x_k)) = \| G(x_k) \| . \| G^{-1}(x_k) \|)$ is uniformly bounded for all k then a globally convergent algorithm can be developed by taking a step $\alpha_k$ along the Newton direction defined by equation (3.21). A practical definition for $\alpha_k$ is that the slope of the function at $x_k + \alpha p_k$ is sufficiently reduced from that at $x_k$ i.e.

$$|g(x_k + \alpha p_k)^T \, p_k| \leqslant -\, \eta g(x_k)^T \, p_k \tag{3.22}$$

where $\eta$ specifies the accuracy with which $\alpha_k$ approximates a stationary points of $f(x)$ along $p_k$ and $0 \leqslant \eta < 1$. If $G(x_k)$ is not positive definite then the quadratic model function defined by equation (3.19) might not have a minimum nor even a stationary point. This situation could arise when $x_k$ is a saddle point and $G(x_k)$ is indefinite.

According to reference [21], modified Newton methods construct a "related" positive definite matrix $\overline{G}_k$ when $G(x_k)$ is indefinite and then solve equation (3.21) using $\overline{G}_k$ instead of $G(x_k)$. One method to determine whether $G(x_k)$ is positive definite is based on a modified Cholesky factorization giving $\overline{G}_k$ as

$$\overline{G}_k = L \, D \, L^T = G(x_k) + E \tag{3.23}$$

$s[\overline{G}_k] = 0$ suffices if no zero occur on diag of $\overline{G}_k^{\Delta}$.

where L is unit lower-triangular, D is a positive diagonal matrix and E is a non-negative diagonal matrix, which is identically zero when $G(x_k)$ is positive definite.

The main advantage of Newton-type methods is that they use curvature information given by the Hessian matrix to build a local quadratic model of f(x) at the current iteration step. For a general nonlinear function such methods converge quadratically to $x^*$ if the starting point is sufficiently close to $x^*$, the Hessian matrix is positive detinite at $x^*$ and $\alpha_k$ converges to unity. However, in practice, modified Newton methods are used for greater computational efficiency.

Quasi-Newton Methods: In contrast to Newton-type methods where all curvature information is computed at a single point, these use the observed behaviour of f(x) and its gradient vector g(x) to build up curvature information as the iteration of a descent method proceeds. An approximation $B_k$ to the Hessian $G(x_k)$ is maintained and updated at each iteration, which [21] is performed using the relation:

$$B_{k+1} = B_k + \frac{y_k\, y_k^T}{\alpha_k y_k^T p_k} + \frac{g_k\, g_k^T}{g_k^t\, p_k} \tag{3.24}$$

where $y_k = g_{k+1} - g_k$. In practice however, a Cholesky factorization of $B_k$ is kept and updated and the search direction is computed by equation (3.21).

## 3.2 FORMULATING THE ENGINE ISOLATION PROBLEM

In this section the objective function and the constraints for the investigation of optimum engine isolation systems will be derived and formulated according to the definition of the general optimization problem given in equation (3.1).

The objective function: Following the decision that the investigation of optimum engine isolation systems will be based on the forced response of a six-degree of freedom rigid engine isolator model, for reasons discussed during the introductory chapter, it was thought sensible that the optimization objective should be to minimize the magnitude of the forces transmitted to the rigid supporting structure. It is clear from the mathematical statement of the general optimization problem that the optimization objective must be expressed in terms of a single function of the design variables,Bearing in mind that the principal reason for using engine isolators is to minimize the transmission of engine generated forces to the vehicle chassis, it seemed reasonable to define the objective function as the sum of the mean square values of the forces over all the isolator local directions and over all the harmonics of the excitation. To derive the analytical expression for this mean square transmitted force, the dynamic displacement vector at the power train mass centre computed by equation (2.29) for the $r^{th}$ harmonic of the excitation is transformed by equation (2.36), after substitution of the static displacement vectors $u^{(s)}$, $v^{(s)}$ by the equivalent dynamic vectors of the power train mass centre, to give the deflection at the $i^{th}$ isolator. The forces on the $i^{th}$ isolator are then computed by the following equation:

$$f_{ij}^{(r)} = k_{ij}\, x_{ij}^{(r)} \tag{2.25}$$

where $f_{ij}^{(r)}$ is the force on the $i^{th}$ isolator in the $j^{th}$ local direction due to the $r^{th}$ harmonic of the excitation

$k_{ij}$ is the stiffness of the $i^{th}$ isolator in the $j^{th}$ local direction

$x_{ij}^{(r)}$ is the deflection of the $i^{th}$ isolator in the $j^{th}$ local direction due to the $r^{th}$ harmonic of the excitation.

The objective function is then expressed as:

$$f(X) = \frac{1}{2} \sum_{r=1}^{m} \left[ \sum_{i=1}^{n} \sum_{j=1}^{6} (k_{ij})^2 \, (x_{ij}^{(r)})^2 \right] \tag{3.26}$$

where **X** is the optimization vector comprised of the design variables; viz, isolator stiffness rates, global position coordinates and orientation Euler angles.

The necessary steps to compute this function for a given set of design variables is illustrated by the flow chart given in Figure 3.3. Although the computation steps are not particularly complex, they do involve a great number of matrix multiplications. During early computer runs the objective function described by equation (3.26) was optimized using an algorithm for unconstrained optimization and it was realised that the objective function was computed at least once for each design variable free from its bounds. The reason for this is attributed to the numerical approximation of the derivatives of the objective function. Further it was observed that a typical optimization run would require a few hundred iterations to converge to the minimum. Bearing in mind that the calculation loop shown in Figure 3.3 is executed for each harmonic of the excitation, it can be appreciated that during a typical optimization run the computer will execute that loop several thousand times. Consequently efforts were made to reduce the computation time of the objective function to a minimum and as a result two alternative definitions of the objective function were considered. The quickest way to compute the objective function, in terms of the forced response, is of course to define it as the mean square displacement at the power train mass centre expressed by equation (3.27) as the sum of the mean square value of the power train mass centre displacements over all global directions and over all the excitation harmonics

$$f(X) = \frac{1}{2} \sum_{r=1}^{n} \sum_{i=1}^{6} |\hat{x}_i^{(r)}|^2 \qquad (3.27)$$

However, this definition was discarded on the grounds that minimizing mean square displacement at the power train mass centre does not necessarily imply force transmission minimization.

The second alternative was to define the objective function as the maximum strain energy stored in the dynamic system as a result of the harmonic excitation. By definition the strain energy of a dynamic system is expressed as

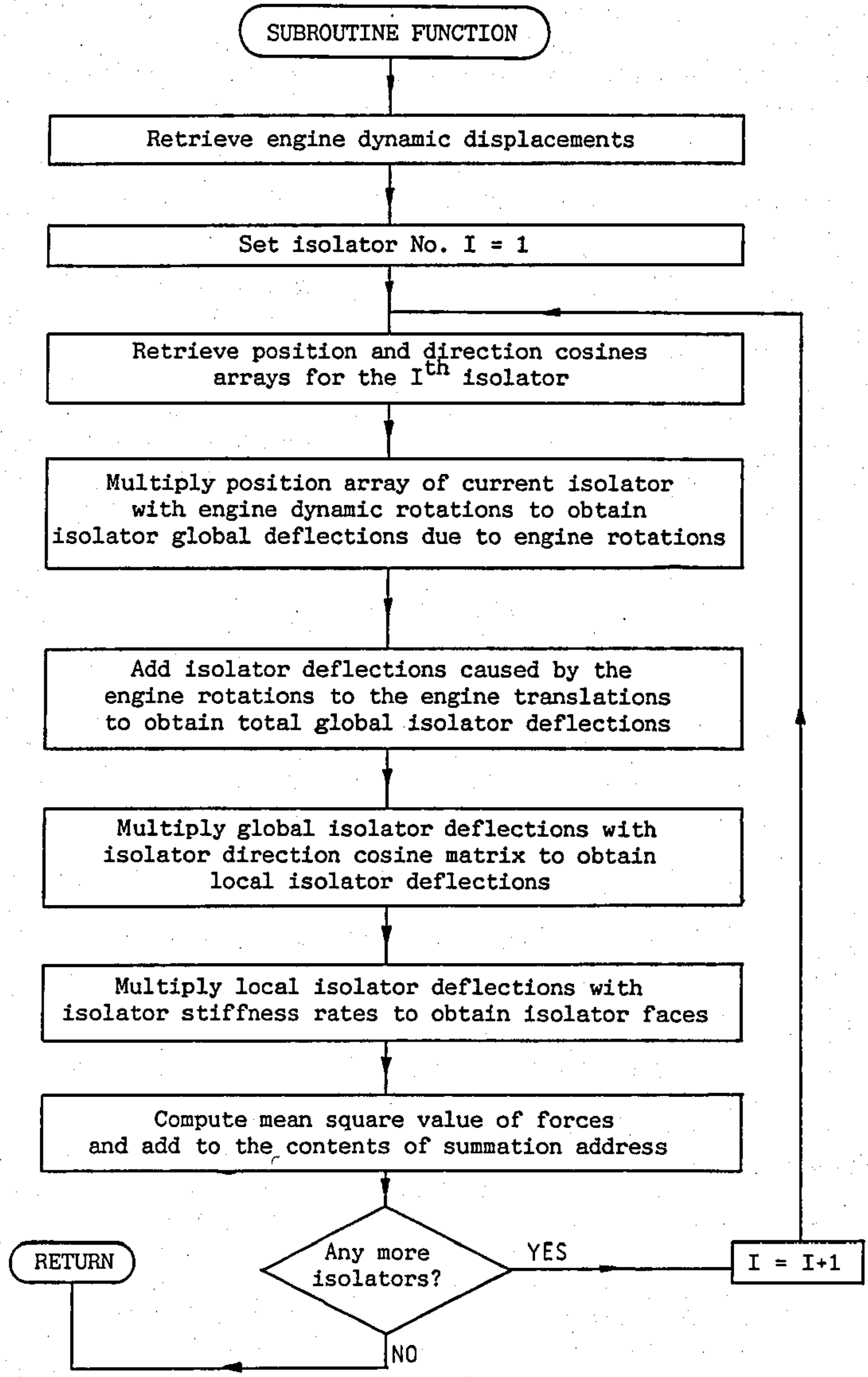


FIGURE 3.3: FLOW CHART FOR COMPUTING MEAN SQUARE FORCE

$$V = \frac{1}{2} \sum_{i=1}^{n} \sum_{j=1}^{n} k_{ij} \; q_i \; q_j \tag{3.28}$$

where $k_{ij}$ is the element in the $i^{th}$ row and $j^{th}$ column of the global stiffness matrix and $q_i$, $q_j$ are the $i^{th}$ and $j^{th}$ generalized coordinates. The objective function is then expressed as

$$f(X) = \frac{1}{2} \sum_{r=1}^{n} [ \sum_{i=1}^{6} \sum_{j=1}^{6} k_{ij} |\hat{x}_i^{(r)}| |\hat{x}_j^{(r)}| ] \tag{3.29}$$

where $|\hat{\underline{x}}_i^{(r)}|$ is the magnitude of the complex displacement at the power train mass centre due to the $r^{th}$ harmonic of the excitation, computed by equation (2.29). It is easy to calculate as may be seen from Figure 3.4 whilst retaining a direct connection with the force transmitted to the supporting structure.

This relationship can be shown by considering the simple oscillator shown in Figure 3.5. The transmitted force can be expressed as:

$$F_T = k \; \hat{x} \tag{3.30}$$

and hence the mean square force is given as:

$$\langle F_T^2 \rangle = k^2 \frac{x^2}{2} \tag{3.31}$$

The time averaged strain energy is given by:

$$\langle V \rangle = \frac{k}{2} \langle x^2 \rangle = \frac{k}{4} x^2 \tag{3.32}$$

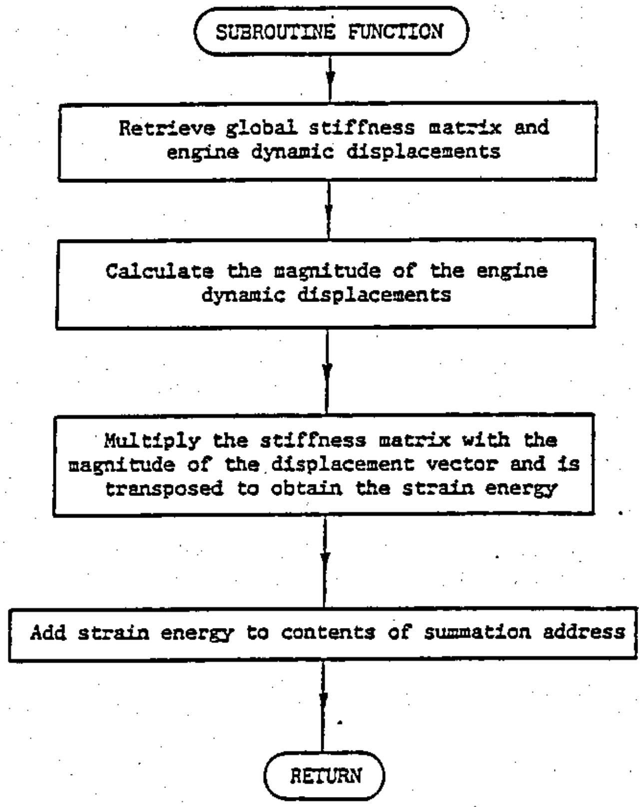


FIGURE 3.4: FLOW CHART FOR COMPUTING STRAIN ENERGY

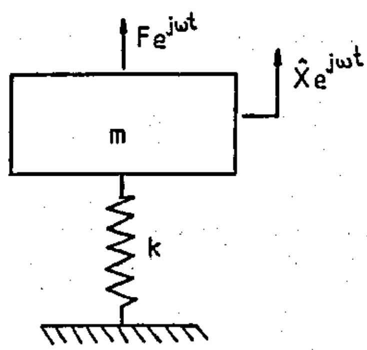


FIGURE 3.5: SINGLE OSCILATOR

and hence the relation between strain energy and transmitted force can be derived form equations (3.31) and (3.32) as

$$\langle F_T^{2} \rangle = 2k \langle V \rangle \tag{3.33}$$

It is quite clear now that using strain energy as the optimization objective, the primary objective of minimizing the forces transmitted to the supporting structure is not violated while comparison of Figures 3.3 and 3.4 clearly suggests that the computation time of the objective function will be reduced considerably.

<u>The constraints:</u> As was discussed during the static analysis of the rigid-engine isolator model presented in the previous chapter, it is desirable to place constraints on the isolator maximum allowable static deflections and power train maximum allowable static rotations. It was further discussed that separation of engine vibration from engine shake is desirable as low frequency road inputs can excite the lower rigid-engine modes. In order to achieve this it would be essential to isolate a particular degree of freedom from the coupled modes of vibration and hence "force" that chosen degree of freedom to be excited within a specified frequency using frequency constraints. Effectively what is required is to identify the modal frequency corresponding to the mode shape in which the chosen degree of freedom dominates the rigid-body response. If a numerical procedure could be used to carry out such identification, every time the eigenvalue problem is solved during optimization, then it would be possible to partially separate engine shake from engine vibration. Total separation could not be achieved with a coupled system as it is highly unlikely that the constrained degree of freedom would not be excited at all the other modal frequencies as it can be appreciated from Table 2.1. Here, for example, it is clear that the vertical degree of freedom is excited in most other modes of vibration. If the mode of vibration where the vertical degree of freedom dominates the response

is constrained within a specified frequency band there is no guarantee that the vertical mode will not be excited outside that frequency band. It can be appreciated now that attempting to separate engine shake from engine vibration using frequency constraints in the way just discussed, the only result will be to increase the computation time with doubtful benefits. A much simpler way to partially solve the problem is to identify the frequency band where the road excitation is expected to interfere with the rigid-engine frequency spectrum and then introduce frequency constraints which will ensure that all the rigid power train modes are beyond that frequency band. spl inf

These frequency constraints, together with the displacement constraints mentioned earlier, fix the general design space which is defined by the upper and lower bounds of the design variables in a feasible and an infeasible subspace. As there is no reason to restrict the optimum solution to lie on the borders between the feasible and the infeasible subspace, all the constraint functions will be of the inequality type and will be formulated as follows.

Let $u_{ij}^{(s)}$ represent the static deflections of the $i^{th}$ isolator in the $j^{th}$ local direction, computed by equation (2.36) and $v_r^{(s)}$ the static engine rotation about the $r^{th}$ global axis computed by equation (2.35). If $C_{ij}$ denotes the maximum allowable value for $v_r^{(s)}$ then the inequality constraint functions can be expressed as

$$C_{i+j}(X) = |C_{ij}| - |U_{ij}^{(s)}| \geqslant 0, \quad i = 1, 2, \ldots, N \qquad (3.34)$$
$$j = 1, 2, 3$$

$$C^{i+j+r}(X) = |C_r| - |V_r^{(s)}| \geqslant 0, \quad r = 1, 2, 3 \qquad (3.35)$$

Similarly if h denotes the minimum allowable value for the rigid engine isolator spectrum ($\omega_n$, $n = 1, 2, \ldots, 6$) then the frequency constraints can be expressed as follows:

$$C_{i+j+r+n}(X) = |\omega_n| - |h_n| \geqslant 0, \quad n = 1, 2, \ldots, 6 \qquad (3.36)$$

Equations (3.29) and (3.34) to (3.36) completely describe the objectives for the investigation of optimum engine isolation systems. What will follow is a description of the numerical algorithm and a discussion of a number of important numerical issues such as local and global minima, numerical accuracy and scaling.

## 3.3 THE NUMERICAL ALGORITHM

Choosing the appropriate routine to solve the optimization problem previously defined, proved to be an easier task than had been anticipated mostly due to the limited range of readily available software. Optimization routines supported at Loughborough University are only those included in the NAG Library which is implemented on both the PRIME and the Honeywell Multics computer systems of the University. The documentation for the optimization routines, supplied by NAG, describes all the algorithms available in the library and users are advised to select the appropriate routine using one of the two available decision trees depending on whether the problem to be solved is of the constrained or unconstrained type. Then the selection of the appropriate routine simply depends on the type of constraint (i.e. simple bounds on the design variables or function constraints) and the availability of analytical expressions for the derivatives of the objective functions with respect to the design variables. expected

The optimization problem defined previously is of the constrained type and further analytical expressions for first and second derivatives of the objective function are impossible to develop. Under these specifications the decision tree for constrained optimization problems pointed to the routine named E04UAF which will be described next.

NAG E04UAF: This procedure uses the augmented Lagrangian function defined earlier by equation (3.18) to transform the general constraint problem into a sequence of "bounds-constrained" subproblems. Once the augmented Lagrangian is constructed using current estimates of the Lagrange multipliers $\lambda$, and the penalty parameter $\rho$, then EO4UAF passes control to NAG subroutine EO4JBF which solves the current "bounds-constrained" subproblem by a quasi-Newton method.

The user is requested to supply three subroutines named FUNCT1, CON1, AMONIT the functions of which are as follows:

FUNCT1: computes the objective function of any **x** set by the NAG routine

CON1: computes the constraints at any **x**

AMONIT is a routine which can be used to monitor the progress of the algorithm.

Subroutines FUNCT1 and CON1 have been discussed in the previous chapter concerned with the dynamic and static analysis of the rigid engine isolator model. However flow charts for all three routines can be found in Appendix D where a description of the whole computer program is presented in terms of fairly detailed flow diagrams. A call to EO4UAF is made by the following statement:

```
CALL EO4UAF (N, MEQ, MINEQ, MRNGE, M, MONAUX, IPRINT, MAXCAL, ETA,
             XTOL, STEPMX, CL, CU, LCLU, IBOUND, XL, XU, LAMSET, X,
             RHO, RLAM, F, C, IW, LIW, W, LW, IFAIL)
```

Although all the parameters involved in the argument are fully explained in the NAG documentation [23], the meaning of some of these is explained below for quick reference purposes.

N - number of independent design variables

MINEQ - number of inequality constraints

M - total number of constraints

MAXCAL - maximum allowable number of function evaluations

ETA - specifies how accurately the minimum of a "cross section" of the augmented Lagrangian function is to be determined (can be related to $\eta$ of equation (3.22))

X - the N-dimensional array containing initial values of the design variables

RHO - is the penalty parameter $\rho$ of equation (3.18)

RLAM - the M-dimensional array containing estimates of the Lagrange multipliers

F - contains the current value of the objective function

C - the M-dimensional array containing the current values of the constraint functions

IFAIL - this is the report flag parameter which is set by the routine before exit to give some indication of the status of the final solution

On entry, EO4UAF checks all the parameters in its argument for consistency and if an error is detected then IFLAG is set to 1 and the algorithm terminates with an error report. Otherwise the algorithm commences by constructing the Lagrangian function defined in equation (3.18). First the inequality constraints are transformed into equality constraints by the addition of slack variables and further bounds. For example the constraint $C_i(x) \geqslant 0$ is replaced by the equality constraint and simple bound:

$$C_i(x) - x_{m+i} = 0 \tag{3.37}$$

$$x_{m+i} \geqslant 0$$

Using current information on the Lagrange multipliers and the penalty parameter $\rho$, the Lagrangian function is then constructed and is passed to EO4JBF where it is minimized subject to bounds on the original and the slack variables.

The main steps of the numerical algorithm are illustrated by the flow chart diagram in Figure 3.6. This brief explanation of the numerical algorithm gives some idea of the numerical procedures involved in the computation of the minimum. Decisions within the algorithm are taken

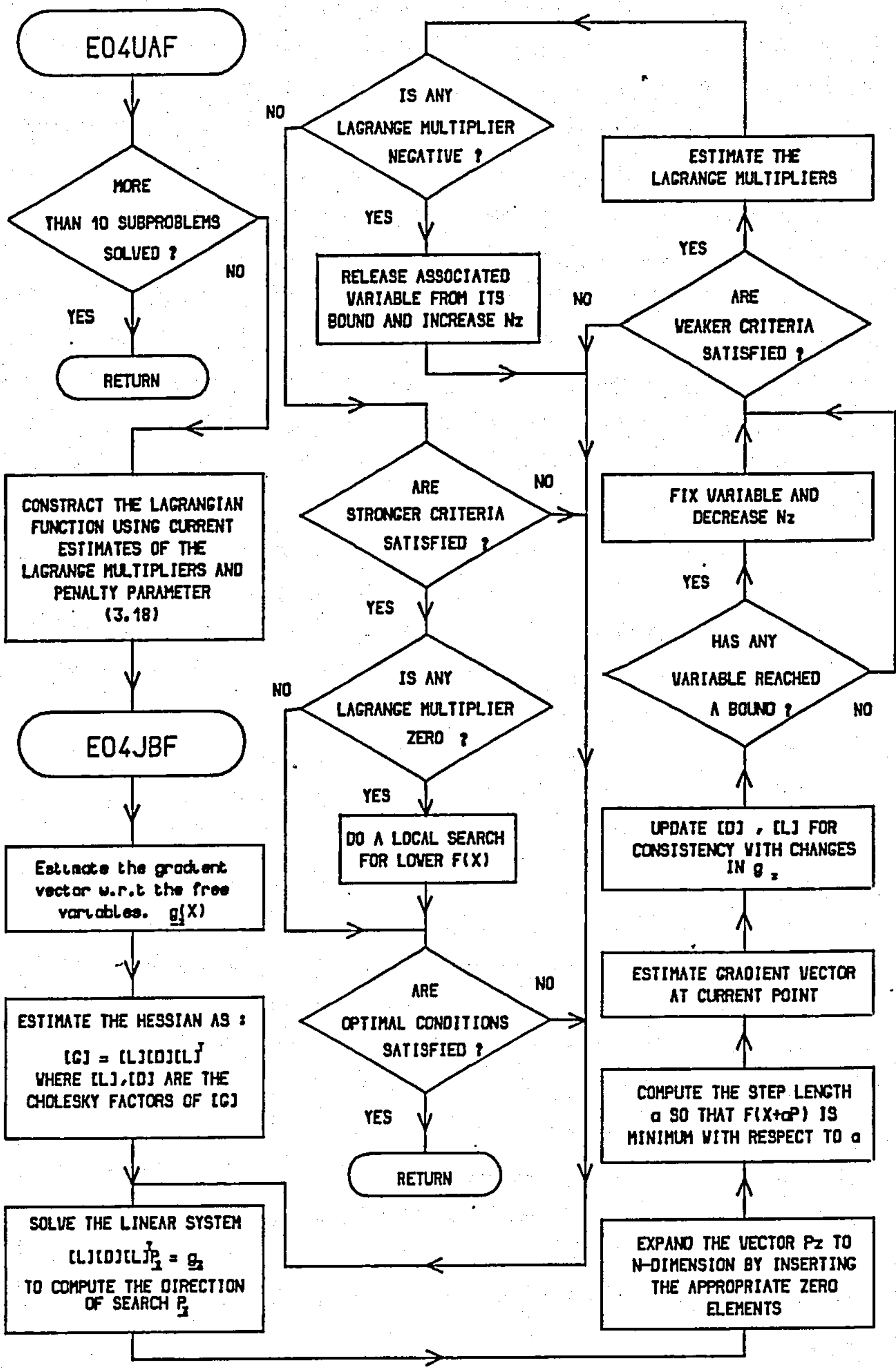


Fig. 3.6 Flow chart of numerical optimization algorithm

by observing numerical changes in key parameters and consequently numerical precision is of vital importance. Further when the problem involves many design variables and constraints it is impossible for the user to construct a geometrical representation for the problem which would help in visually locating undesirable areas or even strong minima. Undesirable areas within the design space are areas where the function surface resembles a "flat valley". Such areas create numerical problems due to the fact that the function undergoes little change by moving along such a "valley" and consequently errors are introduced in the estimate of the gradient vectors, which cause even larger errors in the computation of second derivatives. It can be appreciated that under such conditions the computed directions of search are unlikely to be a direction that will minimize the objective function and consequently the algorithm might get "stuck" or even fail. Unfortunately there is no way to prevent the occurrence of such situations in complex problems nor is there a way to ensure that algorithms of the type described will converge to the global minimum. One common technique used to reduce the chance of serious error is to solve the same problem using many different starting points from which the best solution is chosen (although even such a trial and error kind of approach does not guarantee that the global minimum is not missed).

Apart from the problem mentioned above, there are a number of other numerical problems that can arise and which can be prevented once the sources are established. The nature of such problems as well as possible remedies will next be discussed during an introduction to the importance of "scaling" on the behaviour of the optimization algorithm. which

Scaling is the term used in optimization literature to describe in a vague sense the numerical difficulties associated with optimization algorithms. With respect to scaling, the NAG documentation manual [23] suggests that the user should scale the objective function, the constraints and the design variables in such a way so that:

a) at the solution they all lie in the range [-1, +1] and
b) at points one unit away from the solution $F(\mathbf{x})$ and $c_I(\mathbf{x})$ differ from their values at the solution by approximately one unit.

Unfortunately it is not always possible to follow the above scaling recommendations when dealing with practical problems. Scaling $F(\mathbf{x})$ and $c_I(\mathbf{x})$ so that they are in the range [-1, +1] will not be possible unless the exact range of values of these functions is known from the start. Further it will be extremely difficult to follow recommendation (b) especially when $F(\mathbf{x})$ and $c_I(\mathbf{x})$ are nonlinear functions. However it is possible to scale the design variables so that they are in the range [-1, +1] as their exact range of values (upper and lower limits) are usually specified in practical problems.

Gill, Murray and Wright [21] briefly discuss the reasons for such variable transformations. They argue that numerical problems can arise due to the fact that the design variables involved in practical problems when expressed in physical units will generally have widely varying orders of magnitude or differences in the range of typical values. The main principle of variable transformation is to "map" all the variables to a common numerical range so that numerical changes on the variables can be carried out on a common basis. Consider for example two of the variables involved in the definition of the optimization objective function given earlier by equation (3.29). The stiffness of the isolator will be of the order of $10^6$ N/m while the position of the isolator with respect to the power train mass centre will be of the order of $10^{-1}$m. It can be appreciated that a numerical change of 0.1 to these variables does not reflect equivalent numerical changes. The numerical algorithm must therefore decide in some way what is a reasonable numerical change for each of the variables involved. Even if the variables are of the same order of magnitude the same problem can arise when the range of typical values of the variables involved is substantially dissimilar. Consider, for instance, the case where the variables $x_1$, $x_2$ are constrained as follows:

$$0.1 \leqslant x_1 \leqslant 0.7$$

$$0.1 \leqslant x_2 \leqslant 0.2$$

Although both variables are of the same order of magnitude the variable $x_2$ is much more restricted and consequently a finer numerical change might be more appropriate. Again the numerical algorithm will have to decide what is a reasonable numerical change for each of the variables. However, if the design variables are "mapped" onto the same numerical range by some linear (or otherwise) transformation, then it will be much easier for the numerical procedure to select a reasonable numerical step.

Assuming that the <u>exact</u> bounds of the design variables can be specified, the following transformation relationship is given in [21]

$$y_j = \frac{2x_j}{b_j - a_j} - \frac{a_j + b_j}{b_j - a_j} \tag{3.38}$$

where $x_j$ is the $j^{th}$ original design variable, $y_j$ is the $j^{th}$ transformed design variable and $a_j \leqslant x_j \leqslant b_j$. Obviously the transformed variables $y_j$ are only visible to the optimization routine (E04UAF) while the computation of the objective function is carried out (by FUNCT1) using the original variables. This is achieved by transforming the variables $y_j$ back to physical units (within FUNCT1) using the inverse of equation (3.38) i.e.

$$x_i = \frac{1}{2} [y_j + \frac{a_j + b_j}{b_j - a_j}] (b_j - a_j) \tag{3.39}$$

Equations (3.38) and (3.39) conclude the scaling of the design variables. What remains to be discussed is the scaling of the objective function and the constraints.

Unfortunately scaling these functions is not as straightforward, and indeed it was this part of the problem that consumed most of the author's time. The objective function F(x) and the constraints $c_I(x)$ were scaled on a trial and error basis by observing the behaviour of the numerical algorithm during a series of optimization attempts. Starting these attempts with no scaling whatsoever on F(x) and $c_I(x)$ and by observing intermediate optimization results as well as the final solution it was decided, for reasons which will be discussed in the next chapter, that each of the constraint functions should be multiplied by a constant weighting factor each time these functions are evaluated within CON1. Equations (3.34) to (3.36) were thus modified as follows:

$$c_{i+j}(x) = [|c_{ij}| - |u_{ij}^{(s)}|]\, W_{i+j} \geqslant 0 \quad i = 1, 2, \ldots, N \quad j = 1, 2, 3 \tag{3.40}$$

$$c_{i+j+r}(x) = [|c_r| - |v_r^{(s)}|]\, W_{i+j+r} \geqslant 0, \; r = 1, 2, 3 \tag{3.41}$$

$$c_{i+j+r+n}(x) = [|\omega_n| - |h|]\, W_{i+j+r+n} \geqslant 0, \; n = 1, 2, \ldots, 6 \tag{3.42}$$

where W denotes the weighting factor associated with each constraint. It was further observed that scaling F(x) in a similar way had no visible effects on the behaviour of the numerical algorithm and subsequently the objective function was left unscaled.

Further comments on the effect of scaling and the trial and error approach in choosing "appropriate" weighting factors will be discussed in the next chapter during an extensive discussion of the computer results obtained in an attempt to compute an optimum isolation system for the power train-isolator arrangement which was briefly discussed in the second chapter of this thesis.

# CHAPTER 4

## A CASE STUDY

The previous two chapters developed the required theoretical analysis for the investigation of optimum isolation systems for reciprocating engines. The computer program which reads the data and calls the NAG routine E04UAF to minimize the objective function computed by subroutine FUNCT1 subject to bounds on the design variables and constraints set by subroutine CON1, is named "ENGVIB". The flow chart of ENGVIB can be found in Appendix D with a brief description of the structure of the entire computer program. The structure of the data file required to intialize ENGVIB is also illustrated in this appendix, while the engine-isolator arrangement which is represented by the data is described in Appendix C.

### 4.1 OPTIMIZATION PARAMETERS

From the theoretical analysis previously presented, it will be appreciated that the numerical algorithm can only partially satisfy the complex requirements associated with minimizing the transmission of engine induced vibration whilst simultaneously satisfying the static conditions specified. The main modelling assumptions which limit the usefulness of the algorithm are:

1. the engine supporting structure is rigid, and
2. that the isolators behave like linear springs.

However the implications of these two assumptions on the optimum solution obtained by the computer program are unlikely to be serious if certain key optimization parameters are carefully selected at the start. Effectively these parameters can be classified into two general categories; those which define the specifications of the optimum isolation system (i.e. the constraint constants) and those which are related to the scaling (i.e. the weighting factors).

With respect to the first type of parameter, the main problem to be dealt with, prior to running the computer program, is that of choosing appropriate values for the maximum allowable deflections $c_{ij}$ of the isolators as set out in equation (3.34). Recalling the discussion on the problems associated with the linear model of the engine mounts it can be appreciated that special allowance must be made in the numerical values of these constants to account for their nonlinear load-deflection characteristics. Load-deflection characteristics of isolators with elastic properties resembling those specified by the stiffness bounds can be used to give a gross approximation to the numerical values of the constants $c_{ij}$. The program can then be run for a series of $c_{ij}$ values about these gross estimates. The values of $c_{ij}$ for which the optimum isolation system possesses the most desirable static behaviour can thus be selected for further optimization attempts if needed. When the program was run for the power train-isolator arrangement shown in Figure 2.7 and the static torque was set to the assumed maximum torque of the power train (2437 Nm) the isolator deflections were computed as follows:

| Isolator No. | X-Deflection | Y-Deflection | Z-Deflection |
|---|---|---|---|
| 1 | 1.63 mm | 0.56 mm | 4.7 mm |
| 2 | 2.43 mm | 9.75 mm | 20.8 mm |
| 3 | 0.06 mm | 10.71 mm | 15.6 mm |

The stiffness of the second isolator in the Z-direction was 226 N/mm and consequently equation (2.33) gives an applied force of 4.69 kN. From Figure 2.17 the isolator deflection at a load of 4.69 kN is found to be 12.8 mm according to the upper graph, and 15.8 mm according to the lower graph. Suitable values of $c_{ij}$ for running the program are thus expected to be in the range of 10 to 20 mm. However, apart from the maximum isolator deflections, three more constants are required to specify the maximum allowable static rotations of the power train (see equation (3.35)). Fortunately the computation of the power train rotations is not significantly affected by the linear model and consequently real tolerances can be used. It was advised [10] that the power train should not be allowed to rotate more than 10 degrees in any direction and the appropriate constants were set to this value although a value of 5 degrees was also used in some computer runs for testing purposes. With respect to the constants $c_{ij}$, two sets of test runs were carried out, one with $c_{ij}$ set at 15 and another with $c_{ij}$ set at 20 mm.

The next problem is to decide whether frequency constraints should be applied. The option of frequency constraints was introduced into the program so that the rigid power train frequency spectrum could be intentionally shifted away from undesirable frequency bands. The option is switched on by setting the parameter INAT to 1 in which case the user must supply a minimum numerical value $c_n$, see equation (3.36) for each modal frequency. As was stated previously, frequency constraints can be used to separate engine vibration from engine shake. For the purpose of testing the optimization program a series of test runs was carried out to determine whether the program could reach an optimum when the modal frequency spectrum (initially in the range 5 to 19 Hz) was forced to exceed an 8 Hz lower limiting frequency which was suggested [10] to be the highest frequency of road input excitations that the engine isolation system would experience.

The problems described in the previous two paragraphs are relatively easy to deal with. The difficult and time consuming part is that of choosing numerical values for the weighting factors $w_i$ for the constraint functions (see equations (3.40) to (3.42)) and for the penalty parameter $\rho$ (see equation (3.18)). The main problems which can occur as a result of inexperienced choice of numerical values for these parameters can be summarized as follows:

a) the optimization algorithm ignores constraint violations;
b) slow or oscillating changes of the objective function;
c) too many iterations required for each unconstrained subproblem;
d) the algorithm appears to be stuck (no substantial change is observed in the objective function for a great number of iterations)

e) the algorithm terminates and the value of the objective function on exit is greater than that on entry.

It is the source of these problems that the following discussion aims to clarify on a practical basis since they play a crucial role in determining whether or not the optimum isolation system eventually identified will be associated with a strong minimum of the objective function. Unfortunately, the algorithm is unable to flag a global minimum which leaves the user with no alternative but to run the program, using many different starting points and then to pick the lowest minimum obtained. However, if all the previously stated problems are reasonably dealt with, then it is only a matter of computer time or better definition of the original optimization problem before a strong optimum solution is obtained. Based on considerable experience of successfully running the program, it was found that for a reasonably well defined and scaled problem the algorithm would converge to a local minimum within no more than 1.5 to 2 hours. Typically only about 1.0 hr cpu time was required.

As was stated at the end of Chapter 3, the weighting factors were introduced into the program after certain experience was gained by running the program without scaling the constraint functions. The problem which emerged from those early optimization attempts was that the algorithm was not able to detect violation of constraints. On exit, several constraints would be violated but as far as the algorithm was concerned there was nothing wrong with the solution obtained (IFAIL was set to zero on exit meaning that a local minimum for the constrained problem had successfully been found). With respect to scaling of the constraint functions Gill, Murray and Wright [21] argue that the constraints should be well scaled with respect to the design variables but should also be balanced with respect to each other. As far as the first requirement is concerned, it is expected that the transformation applied to the design variables (equation (3.38) should be adequate for this purpose. Balancing of the constraints requires that each constraint should be appropriately weighted. However, this is not the only effect of introducing weighting factors, and in fact it is a less obvious effect that was responsible for the undetected constraint violation which was observed during the early optimization attempts. It should be mentioned at this point that throughout the progress of the algorithm the Lagrange multipliers remained zero.

Zero Lagrange multipliers are known to be a 'bad sign' even when the solution obtained satisfies all the required conditions. Discussing the subject of Lagrange multipliers Gill, Murray and Wright argue that no comment can be made about the optimality of a point associated with zero Lagrange multipliers before higher derivatives are examined (which are unlikely to be available). Further it is argued that a Lagrange multiplier which is zero at the solution point could indicate that the associated constraint is redundant or that the solution is at a saddle point.

Constraints which are associated with zero Lagrange multipliers are deleted from the active set and consequently cannot influence the sequence of iterates of the algorithm. Due to the limiting precision of computation, difficulties can arise in determining the correct sign of a very small multiplier which could be caused by a small perturbation, initiated by a rounding error. Substantially greater errors can be involved in the computation of the Lagrange multipliers due to ill-conditioning of the Jacobian matrix of the constraints on which the computation of the Lagrange multipliers is known to be critically dependent. According to reference [21] the effect of multiplying a constraint by a constant $w_i$ is to alter the rows of the Jacobian and consequently the values of the Lagrange multipliers. It can be appreciated now why weighting of the constraints can change the sequence of iterates dramatically.

Once the weighting factors were introduced, violation of constraints became detectable by the algorithm but that involved careful assignment of the weights so that the constraints were properly balanced. Initially certain constraints would still be violated at the solution. However, investigation of intermediate optimization results revealed that this was due to the numerical domination of the other (satisfied) constraints. In particular it was the isolator deflections that appeared to be invisible to the algorithm in contrast to the engine rotations to which the algorithm appeared to be most sensitive. (Frequency constraints were not applied during those early optimization attempts). It was observed that the isolator deflections were numerically smaller than the engine rotations by a factor of at least 10 throughout the progress of the algorithm. Considering the Lagrangian function (equation (3.18)), it can be appreciated that a numerical difference among the constraints leads to a square of that difference on the associated penalty term of the Lagrangian ($\frac{1}{2}\rho\, \mathbf{c}^T\mathbf{c}$) which in turn implies that the algorithm will be biased towards certain directions of search.

Better to consider $\theta l = \xi$ deflection to represent the various rotations

There appear to be no other guidelines on choosing weighting factors apart from those mentioned above. Closing the subject of constraint scaling Gill, Murray and Wright discuss the possibility of future software which will automatically scale all the constraint functions. Although this kind of software development will be of great value in conditioning optimization problems from a numerical point of view, it could distance the engineer from vital features of his particular problem, which at present cannot be considered an exhilarating expectation. On the contrary it is believed that users of numerical optimization algorithms should acquire the necessary background on optimization theory.

One further parameter of importance which must be initially set by the user and which can cause a lot of problems (if it is too large or too small on entry to E04UAF) is the penalty parameter $\rho$ involved in the definition of the Lagrangian. According to Gill, Murray and Wright [21], the Hessian matrix of the augmented Lagrangian function will be ill-conditioned for certain ranges of $\rho$ which implies that the unconstrained subproblem will be ill-conditioned too. On the choice of $\rho$ the NAG routine manual suggests that the user should set $\rho$ to 1 initially and if this causes overflow or convergence to a non-feasible point then $\rho$ = 100 should be tried. Neither overflow nor convergence to a non-feasible point was observed irrespective of what value was assigned to $\rho$. However, the problems described earlier by (c) and (d) are largely attributed to unsuitable values for $\rho$. For the current problem, suitable values of $\rho$ can be found in the range of 1 to 1000, although the actual value will largely depend on the chosen constraint constants and the weighting factors.

## 4.2 RESULTS

The following presentation of computer results aims to demonstrate the potential of the computer program whilst also illustrating the sensitivity of the algorithm to the scaling parameters. Tables 4.1 to 4.4 describe four optimization attempts which were made without frequency constraints. It can be appreciated that the algorithm reached a minimum of the objective function each time while satisfying all the conditions specified. However, the optimum obtained each time was a different local minimum of the objective function as is indicated by the value of F(x) after optimization. In the first two attempts the engine static rotations were limited to 5 degrees (0.08727 rads) while the isolators were allowed to deflect up to 15 and 20 mm respectively. Both attempts yielded almost the same reduction in the objective function although E04UAF indicated that the solution of the second run (RES2) is the optimum (IFAIL = 0 on exit).

The flag IFAIL is set before exit from E04UAF to indicate the confidence of the algorithm on the optimum obtained. If IFAIL is set to 2 then this indicates that either the maximum allowable number of function evaluations has been exceeded or that 10 cycles of E04UAF have been completed (i.e. ten subproblems have been solved) and the routine was unable to converge to a better optimum. Usually this means that convergence criteria are not satisfied to the precision specified by XTOL (which on entry was set to E04UAF to approximately 1.0E-19). The NAG Manual states that the precise test for convergence is

$$\mathrm{GLNORM}/(1.0 + |F|) + || D^{-\frac{1}{2}} r || < \mathrm{XTOL}$$

FILE : RES1

RHO = 10 ENGINE SPEED = 800.0 rpm

Before optimization F(X) = 0.7620E-1
After optimization F(X) = 0.1668E-1
Percentage change D % = -78.11
IFAIL = 2
No of function evaluations = 6836
Norm of gradient of Lagrangian = 0.4855E-8
Condition of Hessian = 0.3455E+5
Norm of residual = 0.3822E-8
RHO on exit = 0.3559E+6

| | CONSTRAIN CONSTANT | WEIGHT |
|---|---|---|
| X1 | 15 | 5 |
| Y1 | 15 | 5 |
| Z1 | 15 | 1 |
| X2 | 15 | 5 |
| Y2 | 15 | 5 |
| Z2 | 15 | 10 |
| X3 | 15 | 5 |
| Y3 | 15 | 5 |
| Z3 | 15 | 10 |
| XX | 0.08727 | 0.001 |
| YY | 0.08727 | 0.1 |
| ZZ | 0.08727 | 0.001 |

ISOLATOR STATIC DISPLACEMENTS (mm)

| | | X | Y | Z |
|---|---|---|---|---|
| 1 | BEFORE OPT. | 1.63 | 0.56 | 4.70 |
| | AFTER OPT. | 1.36 | 1.33 | 7.71 |
| 2 | BEFORE OPT. | 2.43 | 9.74 | 20.77 |
| | AFTER OPT. | 9.79 | 4.05 | 15.00 |
| 3 | BEFORE OPT. | 0.061 | 10.71 | 15.65 |
| | AFTER OPT. | 12.15 | 5.54 | 13.73 |

ENGINE STATIC ROTATIONS (Degrees)

| | XX | YY | ZZ |
|---|---|---|---|
| BEFORE OPT. | 0.23 | 4.28 | 2.39 |
| AFTER OPT. | 0.64 | 5.00 | 1.13 |

NATURAL FREQUENCIES (Hz)

| | 1 | 2 | 3 | 4 | 5 | 6 |
|---|---|---|---|---|---|---|
| BEFORE OPT. | 5.19 | 6.92 | 9.10 | 12.22 | 12.37 | 19.50 |
| AFTER OPT. | 5.01 | 5.69 | 7.46 | 9.90 | 10.19 | 14.39 |

Table 4.1 Computer results from output file RES1

FILE : RES2

RHO = 100 ENGINE SPEED = 900.0 rpm

Before optimization F(X) = 0.7620E-1
After optimization F(X) = 0.1618E-1
Percentage change D % = -78.77
IFAIL = 0
No of function evaluations = 41316
Norm of gradient of Lagrangian = 0.4136E-11
Condition of Hessian = 0.6340E+9
Norm of residual = 0.2889E-12
RHO on exit = 0.7644E+6

| | CONSTRAIN CONSTANT | WEIGHT |
|---|---|---|
| X1 | 20 | 10 |
| Y1 | 20 | 10 |
| Z1 | 20 | 1 |
| X2 | 20 | 10 |
| Y2 | 20 | 10 |
| Z2 | 20 | 10 |
| X3 | 20 | 10 |
| Y3 | 20 | 10 |
| Z3 | 20 | 10 |
| XX | 0.08727 | 1 |
| YY | 0.08727 | 1 |
| ZZ | 0.08727 | 1 |

ISOLATOR STATIC DISPLACEMENTS (mm)

| | | X | Y | Z |
|---|---|---|---|---|
| 1 | BEFORE OPT. | 1.63 | 0.56 | 4.70 |
| | AFTER OPT. | 2.52 | 2.84 | 10.12 |
| 2 | BEFORE OPT. | 2.43 | 9.74 | 20.77 |
| | AFTER OPT. | 5.23 | 7.89 | 15.94 |
| 3 | BEFORE OPT. | 0.061 | 10.71 | 15.65 |
| | AFTER OPT. | 8.58 | 2.78 | 13.67 |

ENGINE STATIC ROTATIONS (Degrees)

| | XX | YY | ZZ |
|---|---|---|---|
| BEFORE OPT. | 0.23 | 4.28 | 2.39 |
| AFTER OPT. | 0.57 | 5.0 | 1.02 |

NATURAL FREQUENCIES (Hz)

| | 1 | 2 | 3 | 4 | 5 | 6 |
|---|---|---|---|---|---|---|
| BEFORE OPT. | 5.19 | 6.92 | 9.10 | 12.22 | 12.37 | 19.50 |
| AFTER OPT. | 4.58 | 5.28 | 6.29 | 9.94 | 10.09 | 14.46 |

Table 4.2 Computer results from output file RES2

FILE : RES3

RHO = 10    ENGINE SPEED = 800.0 rpm

```
Before optimization  F(X) = 0.7620E-1
After  optimization  F(X) = 0.1264E-1
Percentage change    D %  = -83.41
IFAIL                     = 2
No of function evaluations      = 3329
Norm of gradient of Lagrangian  = 0.2129E-6
Condition of Hessian            = 0.2215E+2
Norm of residual                = 0.5128E-6
RHO on exit                     = 0.5408E+6
```

| | CONSTRAIN | CONSTANT WEIGHT |
|---|---|---|
| X1 | 15 | 10 |
| Y1 | 15 | 10 |
| Z1 | 15 | 10 |
| X2 | 15 | 10 |
| Y2 | 15 | 10 |
| Z2 | 15 | 10 |
| X3 | 15 | 10 |
| Y3 | 15 | 10 |
| Z3 | 15 | 10 |
| XX | 0.1745 | 0.01 |
| YY | 0.1745 | 0.01 |
| ZZ | 0.1745 | 0.01 |

ISOLATOR STATIC DISPLACEMENTS (mm)

| | | X | Y | Z |
|---|---|---|---|---|
| 1 | BEFORE OPT. | 1.63 | 0.56 | 4.70 |
| | AFTER OPT. | 2.44 | 2.18 | 11.69 |
| 2 | BEFORE OPT. | 2.43 | 9.74 | 20.77 |
| | AFTER OPT. | 15.00 | 5.11 | 15.00 |
| 3 | BEFORE OPT. | 0.061 | 10.71 | 15.65 |
| | AFTER OPT. | 15.00 | 7.47 | 15.00 |

ENGINE STATIC ROTATIONS (Degrees)

| | XX | YY | ZZ |
|---|---|---|---|
| BEFORE OPT. | 0.23 | 4.28 | 2.39 |
| AFTER OPT. | 1.056 | 6.43 | 1.54 |

NATURAL FREQUENCIES (Hz)

| | 1 | 2 | 3 | 4 | 5 | 6 |
|---|---|---|---|---|---|---|
| BEFORE OPT. | 5.19 | 6.92 | 9.10 | 12.22 | 12.37 | 19.50 |
| AFTER OPT. | 5.13 | 5.75 | 7.53 | 9.02 | 10.52 | 14.71 |

Table 4.3 Computer results from output file RES3

FILE : RES4

RHO = 10 ENGINE SPEED = 800.0 rpm

Before optimization F(X) = 0.7620E-1
After optimization F(X) = 0.6940E-2
Percentage change D % = -90.89
IFAIL = 2
No of function evaluations = 14076
Norm of gradient of Lagrangian = 0.2540E-7
Condition of Hessian = 0.6905E+3
Norm of residual = 0.2521E-6
RHO on exit = 0.9878E+6

| | CONSTRAIN | CONSTANT | WEIGHT |
|---|---|---|---|
| X1 | 15 | | 10 |
| Y1 | 15 | | 10 |
| Z1 | 15 | | 10 |
| X2 | 15 | | 10 |
| Y2 | 15 | | 10 |
| Z2 | 15 | | 10 |
| X3 | 15 | | 10 |
| Y3 | 15 | | 10 |
| Z3 | 15 | | 10 |
| XX | 0.1745 | | 0.1 |
| YY | 0.1745 | | 0.1 |
| ZZ | 0.1745 | | 0.1 |

ISOLATOR STATIC DISPLACEMENTS (mm)

| | | X | Y | Z |
|---|---|---|---|---|
| 1 | BEFORE OPT. | 1.63 | 0.56 | 4.70 |
| | AFTER OPT. | 4.71 | 1.25 | 15.00 |
| 2 | BEFORE OPT. | 2.43 | 9.74 | 20.77 |
| | AFTER OPT. | 15.00 | 0.69 | 14.92 |
| 3 | BEFORE OPT. | 0.061 | 10.71 | 15.65 |
| | AFTER OPT. | 15.00 | 3.32 | 15.00 |

ENGINE STATIC ROTATIONS (Degrees)

| | XX | YY | ZZ |
|---|---|---|---|
| BEFORE OPT. | 0.23 | 4.28 | 2.39 |
| AFTER OPT. | 1.00 | 9.99 | 1.91 |

NATURAL FREQUENCIES (Hz)

| | 1 | 2 | 3 | 4 | 5 | 6 |
|---|---|---|---|---|---|---|
| BEFORE OPT. | 5.19 | 6.92 | 9.10 | 12.22 | 12.37 | 19.50 |
| AFTER OPT. | 4.87 | 5.71 | 7.68 | 8.72 | 15.16 | 17.00 |

Table 4.4 Computer results from output file RES4

where GLNORM is the Euclidean norm of the vector Gz - A x RLAM (Gz is an approximation to the gradient vector of F(X) with respect to the free variables and A is the Jacobian of the active constraints)

D is a diagonal matrix ~~with~~ whose elements are the diagonal elements of $(I + A^TA)$.

The quantity of the left hand side of the inequality (4.1) is estimated at the end of each cycle of E04UAF. On exit of run RES2 this convergence parameter was estimated as 0.1657E-8 which is certainly not less than XTOL. It is therefore not clear why the algorithm set IFAIL = 0.

One point that is clear from Tables 4.1 to 4.2 is that certain constraints will be inactive at the solution. In fact, with the exception of ZZ and YY, all the other constraints are inactive at the solution. These constraints, as expected, were associated with zero Lagrange multipliers. However, they were not removed from successive runs because it was not certain if their redundancy was genuine or due to inappropriate scaling. It was found at a later stage that under certain conditions some of them became active as can be observed in Tables 4.3 and 4.4. Comparing the scaling factors and the final results of Tables 4.3 and 4.4, the sensitivity of the algorithm to the scaling of the constraint functions becomes evident. The results show that a change in the weighting factors of the engine rotation constraints by a factor of ten caused the algorithm to converge to a lower local minimum, Unfortunately, the condition number of the Jacobian matrix of the constraints is not monitored by E04UAF and as a result it is not possible to investigate whether the observed change in the sequence of iterates was connected with improved conditioning of the Jacobian. The parameters which are available for monitoring at the end of each iteration of E04JBF are:

1. the iteration number;
2. the number of function evaluations;

3. the norm of the gradient vector of the Lagrangian function, and
4. the condition of the projected Hessian.

However, these parameters give no indication of the effectiveness of the applied scaling although they do indicate changes in the sequence of iterates of the algorithm.

Due to the fact that there is no test available to check whether a particular type of scaling will improve the conditioning of the optimization problem it was decided to adjust the scaling factors by observing the values of the constraint functions at the solution. Hence, constraints which appeared to change little and which were numerically large in relation to the others, and those which appeared to be redundant, were scaled down. On the other hand, those constraints which were considered to be relatively more important for the validity of the solution or numerically small compared with the others were scaled up. However, the magnitude of the scaling factors in a particular case was obtained on a trial and error basis. For the optimization problem described so far it was decided that the important constraints were:

1. engine rotation in the YY direction since this is the direction of the applied torque;
2. isolator deflection in the Z direction since the isolator orientation (design variable subject to bounds) was limited to 10 degrees and consequently the applied torque and the engine weight were most likely to cause large deflections in a vertical plane;
3. frequency constraints for subsequent runs because of their influence on the engine shake problem.

Although the solution obtained from RES4 does not meet the 8 Hz frequency minimum discussed earlier, it was decided to check this solution simply because the frequency spectrum of the optimum isolation system is fairly close to that of the initial system and out of curiosity to find out the physical meaning of the changes made to the design variables by the numerical algorithm. Table 4.5 shows the

| DESIGN VARIABLES | BEFORE OPTIMIZATION | AFTER OPTIMIZATION |
|---|---|---|
| Stiffness KX1 | 418 N/mm | 202 N/mm |
| Stiffness KY1 | 132 N/mm | 103 N/mm |
| Stiffness Kz1 | 165 N/mm | 126 N/mm |
| Position X1 | 124 mm | 160 mm |
| Position Y1 | 292 mm | 257 mm |
| Position Z1 | 81 mm | 60 mm |
| Orientation FI1 | 0 Degrees | 0 Degrees |
| Orientation THETA1 | 0 Degrees | -0.21 Degrees |
| Orientation PSI1 | 0 Degrees | 0 Degrees |
| Stiffness KX2 | 288 N/mm | 408 N/mm |
| Stiffness KY2 | 77 N/mm | 71 N/mm |
| Stiffness Kz2 | 226 N/mm | 398 N/mm |
| Position X2 | 308 mm | 103 mm |
| Position Y2 | -279 mm | -325 mm |
| Position Z2 | -292 mm | 6 mm |
| Orientation FI2 | 0 Degrees | 0 Degrees |
| Orientation THETA2 | 0 Degrees | -1.79 Degrees |
| Orientation PSI2 | 0 Degrees | 0.99 Degrees |
| Stiffness KX3 | 288 N/mm | 465 N/mm |
| Stiffness KY3 | 77 N/mm | 82 N/mm |
| Stiffness Kz3 | 226 N/mm | 400 N/mm |
| Position X3 | -181 mm | -63 mm |
| Position Y3 | -303 mm | -246 mm |
| Position Z3 | -272 mm | -149 mm |
| Orientation FI3 | 0 Degrees | 0 Degrees |
| Orientation THETA3 | 0 Degrees | -2.78 Degrees |
| Orientation PSI3 | 0 Degrees | 0 Degrees |

Table 4.5 Original and final values of optimization variables for the computer results of table 4.4

initial and final values of the optimization variables, while Figure 4.1 shows the position of the isolators with respect to the power train before and after optimization. From this figure it can be appreciated that the algorithm reduced the objective function by moving the isolators closer to the power train and effectively reducing the roll stiffness. However, from Table 4.5 it is obvious that in order to satisfy the static constraints the stiffnesses of the second (rear left) and the third (rear right) isolators in the Z and X local directions were substantially increased. Table 4.6 shows the kinetic energy modal distributions of the optimized system while Table 4.7 shows those of the original system.

Comparison of Tables 4.6 and 4.7 shows that the algorithm effectively reduced the roll mode frequency from 19.51 Hz to 8.72 Hz. Recalling the discussion on the dynamic response of the model (in Chapter 2), it is obvious that reducing the frequency of the roll mode effectively reduces the transmission of vibration generated by the second harmonic of the excitation.

The dynamic response of the optimum isolation system is superimposed on that of the original system and is presented for comparison in Figures 4.2 to 4.8. The advantages for vibration isolation of a low frequency roll mode are evident in all the plots. Such a low frequency roll mode is, of course, undesirable because of its susceptibility to road surface indirect vibration which makes this particular solution undesirable. This solution also has one further disadvantage from a practical point of view. The dotted triangles on the X-Y plane (plan view) in Figure 4.1 outline the supporting base defined by the isolators before and after optimization. It may be seen that the power train mass centre is outside the base defined by the optimized position of the isolators which is certainly not traditional engineering practice. However, it was not possible in the time available to investigate the possibility of additional constraints which would eliminate the problem apart from careful definition of the design space.

| Frequency | X | Y | Z | XX | YY | ZZ | COUPL. |
|---|---|---|---|---|---|---|---|
| 1. 4.87 | 0 | 12.34 | 37.94 | 23.32 | 20.5 | 2.47 | 3.43 |
| 2. 5.71 | 2.46 | 83.34 | 5.20 | 3.77 | 2.66 | 0.95 | 1.62 |
| 3. 7.68 | 55.07 | 3.39 | 2.54 | 3.68 | 11.67 | 18.34 | 5.31 |
| 4. 8.72 | 8.17 | 0.76 | 11.94 | 13.48 | 72.88 | 21.0 | -28.23 |
| 5. 15.16 | 0.51 | 0.01 | 41.92 | 58.04 | 0.29 | 0.17 | -0.94 |
| 6. 17.00 | 33.72 | 0.11 | 0.29 | 0.65 | 0.27 | 63.18 | 1.78 |

TABLE 4.6: KINETIC ENERGY MODAL DISTRIBUTIONS FOR RES4

| Frequency | X | Y | Z | XX | YY | ZZ | COUPL. |
|---|---|---|---|---|---|---|---|
| 1. 5.19 | 2.26 | 64.83 | 14.30 | 8.20 | 5.63 | 5.00 | -0.22 |
| 2. 6.92 | 8.32 | 32.95 | 40.60 | 5.24 | 9.94 | 3.35 | -0.40 |
| 3. 9.08 | 48.25 | 0.01 | 19.64 | 11.37 | 21.03 | 12.26 | -12.56 |
| 4. 12.23 | 23.00 | 0.00 | 3.66 | 33.40 | 9.95 | 47.23 | -17.24 |
| 5. 12.38 | 8.97 | 2.12 | 21.34 | 42.64 | 4.56 | 19.44 | 0.93 |
| 6. 19.51 | 9.3 | 0.06 | 0.042 | 1.98 | 57.10 | 18.70 | 12.44 |

TABLE 4.7: KINETIC ENERGY MODAL DISTRIBUTIONS OF ORIGINAL SYSTEM

Tables 4.8 to 4.11 show the scaling and the results of the optimization attempts which were made with frequency constraints. Tables 4.8 and 4.9 give evidence of the previously stated problem of termination of the algorithm at a point where the value of the objective function is greater than that at the starting point. It is beyond any doubt that in this particular case the algorithm was misled by an ill-conditioned problem as a result of bad scaling. However, there can be cases where such an occurrence is quite genuine. Consider for instance the situation where the algorithm is initiated at a non-feasible point and most of the constraints are violated by substantial margins. It is quite possible then that at the optimum point the objective function will be numerically greater than at the starting point. In other words, it is possible that a better local minimum of the objective function might exist in the unfeasible subspace.

With respect to the frequency constraints three optimization attempts were made. First the lower end of the rigid-power train frequency spectrum was limited to 8 Hz for the reason described above. These attempts are illustrated in Tables 4.10 and 4.11. Although the solutions obtained from these runs were feasible, it was found difficult to obtain a lower minimum and time limitations did not allow further attempts to be carried out on this particular case. Further it was realised that there was no need to constrain every single modal frequency. As previously noted the NAG routine which solves the eigenvalue problem returns the eigenvalues in ascending order. Hence only the first element of the eigenvalue matrix needs to be constrained, thereby implying that five of the six frequency constraints are redundant. Deleting the redundant constraints from the program was considered at first but not implemented. Instead, the constraint constants were changed so that the redundant constraints could be made active on the condition that each modal frequency was constrained at a higher level than the previous one. The six modal frequencies were thus constrained at 8, 10, 12, 14, 16 and 18 Hz respectively so that the modal frequency spectrum will be placed above the frequency band of possible road input excitation and below the second order engine excitation (engine idle at 800 rpm or 13.33 Hz

FILE : RES6

RHO = 1 ENGINE SPEED = 800.0 rpm

Before optimization F(X) = 0.7620E-1
After optimization F(X) = 0.7909E-1
Percentage change D % = +3.79
IFAIL = 2
No of function evaluations = 4890
Norm of gradient of Lagrangian = 0.1610E-5
Condition of Hessian = 0.2480E+4
Norm of residual = 0.7659E-4
RHO on exit = 0.2541E+7

| | CONSTRAIN CONSTANT | WEIGHT |
|---|---|---|
| X1 | 15 | 10 |
| Y1 | 15 | 10 |
| Z1 | 15 | 10 |
| X2 | 15 | 10 |
| Y2 | 15 | 10 |
| Z2 | 15 | 10 |
| X3 | 15 | 10 |
| Y3 | 15 | 10 |
| Z3 | 15 | 10 |
| XX | 0.1745 | 0.01 |
| YY | 0.1745 | 0.01 |
| ZZ | 0.1745 | 0.01 |
| W1 | 8.0 | 0.01 |
| W2 | 10.0 | 0.001 |
| W3 | 12.0 | 0.0001 |
| W4 | 14.0 | 0.00001 |
| W5 | 16.0 | 0.000001 |
| W6 | 18.0 | 0.0000001 |

ISOLATOR STATIC DISPLACEMENTS (mm)

| | | X | Y | Z |
|---|---|---|---|---|
| 1 | BEFORE OPT. | 1.63 | 0.56 | 4.70 |
| | AFTER OPT. | 4.11 | 0.37 | 3.99 |
| 2 | BEFORE OPT. | 2.43 | 9.74 | 20.77 |
| | AFTER OPT. | 9.60 | 2.30 | 10.02 |
| 3 | BEFORE OPT. | 0.061 | 10.71 | 15.65 |
| | AFTER OPT. | 11.39 | 0.81 | 9.06 |

ENGINE STATIC ROTATIONS (Degrees)

| | XX | YY | ZZ |
|---|---|---|---|
| BEFORE OPT. | 0.23 | 4.28 | 2.39 |
| AFTER OPT. | 0.31 | 4.22 | 0.95 |

NATURAL FREQUENCIES (Hz)

| | 1 | 2 | 3 | 4 | 5 | 6 |
|---|---|---|---|---|---|---|
| BEFORE OPT. | 5.19 | 6.92 | 9.10 | 12.22 | 12.37 | 19.50 |
| AFTER OPT. | 8.75 | 9.93 | 11.68 | 12.44 | 20.50 | 22.64 |

Table 4.8 Computer results from output file RES6

FILE : RES5

RHO = 100 ENGINE SPEED = 800.0 rpm

```
Before optimization  F(X) = 0.7620E-1
After  optimization  F(X) = 0.7731E-1
Percentage change    D %  = +1.46
IFAIL                     = 2
No of function evaluations     = 3052
Norm of gradient of Lagrangian = 0.2154E-5
Condition of Hessian           = 0.1540E+2
Norm of residual               = 0.1997E-3
RHO on exit                    = 0.2333E+10
```

| | CONSTRAIN CONSTANT | WEIGHT |
|---|---|---|
| X1 | 15 | 10 |
| Y1 | 15 | 10 |
| Z1 | 15 | 10 |
| X2 | 15 | 10 |
| Y2 | 15 | 10 |
| Z2 | 15 | 10 |
| X3 | 15 | 10 |
| Y3 | 15 | 10 |
| Z3 | 15 | 10 |
| XX | 0.1745 | 0.01 |
| YY | 0.1745 | 0.01 |
| ZZ | 0.1745 | 0.01 |
| W1 | 8.0 | 0.01 |
| W2 | 10.0 | 0.001 |
| W3 | 12.0 | 0.0001 |
| W4 | 14.0 | 0.00001 |
| W5 | 16.0 | 0.000001 |
| W6 | 18.0 | 0.0000001 |

ISOLATOR STATIC DISPLACEMENTS (mm)

| | | X | Y | Z |
|---|---|---|---|---|
| 1 | BEFORE OPT. | 1.63 | 0.56 | 4.70 |
| | AFTER OPT. | 1.38 | 0.11 | 2.35 |
| 2 | BEFORE OPT. | 2.43 | 9.74 | 20.77 |
| | AFTER OPT. | 1.56 | 5.00 | 15.00 |
| 3 | BEFORE OPT. | 0.061 | 10.71 | 15.65 |
| | AFTER OPT. | 3.90 | 4.09 | 7.60 |

ENGINE STATIC ROTATIONS (Degrees)

| | XX | YY | ZZ |
|---|---|---|---|
| BEFORE OPT. | 0.23 | 4.28 | 2.39 |
| AFTER OPT. | 0.11 | 2.25 | 0.83 |

NATURAL FREQUENCIES (Hz)

| | 1 | 2 | 3 | 4 | 5 | 6 |
|---|---|---|---|---|---|---|
| BEFORE OPT. | 5.19 | 6.92 | 9.10 | 12.22 | 12.37 | 19.50 |
| AFTER OPT. | 8.49 | 9.89 | 10.33 | 12.78 | 13.76 | 16.57 |

Table 4.9 Computer results from output file RES5

FILE : RES8a

RHO = 100 ENGINE SPEED = 800.0 rpm

Before optimization F(X) = 0.7620E-1
After optimization F(X) = 0.7294E-1
Percentage change D % = -4.27
IFAIL = 2
No of function evaluations = 2744
Norm of gradient of Lagrangian = 0.8362E-7
Condition of Hessian = 0.6100E+3
Norm of residual = 0.8706E-8
RHO on exit = 0.1375E+9

| | CONSTRAIN CONSTANT | WEIGHT |
|---|---|---|
| X1 | 15 | 10 |
| Y1 | 15 | 10 |
| Z1 | 15 | 10 |
| X2 | 15 | 10 |
| Y2 | 15 | 10 |
| Z2 | 15 | 10 |
| X3 | 15 | 10 |
| Y3 | 15 | 10 |
| Z3 | 15 | 10 |
| XX | 0.1745 | 0.01 |
| YY | 0.1745 | 0.01 |
| ZZ | 0.1745 | 0.01 |
| W1 | 8.0 | 0.01 |
| W2 | 8.0 | 0.001 |
| W3 | 8.0 | 0.0001 |
| W4 | 8.0 | 0.00001 |
| W5 | 8.0 | 0.000001 |
| W6 | 8.0 | 0.0000001 |

ISOLATOR STATIC DISPLACEMENTS (mm)

| | | X | Y | Z |
|---|---|---|---|---|
| 1 | BEFORE OPT. | 1.63 | 0.56 | 4.70 |
| | AFTER OPT. | 1.61 | 0.40 | 3.26 |
| 2 | BEFORE OPT. | 2.43 | 9.74 | 20.77 |
| | AFTER OPT. | 2.45 | 3.67 | 13.44 |
| 3 | BEFORE OPT. | 0.061 | 10.71 | 15.65 |
| | AFTER OPT. | 4.34 | 2.99 | 7.24 |

ENGINE STATIC ROTATIONS (Degrees)

| | XX | YY | ZZ |
|---|---|---|---|
| BEFORE OPT. | 0.23 | 4.28 | 2.39 |
| AFTER OPT. | 0.05 | 1.98 | 0.58 |

NATURAL FREQUENCIES (Hz)

| | 1 | 2 | 3 | 4 | 5 | 6 |
|---|---|---|---|---|---|---|
| BEFORE OPT. | 5.19 | 6.92 | 9.10 | 12.22 | 12.37 | 19.50 |
| AFTER OPT. | 8.00 | 8.03 | 8.91 | 12.16 | 13.75 | 16.82 |

Table 4.10 Computer results from output file RES8a

FILE : RES8b

RHO = 10 ENGINE SPEED = 800.0 rpm

Before optimization F(X) = 0.7620E-1
After optimization F(X) = 0.5517E-1
Percentage change D % = -27.59
IFAIL = 2
No of function evaluations = 5221
Norm of gradient of Lagrangian = 0.2837E-5
Condition of Hessian = 0.7999E+2
Norm of residual = 0.2752E-3
RHO on exit = 0.3123E+9

| | CONSTRAIN CONSTANT | WEIGHT |
|---|---|---|
| X1 | 15 | 10 |
| Y1 | 15 | 10 |
| Z1 | 15 | 10 |
| X2 | 15 | 10 |
| Y2 | 15 | 10 |
| Z2 | 15 | 10 |
| X3 | 15 | 10 |
| Y3 | 15 | 10 |
| Z3 | 15 | 10 |
| XX | 0.1745 | 0.01 |
| YY | 0.1745 | 0.01 |
| ZZ | 0.1745 | 0.01 |
| W1 | 8.0 | 0.1 |
| W2 | 8.0 | 0.00000001 |
| W3 | 8.0 | 0.00000001 |
| W4 | 8.0 | 0.00000001 |
| W5 | 8.0 | 0.00000001 |
| W6 | 8.0 | 0.00000001 |

ISOLATOR STATIC DISPLACEMENTS (mm)

| | | X | Y | Z |
|---|---|---|---|---|
| 1 | BEFORE OPT. | 1.63 | 0.56 | 4.70 |
| | AFTER OPT. | 0.54 | 0.27 | 3.55 |
| 2 | BEFORE OPT. | 2.43 | 9.74 | 20.77 |
| | AFTER OPT. | 7.74 | 1.82 | 13.30 |
| 3 | BEFORE OPT. | 0.061 | 10.71 | 15.65 |
| | AFTER OPT. | 7.44 | 1.59 | 8.12 |

ENGINE STATIC ROTATIONS (Degrees)

| | XX | YY | ZZ |
|---|---|---|---|
| BEFORE OPT. | 0.23 | 4.29 | 2.39 |
| AFTER OPT. | 0.50 | 2.57 | 0.73 |

NATURAL FREQUENCIES (Hz)

| | 1 | 2 | 3 | 4 | 5 | 6 |
|---|---|---|---|---|---|---|
| BEFORE OPT. | 5.19 | 6.92 | 9.10 | 12.22 | 12.37 | 19.50 |
| AFTER OPT. | 8.00 | 10.61 | 12.07 | 12.65 | 16.80 | 18.39 |

Table 4.11 Computer results from output file RES8b

giving the second order excitation at 23.66 Hz). The results of the final attempts are summarised in Tables 4.12 and 4.13 and conclude the selected series of computer runs, out of all those which were made for the purpose of testing the computer program. The following section of the current discussion will deal with the evaluation of this final solution.

The position of the isolators, with respect to the power train mass centre, for the optimum isolation systems obtained from the computer runs described in Tables 4.12 and 4.13, are shown in Figures 4.9 and 4.10 respectively. By comparing the position of the power train mass centre relative to the supporting triangular base defined by the isolators on the X-Y plane it can be appreciated that the optimum isolation system obtained from the optimization attempt described in Table 4.13 is statically more stable than that of Table 4.12. In addition to this, the optimum isolation system of Table 4.13 is associated with a lower minimum of the objective function and consequently it is selected as the best solution. Although on exit from E04UAF the flag IFAIL was set to 2, it is not necessarily true that the solution is not optimum. The only case where IFAIL was set to 0 on exit, is the optimization attempt described in Table 4.2. Table 4.14 below shows the values of the optimization parameters, which are checked by the algorithm before the flag IFAIL is set on exit from E04UAF, for the two optimization attempts described in Tables 4.2 and 4.13 respectively.

From Table 4.14, it is clear that the only substantial difference between the optimality conditions of the two attempts is the amount by which the inequality constraint functions lie outside their range, i.e. the norm of the residual vector. However this difference is not

FILE : RES8

RHO = 1 ENGINE SPEED = 800.0 rpm

```
Before optimization  F(X) = 0.7620E-1
After  optimization  F(X) = 0.2091E-1
Percentage change    D %  = -72.56
IFAIL                     = 2
No of function evaluations     = 9863
Norm of gradient of Lagrangian = 0.2029E-6
Condition of Hessian           = 0.1339E+5
Norm of residual               = 0.3256E-6
RHO on exit                    = 0.2159E+4
```

| | CONSTRAIN CONSTANT | WEIGHT |
|---|---|---|
| X1 | 15 | 10 |
| Y1 | 15 | 10 |
| Z1 | 15 | 10 |
| X2 | 15 | 10 |
| Y2 | 15 | 10 |
| Z2 | 15 | 10 |
| X3 | 15 | 10 |
| Y3 | 15 | 10 |
| Z3 | 15 | 10 |
| XX | 0.1745 | 0.1 |
| YY | 0.1745 | 0.1 |
| ZZ | 0.1745 | 0.1 |
| W1 | 8.0 | 0.1 |
| W2 | 10.0 | 0.1 |
| W3 | 12.0 | 0.1 |
| W4 | 14.0 | 0.1 |
| W5 | 16.0 | 0.1 |
| W6 | 18.0 | 0.1 |

ISOLATOR STATIC DISPLACEMENTS (mm)

| | | X | Y | Z |
|---|---|---|---|---|
| 1 | BEFORE OPT. | 1.63 | 0.56 | 4.70 |
| | AFTER OPT. | 0.26 | 0.53 | 0.98 |
| 2 | BEFORE OPT. | 2.43 | 9.74 | 20.77 |
| | AFTER OPT. | 12.66 | 2.50 | 15.00 |
| 3 | BEFORE OPT. | 0.061 | 10.71 | 15.65 |
| | AFTER OPT. | 9.69 | 0.22 | 11.22 |

ENGINE STATIC ROTATIONS (Degrees)

| | XX | YY | ZZ |
|---|---|---|---|
| BEFORE OPT. | 0.23 | 4.28 | 2.39 |
| AFTER OPT. | 0.05 | 5.33 | 1.00 |

NATURAL FREQUENCIES (Hz)

| | 1 | 2 | 3 | 4 | 5 | 6 |
|---|---|---|---|---|---|---|
| BEFORE OPT. | 5.19 | 6.92 | 9.10 | 12.22 | 12.37 | 19.50 |
| AFTER OPT. | 8.00 | 10.00 | 12.00 | 14.77 | 16.00 | 20.42 |

Table 4.12 Computer results from output file RES8

```
FILE : RES9

RHO = 1                          ENGINE SPEED = 800.0 rpm

Before optimization  F(X) = 0.7620E-1
After  optimization  F(X) = 0.2025E-1
Percentage change    D %  = -73.42
IFAIL                     = 2
No of function evaluations        = 17727
Norm of gradient of Lagrangian    = 0.5792E-10
Condition of Hessian              = 0.4710E+5
Norm of residual                  = 0.1118E-8
RHO on exit                       = 0.5074E+3
```

| | CONSTRAIN CONSTANT | WEIGHT |
|---|---|---|
| X1 | 20 | 10 |
| Y1 | 20 | 10 |
| Z1 | 20 | 10 |
| X2 | 20 | 10 |
| Y2 | 20 | 10 |
| Z2 | 20 | 10 |
| X3 | 20 | 10 |
| Y3 | 20 | 10 |
| Z3 | 20 | 10 |
| XX | 0.1745 | 0.1 |
| YY | 0.1745 | 0.1 |
| ZZ | 0.1745 | 0.1 |
| W1 | 8.0 | 0.1 |
| W2 | 10.0 | 0.1 |
| W3 | 12.0 | 0.1 |
| W4 | 14.0 | 0.1 |
| W5 | 16.0 | 0.1 |
| W6 | 18.0 | 0.1 |

ISOLATOR STATIC DISPLACEMENTS (mm)

| | | X | Y | Z |
|---|---|---|---|---|
| 1 | BEFORE OPT. | 1.63 | 0.56 | 4.70 |
| | AFTER OPT. | 0.87 | 0.18 | 1.24 |
| 2 | BEFORE OPT. | 2.43 | 9.74 | 20.77 |
| | AFTER OPT. | 3.76 | 0.52 | 17.34 |
| 3 | BEFORE OPT. | 0.061 | 10.71 | 15.65 |
| | AFTER OPT. | 11.47 | 0.43 | 14.52 |

ENGINE STATIC ROTATIONS (Degrees)

| | XX | YY | ZZ |
|---|---|---|---|
| BEFORE OPT. | 0.23 | 4.28 | 2.39 |
| AFTER OPT. | 0.04 | 5.63 | 0.99 |

NATURAL FREQUENCIES (Hz)

| | 1 | 2 | 3 | 4 | 5 | 6 |
|---|---|---|---|---|---|---|
| BEFORE OPT. | 5.19 | 6.92 | 9.10 | 12.22 | 12.37 | 19.50 |
| AFTER OPT. | 8.00 | 10.00 | 12.00 | 14.71 | 16.00 | 20.26 |

Table 4.13 Computer results from output file RES9

| IFAIL | 0 | 2 |
|---|---|---|
| Norm of residual | 0.2889E-12 | 0.1118E-8 |
| LHS of condition (4.1) | 0.1657E-8 | 0.3657E-8 |

TABLE 4.14: OPTIMALITY PARAMETERS FROM OPTIMIZATION ATTEMPTS OF TABLES 4.2 AND 4.13, ON EXIT FROM EO4UAF

alarming, bearing in mind that the specified accuracy of the solution defined by XTOL has little practical significance. For practical purposes setting XTOL in the range of 10E-5 to 10E-8 should be quite adequate.

The values of the design variables, before and after optimization, for the optimization attempt described in Table 4.13 are shown in Table 4.15. They indicate that the algorithm increased the isolator stiffnesses in order to satisfy the constraints but brought the isolators closer to the power train mass centre as can be observed in Figure 4.10. The kinetic energy modal distributions for the optimum isolation system, given in Table 4.16, indicate that the roll mode has been moved towards the lower end of the rigid-power train frequency spectrum.

Finally the dynamic behaviour of the optimum isolation system, superimposed on that of the original system, is presented in Figures 4.11 to 4.17 for the purpose of comparison. The discontinuous vertical line on all the plots marks the engine idling speed which is

| DESIGN VARIABLES | BEFORE OPTIMIZATION | AFTER OPTIMIZATION |
|---|---|---|
| Stiffness KX1 | 418 N/mm | 750 N/mm |
| Stiffness KY1 | 132 N/mm | 500 N/mm |
| Stiffness Kz1 | 165 N/mm | 400 N/mm |
| Position X1 | 124 mm | 82 mm |
| Position Y1 | 292 mm | 399 mm |
| Position Z1 | 81 mm | 88 mm |
| Orientation FI1 | 0 Degrees | 10 Degrees |
| Orientation THETA1 | 0 Degrees | -10 Degrees |
| Orientation PSI1 | 0 Degrees | 10 Degrees |
| Stiffness KX2 | 288 N/mm | 500 N/mm |
| Stiffness KY2 | 77 N/mm | 70 N/mm |
| Stiffness Kz2 | 226 N/mm | 400 N/mm |
| Position X2 | 308 mm | 242 mm |
| Position Y2 | -279 mm | -248 mm |
| Position Z2 | -292 mm | -26 mm |
| Orientation FI2 | 0 Degrees | 0 Degrees |
| Orientation THETA2 | 0 Degrees | 10 Degrees |
| Orientation PSI2 | 0 Degrees | 10 Degrees |
| Stiffness KX3 | 288 N/mm | 108 N/mm |
| Stiffness KY3 | 77 N/mm | 234 N/mm |
| Stiffness Kz3 | 226 N/mm | 400 N/mm |
| Position X3 | -181 mm | -81 mm |
| Position Y3 | -303 mm | -244 mm |
| Position Z3 | -272 mm | -149 mm |
| Orientation FI3 | 0 Degrees | 0 Degrees |
| Orientation THETA3 | 0 Degrees | 10 Degrees |
| Orientation PSI3 | 0 Degrees | 0 Degrees |

Table 4.15 Original and final values of design variables from the optimization attempt described in table 4.13

| Frequency | X | Y | Z | XX | YY | ZZ | COUPL. |
|---|---|---|---|---|---|---|---|
| 1. 8.0 | 0.18 | 0.49 | 36.52 | 0.70 | 63.53 | 2.75 | -4.17 |
| 2. 10.0 | 1.63 | 94.42 | 2.85 | 0.00 | 0.28 | 1.08 | -0.26 |
| 3. 12.0 | 84.42 | 1.10 | 4.58 | 0.48 | 1.43 | 6.71 | 1.28 |
| 4. 14.7 | 3.36 | 3.62 | 55.22 | 4.15 | 31.54 | 3.56 | -1.45 |
| 5. 16.0 | 0.63 | 0.18 | 0.74 | 96.85 | 11.67 | 3.63 | -13.70 |
| 6. 20.3 | 9.80 | 0.19 | 0.04 | 0.36 | 0.04 | 88.40 | -1.17 |

TABLE 4.16: KINETIC ENERGY MODAL DISTRIBUTIONS FOR OPTIMUM ISOLATION SYSTEM

also the engine speed used for the optimization. From Figure 4.16 it can be seen that the optimum isolation system is more efficient at engine speeds in the range of 600 to 1600 rpm with the exception of the two peaks which appear at approximately 880 and 960 rpm respectively. These peaks are attributed to the response of the vertical and the pitch modes of vibration to the first harmonic of the excitation as can be deduced from Figure 4.12. At frequencies lower than 600 rpm and higher than 1600 rpm the optimum isolation system is found to be less efficient than the original isolation system. At high frequencies the response of the power train is controlled by its inertia and this is reflected by the decline of the mean square displacement curve where the two systems display almost identical behaviour. The deficiency of the optimum system at high frequencies is undoubtedly due to its having stiffer isolators than the original system. This means that if the level of vibration at high frequencies is to be kept as low as possible, then an upper bound of the isolators stiffnesses should be specified prior to optimization. If no other changes are made to the constraints then it is expected that the algorithm will have little choice but to place the isolators further away from the power train mass centre in order to retain feasibility of the solution. It can be appreciated that under such conditions the roll mode will, most likely, be shifted to a higher position in the rigid-power train frequency spectrum and effectively reduce the efficiency of the isolation system at engine idle. The efficiency of the isolation system below the operating frequency band is of no importance in assessing its overall performance although it gives some indication of its behaviour during engine starting. However, comparison of the two systems in the low frequency region (50-600 rpm) is inconclusive for this kind of assessment.

The dynamic response of the two isolation systems, to the 0.5 and the second order harmonics of the excitation are considered as a final check for the optimum solution. The dynamic response curves shown in Figure 4.13 suggest that overall the response of the two isolation systems to the second harmonic of the excitation is similar. However Figure 4.13 shows also that the response of the optimum system to the 0.5 harmonic of the excitation is generally smoother (less peaks) although the level of the response is generally equivalent for both systems.

It is believed that all the problems which were encountered during the development of the program and all those which emerged while testing the algorithm, have been reasonably analysed. No attempt has been made to discuss the various problems on a mathematical basis due to lack of sufficient mathematical background on optimization theory. Time limitations did not allow the acquisition of such knowledge and consequently the discussion has been limited to the practical, but certainly not unimportant, aspects of the problem.

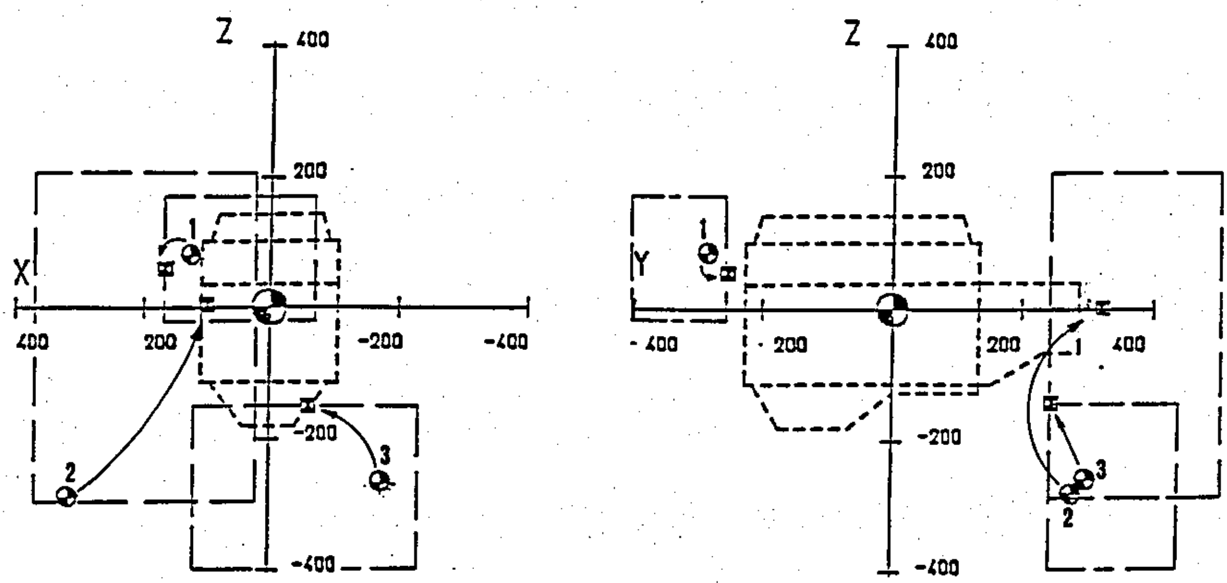


⊖---- Before Optimization

⊠----- After Optimization

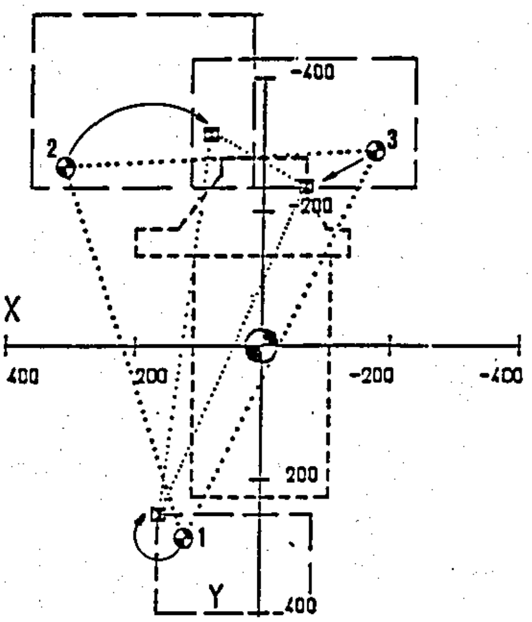


ENGINE DATA

| | | |
|---|---|---|
| TYPE | : | Ford four cylinder Diesel |
| Capacity | : | 1606 cc |
| Power | : | 40 KW |
| Maximum speed reduction of final drive | : | 12.827 |
| Mass | : | 197 Kg |

Inertia matrix :

$$\begin{bmatrix} 13.2 & 1.41 & 0.259 \\ 1.41 & 7.02 & -2.03 \\ 0.259 & -2.03 & 10.7 \end{bmatrix}$$

FIGURE 4.1: ENGINE-ISOLATOR LAYOUT BEFORE AND AFTER OPTIMIZATION (OUTPUT FILE RES4)

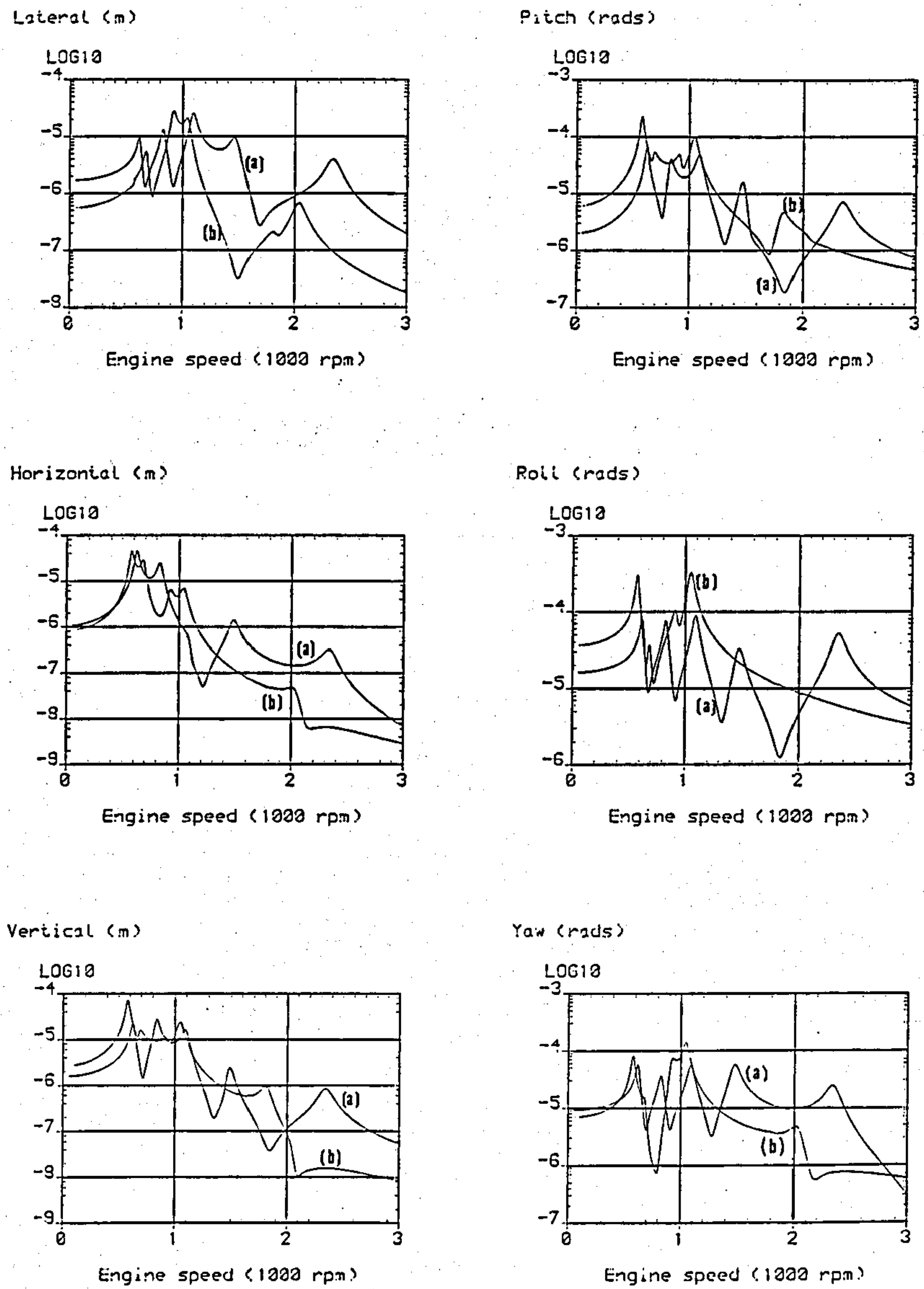


FIGURE 4.2: DYNAMIC RESPONSE OF POWER TRAIN MASS-CENTRE DUE TO THE ½ ORDER EXCITATION HARMONIC (OUTPUT FILE RES4):
(a) ORIGINAL, (b) OPTIMIZED

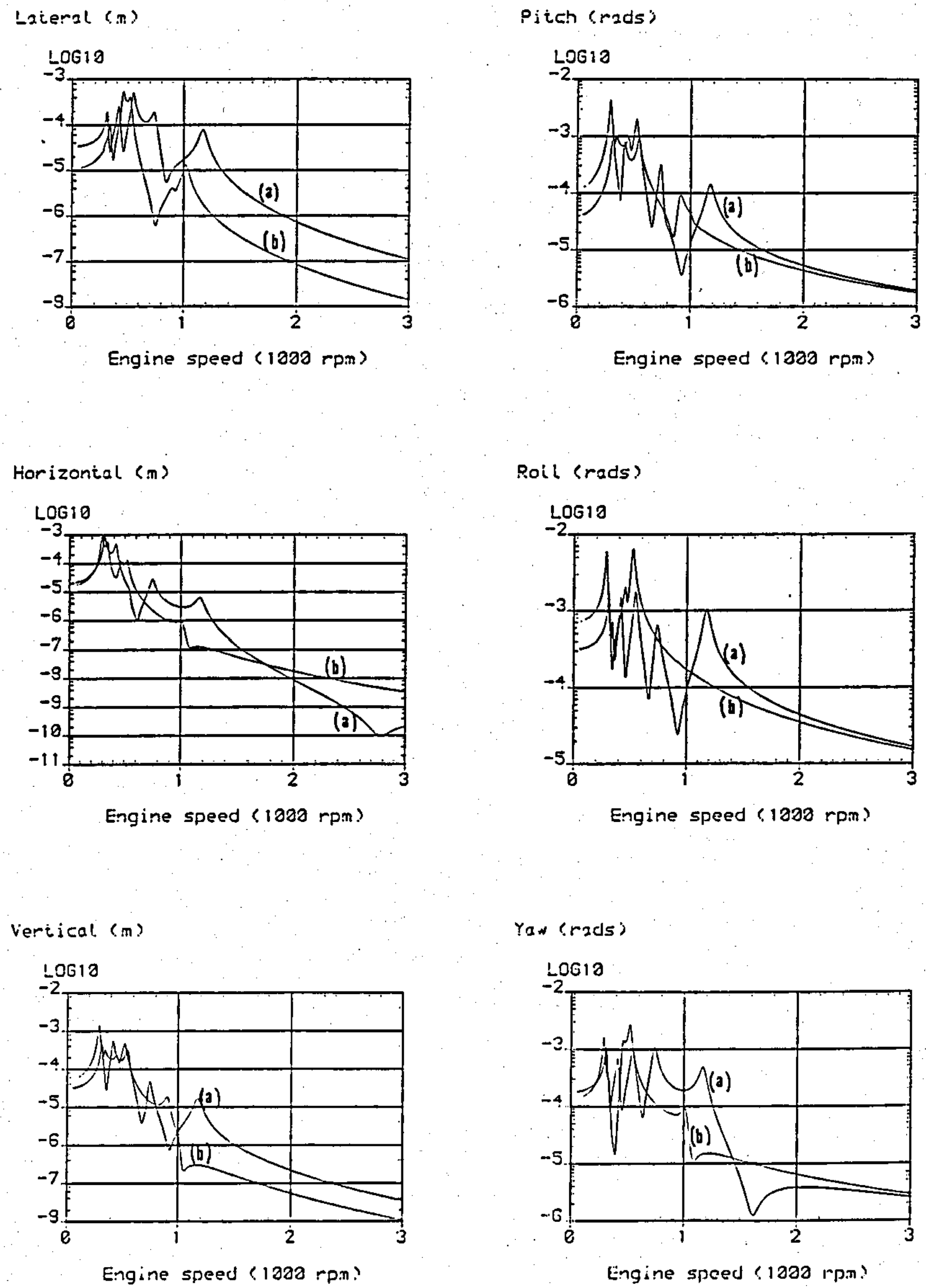


FIGURE 4.3: DYNAMIC RESPONSE OF POWER TRAIN MASS-CENTRE DUE TO THE FIRST ORDER EXCITATION HARMONIC (OUTPUT FILE RES4):
(a) ORIGINAL, (b) OPTIMIZED

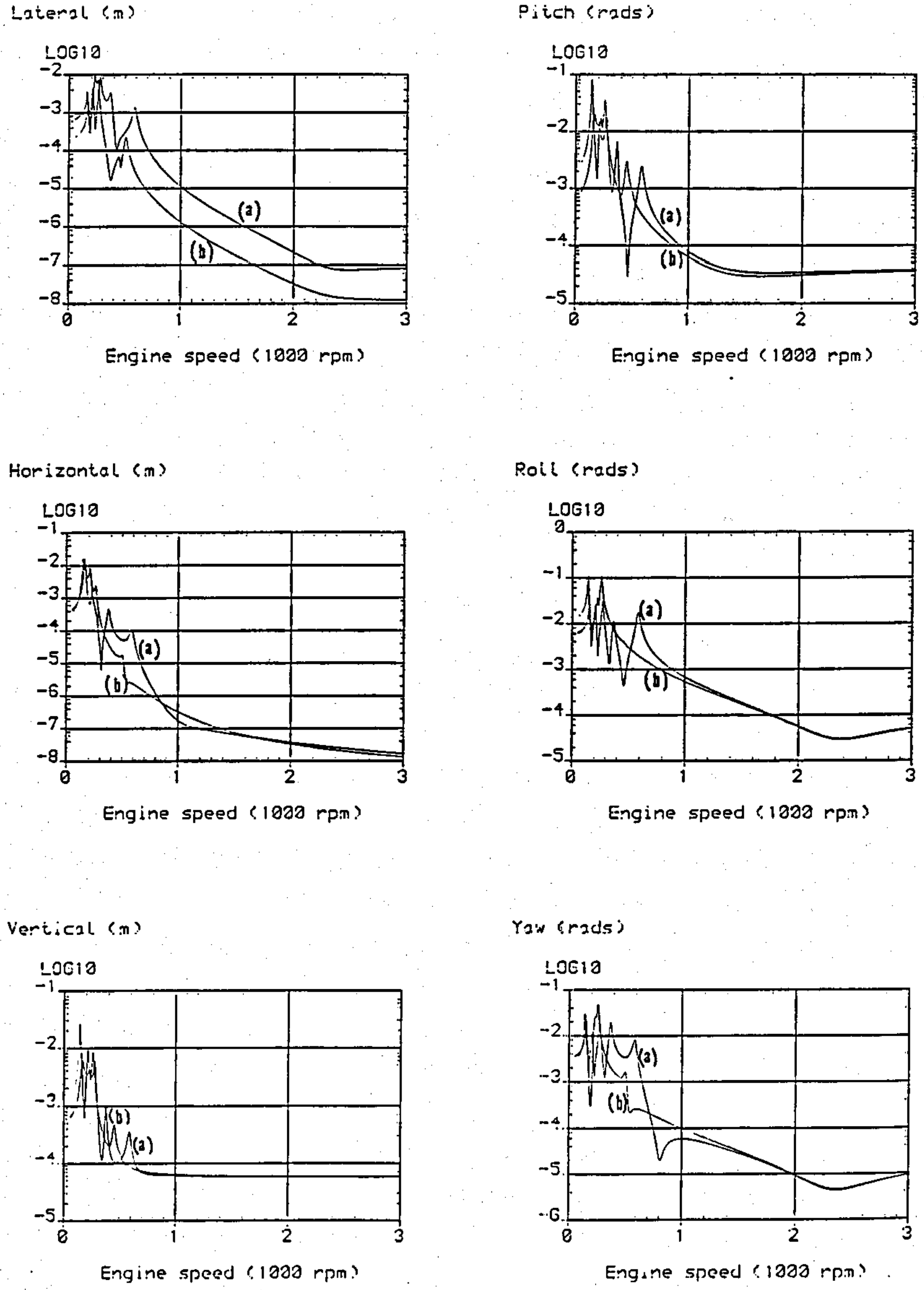


FIGURE 4.4: DYNAMIC RESPONSE OF POWER TRAIN MASS-CENTRE DUE TO THE SECOND ORDER EXCITATION HARMONIC (OUTPUT FILE RES4):
(a) ORIGINAL (b) OPTIMIZED

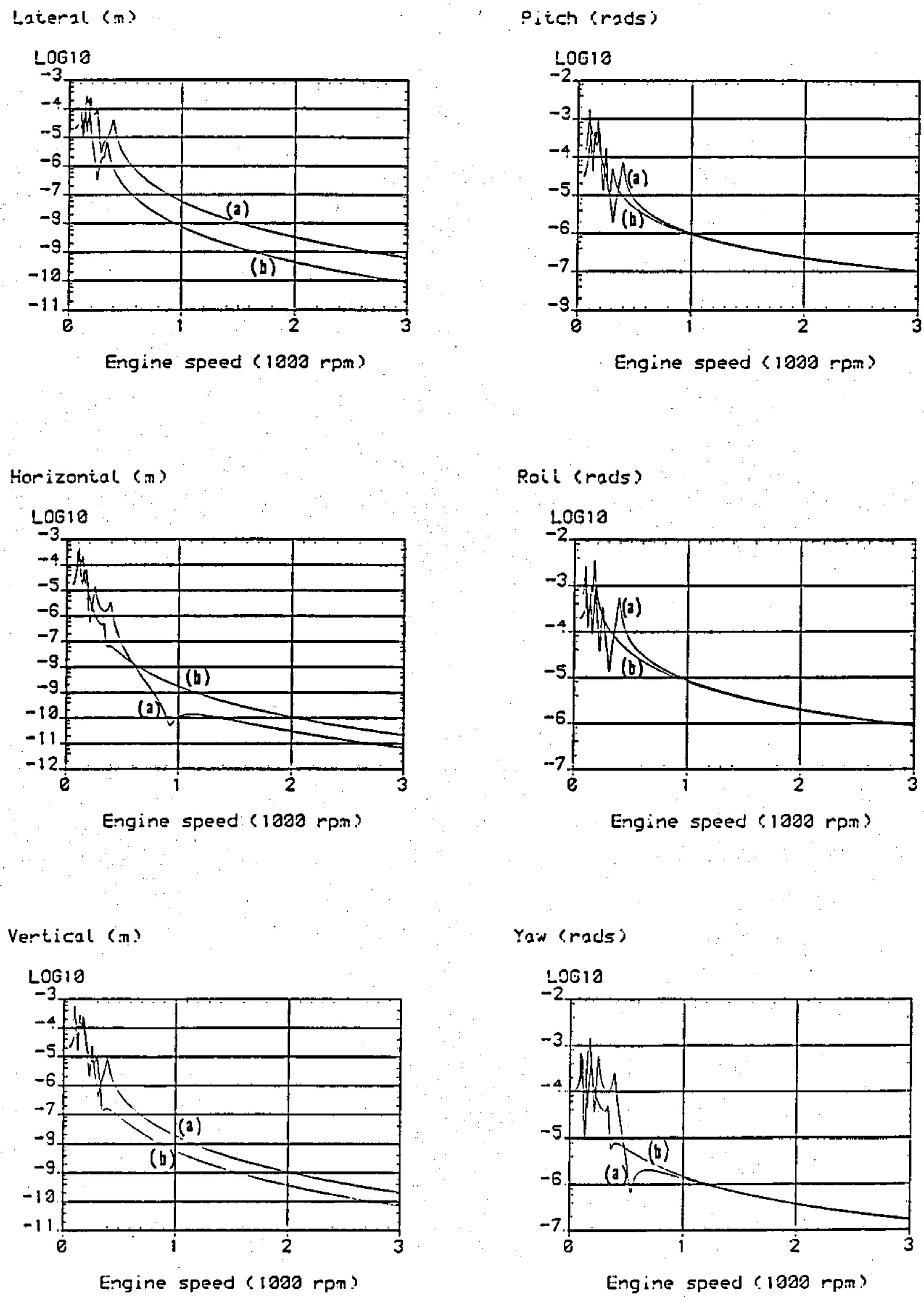


FIGURE 4.5: DYNAMIC RESPONSE OF POWER TRAIN MASS-CENTRE DUE TO THE THIRD ORDER EXCITATION HARMONIC (OUTPUT FILE RES4):
(a) ORIGINAL, (b) OPTIMIZED

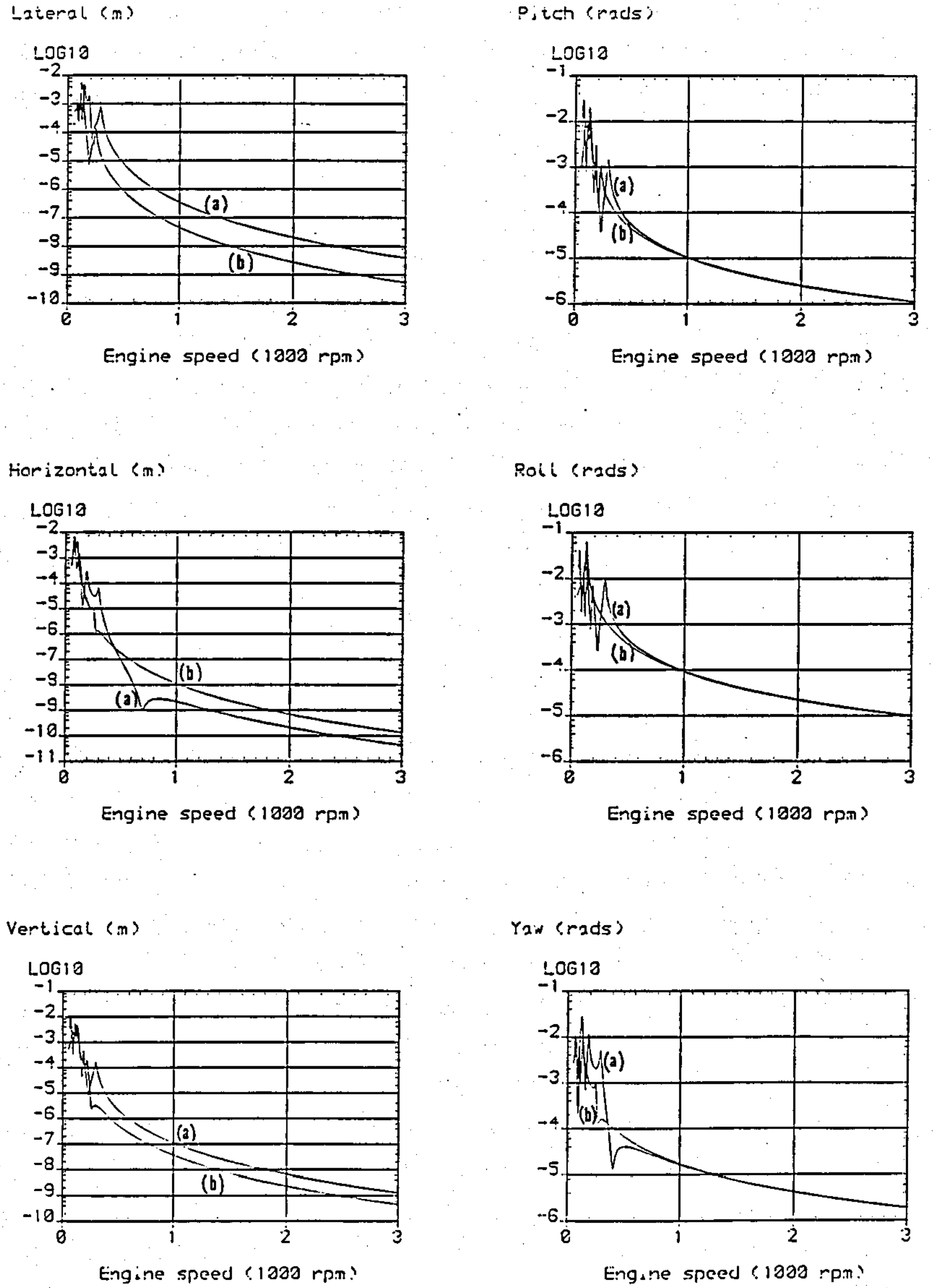


FIGURE 4.6: DYNAMIC RESPONSE OF POWER TRAIN MASS-CENTRE DUE TO THE FOURTH ORDER EXCITATION HARMONIC (OUTPUT FILE RES4):
(a) ORIGINAL, (b) OPTIZIZED

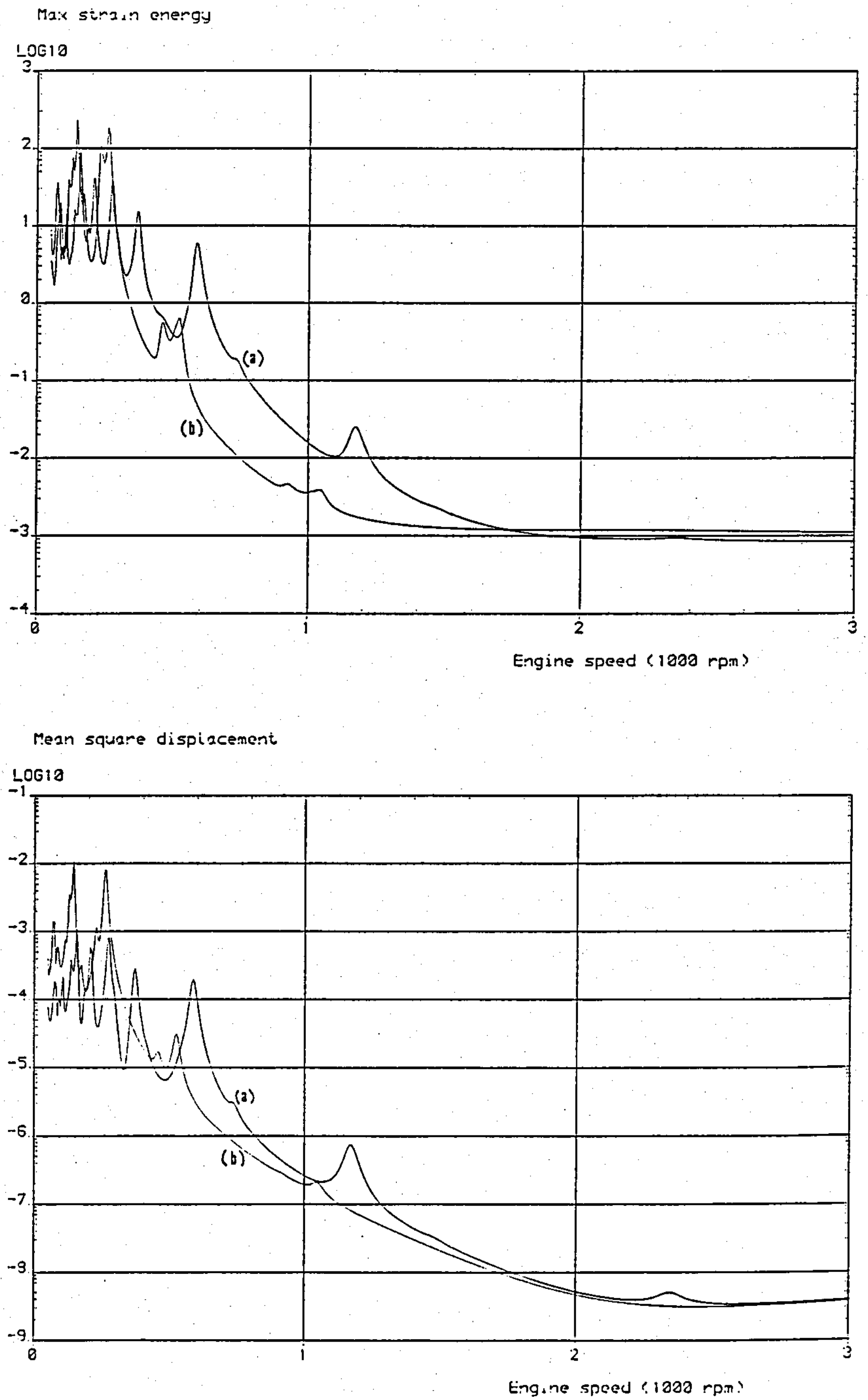


FIGURE 4.7: OPTIMIZATION FUNCTION AND MEAN SQUARE DISPLACEMENT
(OUTPUT FILE [illegible]) (a) ORIGINAL, (b) OPTIMIZED

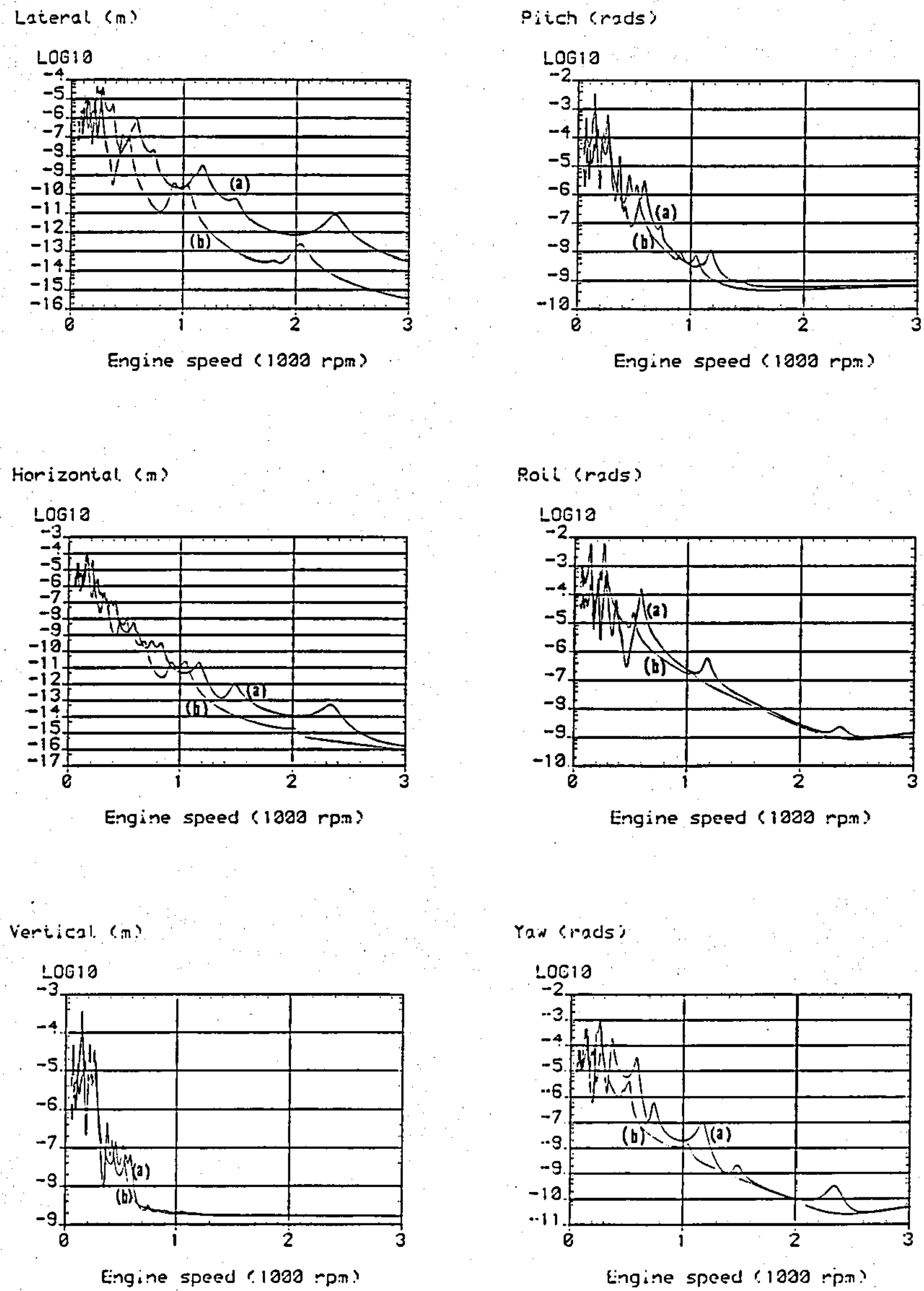


FIGURE 4.8: MEAN SQUARE RESPONSE OF POWER TRAIN MASS CENTRE (OUTPUT FILE RES4) (a) ORIGINAL, (b) OPTIMIZED

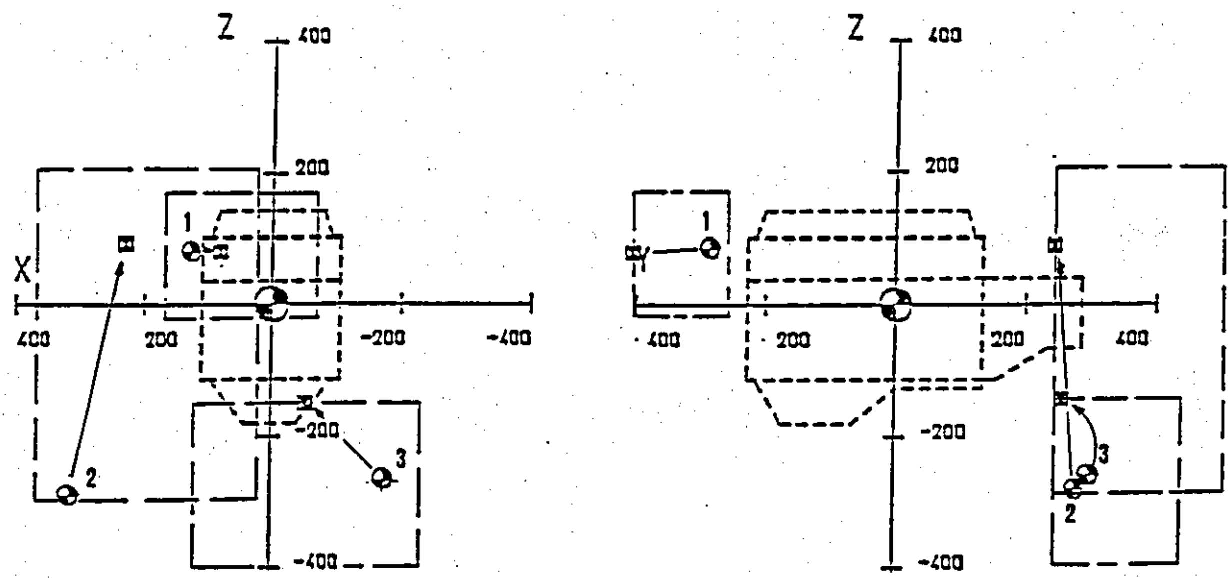


Before Optimization

After Optimization

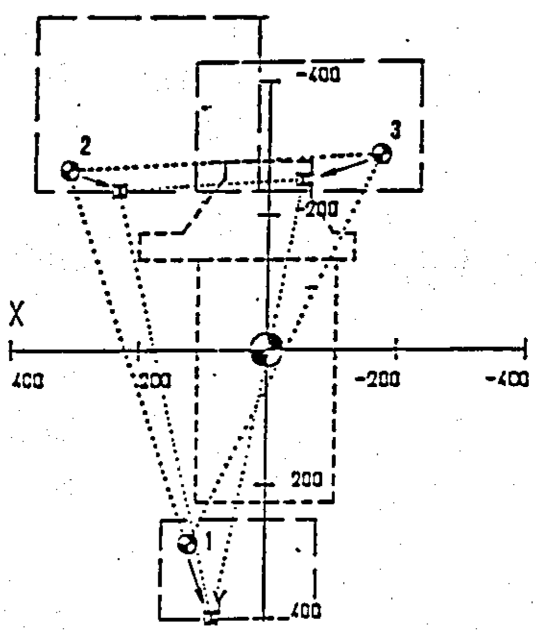


ENGINE DATA

| | | |
|---|---|---|
| TYPE | : | Ford four cylinder Diesel |
| Capacity | : | 1606 cc |
| Power | : | 40 KW |
| Maximum speed reduction of final drive | : | 12.827 |
| Mass | : | 197 Kg |

Inertia matrix :

$$\begin{bmatrix} 13.2 & 1.41 & 0.259 \\ 1.41 & 7.02 & -2.03 \\ 0.259 & -2.03 & 10.7 \end{bmatrix}$$

FIGURE 4.9: ENGINE-ISOLATOR RESPONSE OF POWER TRAIN MASS CENTRE
(OUTPUT FILE RES8)

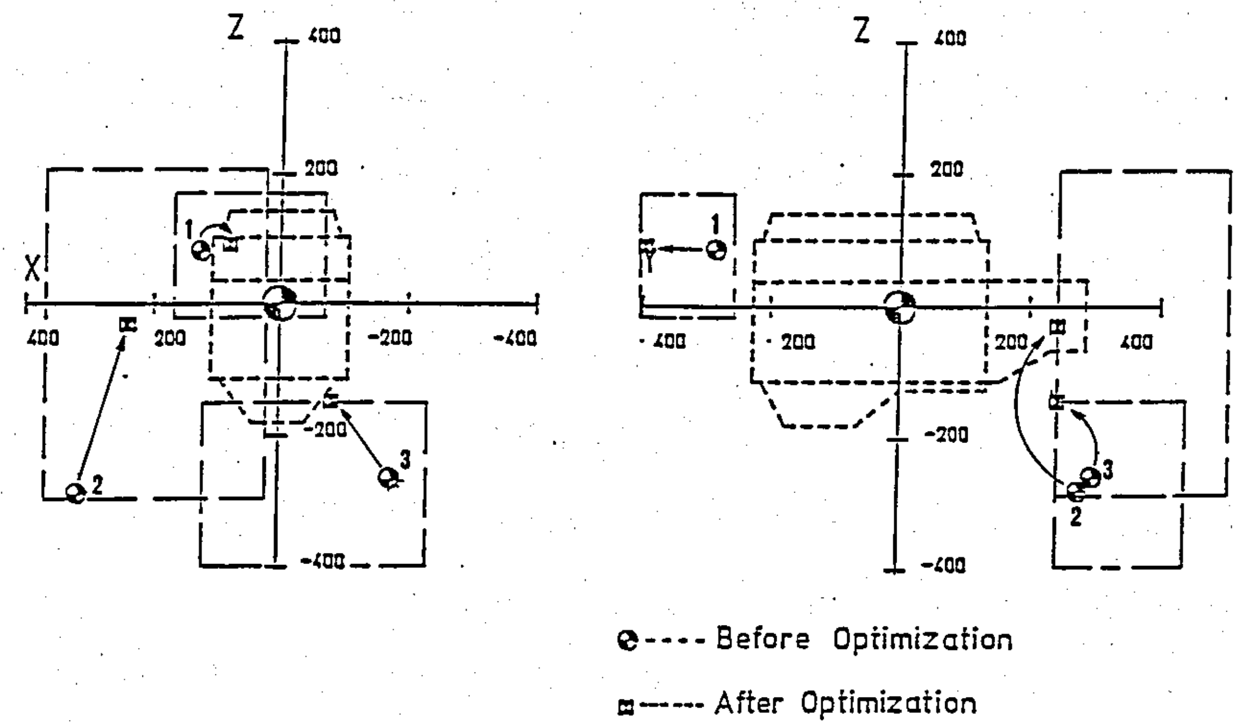


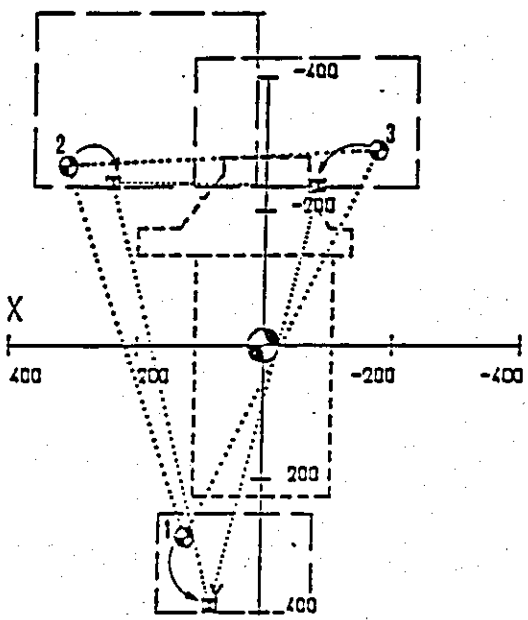


ENGINE DATA

| | | |
|---|---|---|
| TYPE | : | Ford four cylinder Diesel |
| Capacity | : | 1606 cc |
| Power | : | 40 KW |
| Maximum speed reduction of final drive | : | 12.827 |
| Mass | : | 197 Kg |

Inertia matrix .
$$\begin{bmatrix} 13.2 & 1.41 & 0.259 \\ 1.41 & 7.02 & -2.03 \\ 0.259 & -2.03 & 10.7 \end{bmatrix}$$

FIGURE 4.10: ENGINE-ISOLATOR RESPONSE OF POWER TRAIN MASS CENTRE
(OUTPUT FILE RES9)

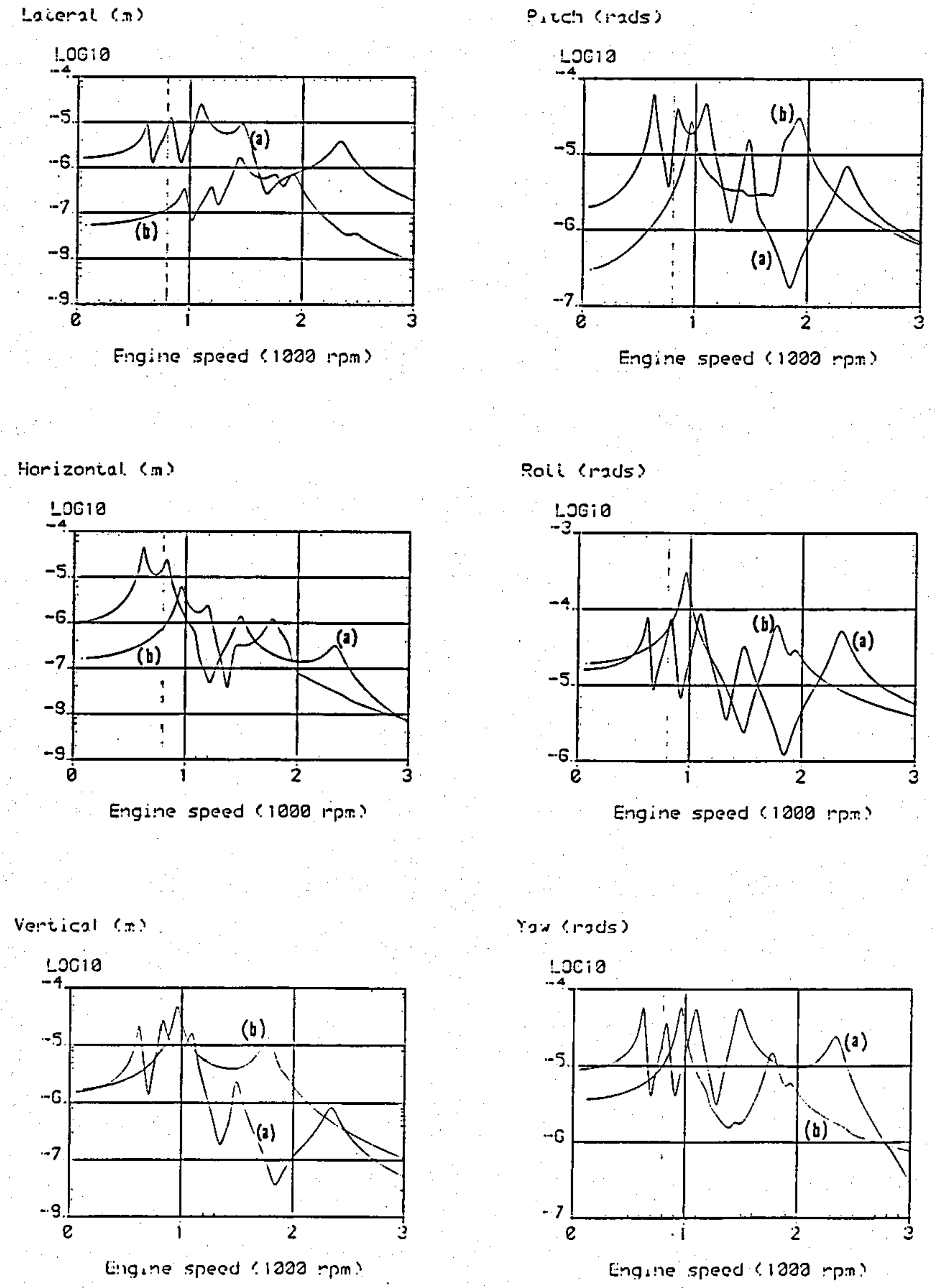


FIGURE 4.11: DYNAMIC RESPONSE OF POWER TRAIN MASS CENTRE DUE TO THE ½ ORDER EXCITATION HARMONIC (OUTPUT FILE RES9)
(a) ORIGINAL, (b) OPTIMIZED

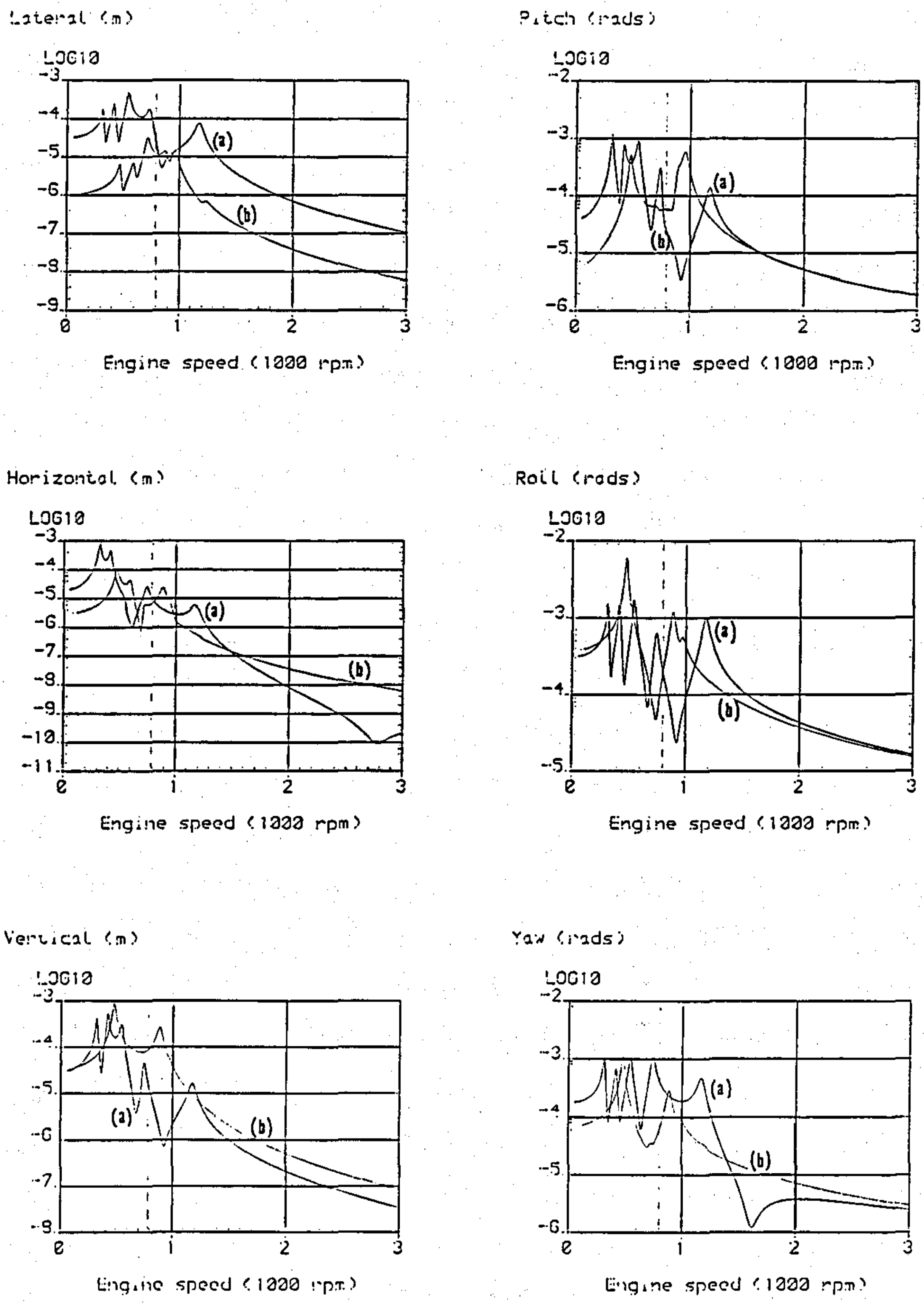


FIGURE 4.12: DYNAMIC RESPONSE OF POWER TRAIN MASS CENTRE DUE TO THE FIRST ORDER EXCITATION HARMONIC (OUTPUT FILE RES9)
(a) ORIGINAL, (b) OPTIMIZED

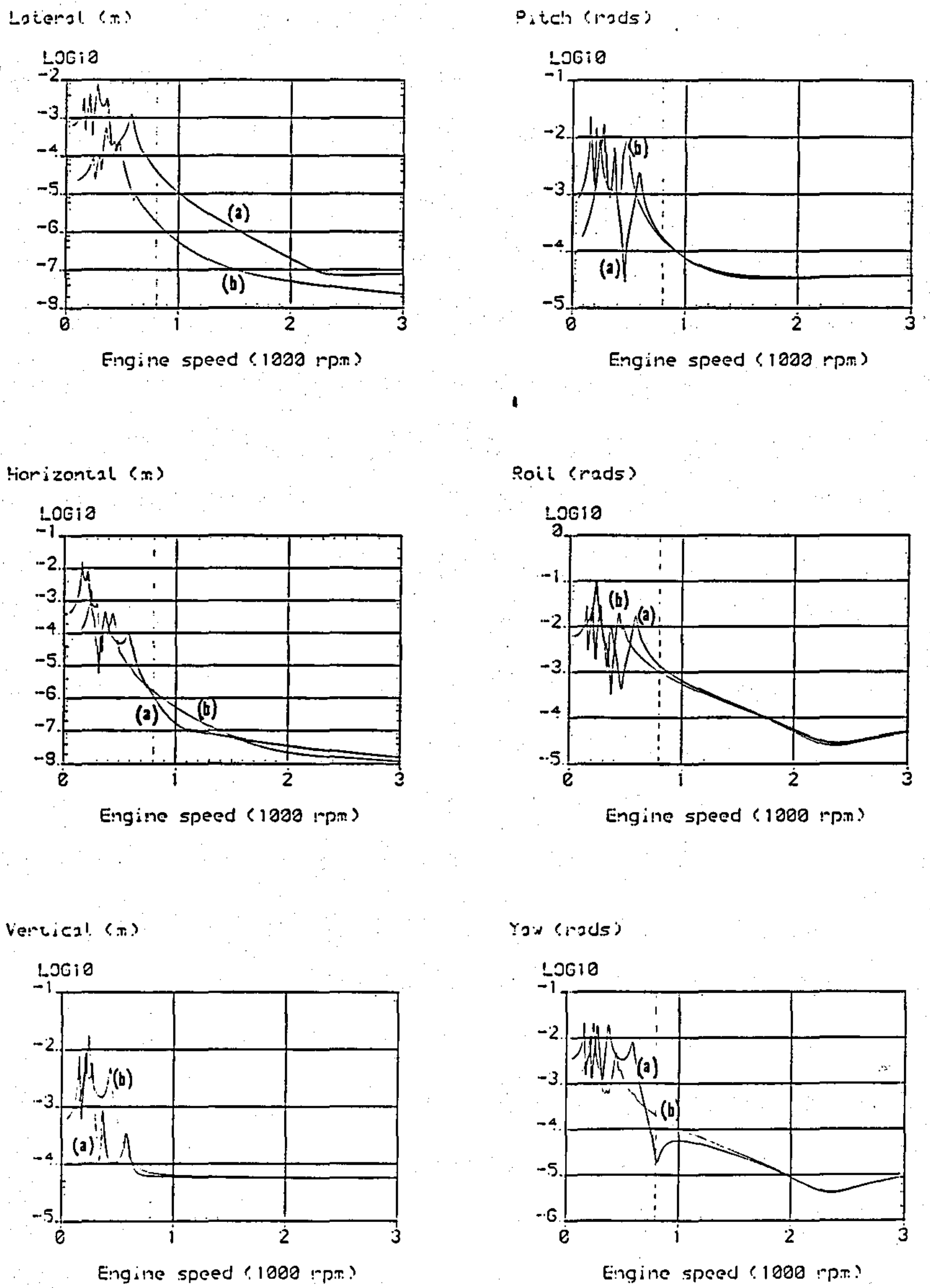


FIGURE 4.13: DYNAMIC RESPONSE OF POWER TRAIN MASS CENTRE DUE TO THE SECOND ORDER EXCITATION HARMONIC (OUTPUT FILE RES9)
(a) ORIGINAL, (b) OPTIMIZED

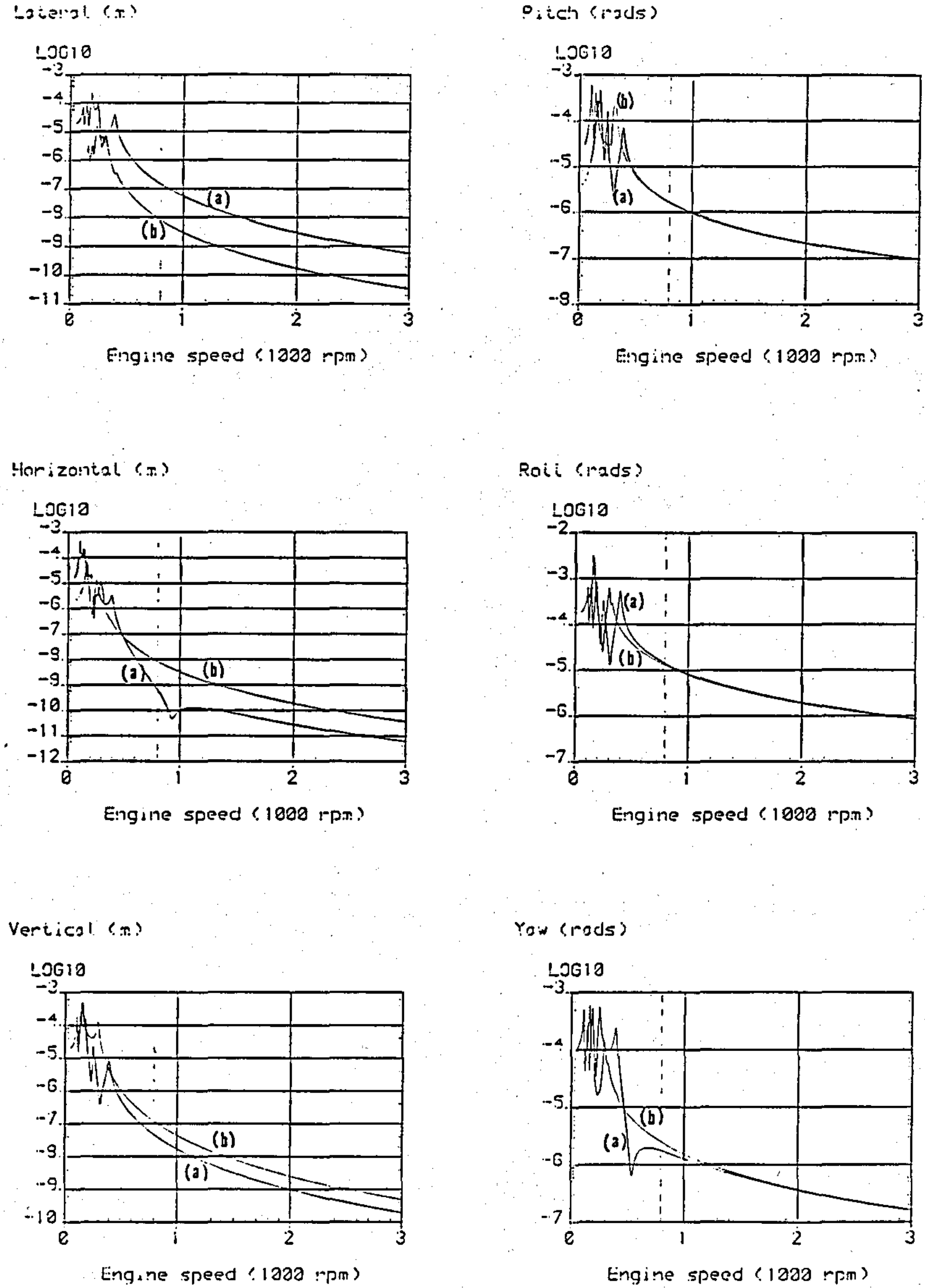


FIGURE 4.14: DYNAMIC RESPONSE OF POWER TRAIN MASS CENTRE DUE TO THE THIRD ORDER EXCITATION HARMONIC (OUTPUT FILE RES9)
(a) ORIGINAL, (b) OPTIMIZED

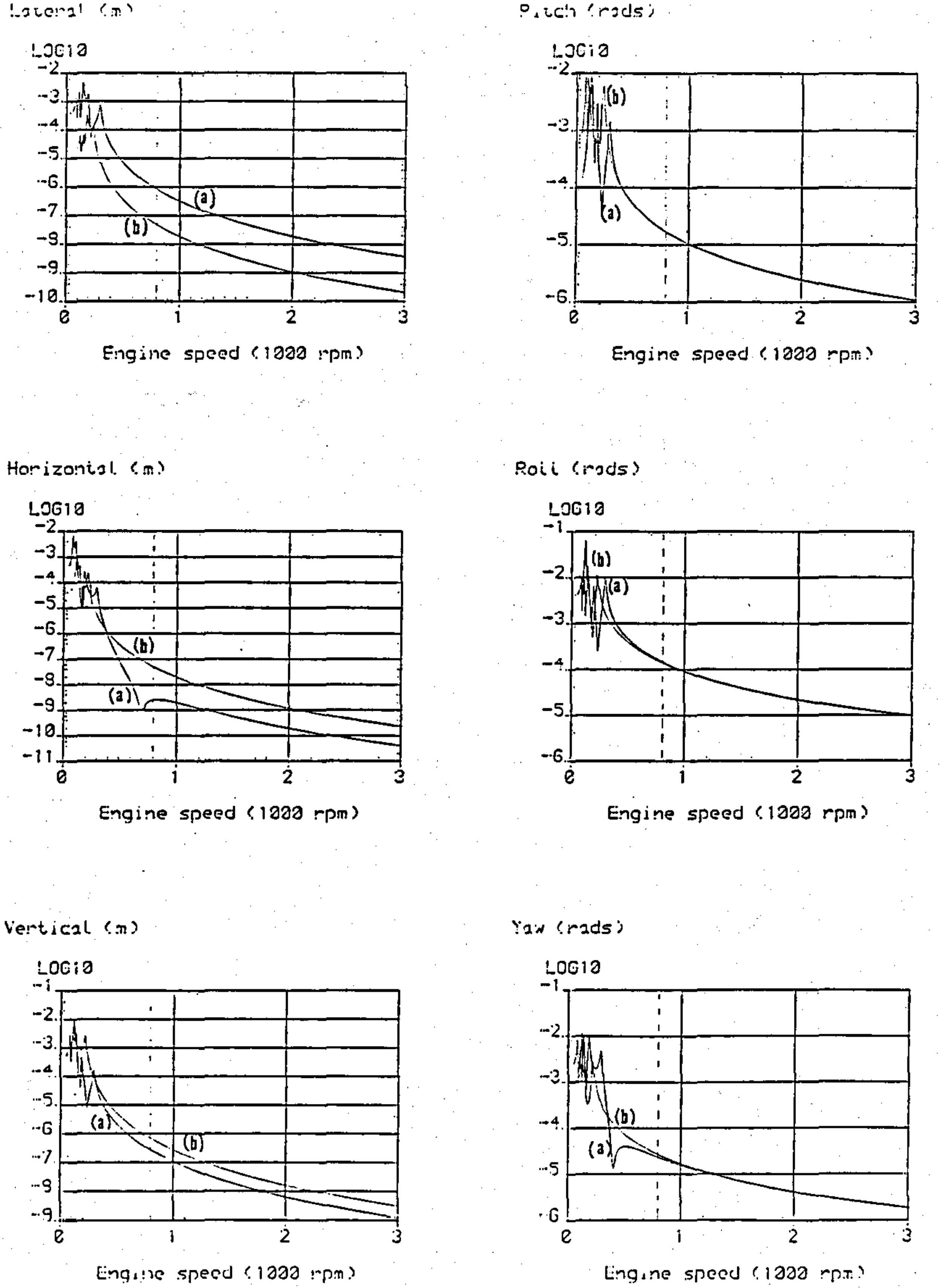


FIGURE 4.15: DYNAMIC RESPONSE OF POWER TRAIN MASS CENTRE DUE TO THE FOURTH ORDER EXCITATION HARMONIC (OUTPUT FILE RES9)
(a) ORIGINAL, (b) OPTIMIZED

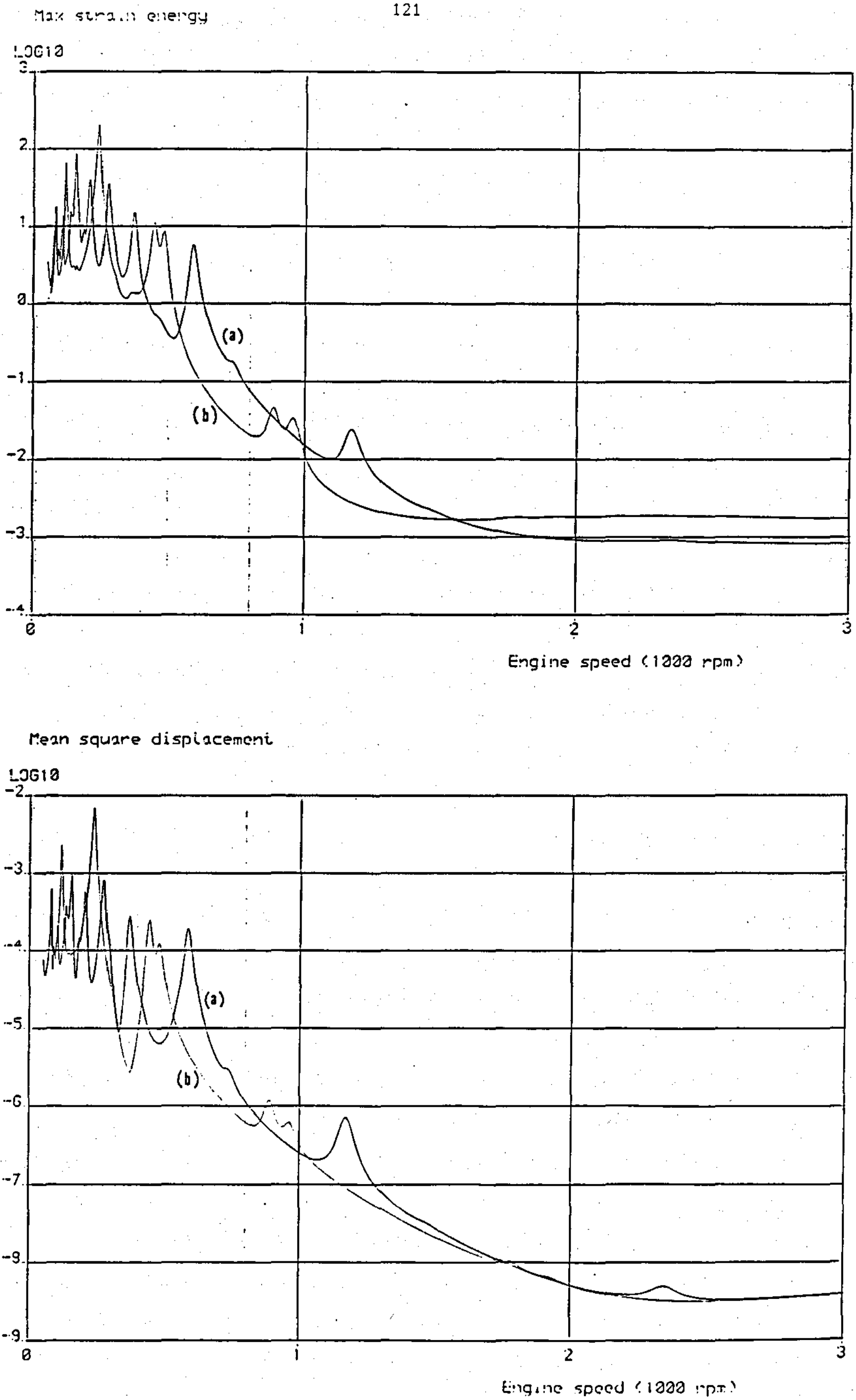


FIGURE 4.16: OPTIMIZATION FUNCTION AND MEAN SQUARE DISPLACEMENT (OUTPUT FILE RES9). (a) ORIGINAL, (b) OPTIMIZED

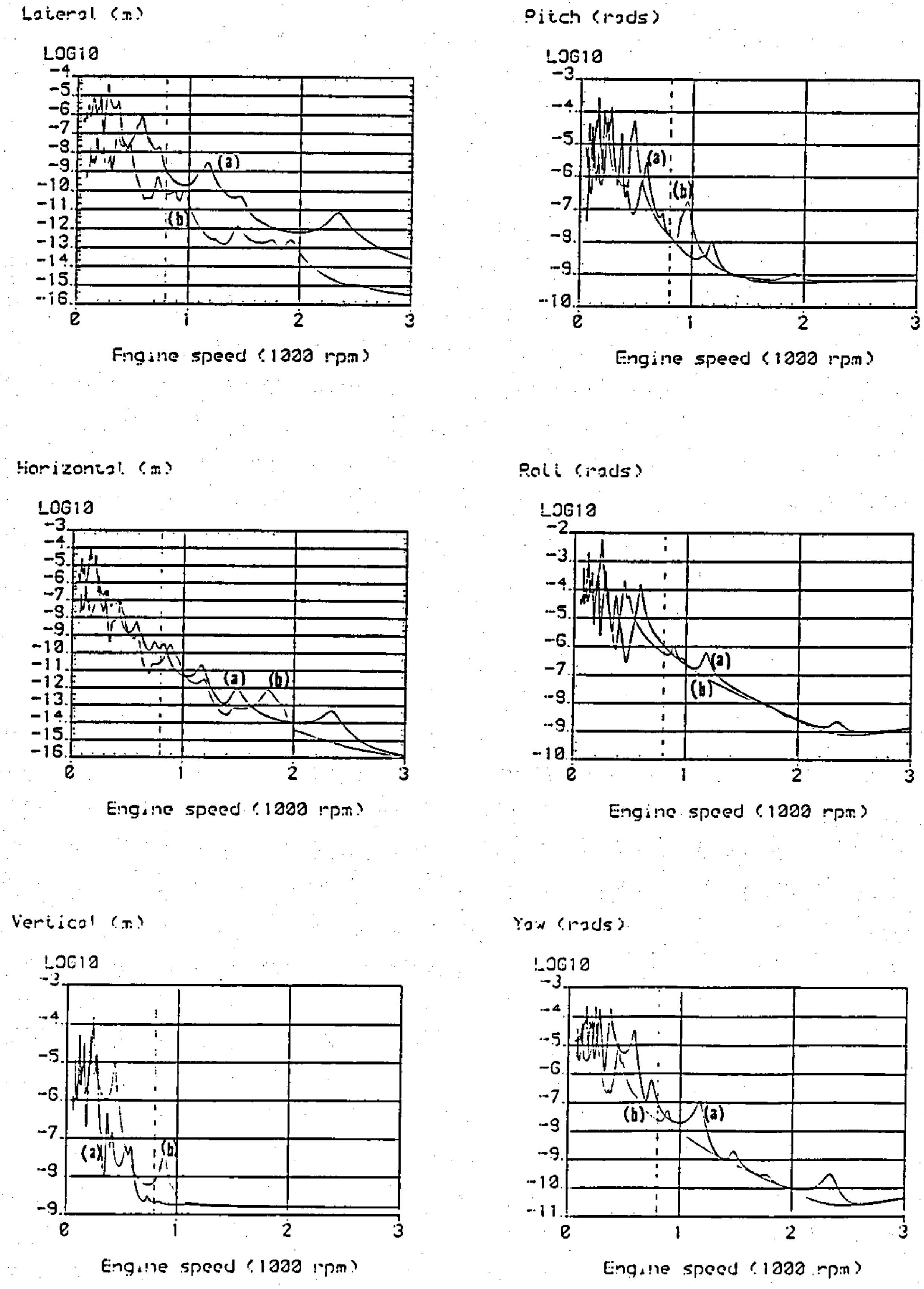


FIGURE 4.17: MEAN SQUARE RESPONSE OF POWER TRAIN MASS CENTRE (OUTPUT FILE RES9). (a) ORIGINAL, (b) OPTIMIZED

# CHAPTER 5

## SUMMARY AND CONCLUSIONS

It was demonstrated in the previous chapter that the program can successfully carry out all the optimization objectives which were set i.e. minimize the objective function while satisfying all the constraints. It was further shown that the numerical algorithm achieved a local minimum of the objective function in a fairly traditional engineering way. That is by moving the isolators closer to the engine mass centre (X-direction) and consequently reducing the roll mode frequency. In fact these changes are performed in the first few iterations while the rest of the computing time is associated with changes that ensure satisfaction of the constraints to the specified tolerance and further search of the local design space for a "better" minimum. Had the specified tolerance been reduced to the value suggested in Chapter 4 then it is expected that the computing time would be reduced considerably.

It would seem that this new approach to optimization of isolation systems has two main advantages over the methods used in the past. The objective function is defined in terms of a quantity which is directly related to force transmission into the chassis, referred to as the maximum strain energy of the dynamic system (see Section 3.2), and the static requirements are incorporated in terms of constraints on the deflection of the isolators and engine rotations, as discussed in Sections 2.4 and 3.2. The main benefit which emerges from this definition of the objective function is that there are no implied constraints on the formation of the stiffness matrix other than those imposed by the static requirements. The final result may also be directly interpreted in terms of isolation efficiency in contrast to other methods where either some form of modal decoupling or spectral penalty function is used. Such methods produce no immediate evidence of the isolation efficiency of the system obtained from the optimization process.

Unfortunately time limitations did not allow the dynamic model to be generalized. It suffers, in its present form, from lack of a non-linear static analysis of the isolators deflections (discussed in Section 2.5) and a lack of consideration of road input excitation (engine shake). With respect to the former it was shown in Section 2.5 that the problem can be adequately solved with the minimum of alterations to the computer program. Frequency constraints were introduced as a remedy to the problem of separating engine vibration from engine shake. However, frequency constraints are regarded as arbitrary constraints on the design space and consequently freedom constraints on the optimization algorithm. It is strongly believed that it would be far more sensible to change the model into one which includes a simple model of the vehicle suspension and indeed that would be the author's reaction had time permitted it.

Another area of concern remains that of the definition of the static constraints. This is due to the fact that in many optimization attempts it was observed that the position of the isolators for the optimum isolation system defined a triangular base on the X-Y plane which did not enclose the power train mass centre. This point was discussed in Chapter 4 and formed one of the acceptance criteria for the optimum isolation system. The question that remains is whether additional constraints are required to make the algorithm aware of this standard engineering practice or whether a completely different definition of the static requirements is needed.

Carefully selecting the upper and lower bounds for the position of each isolator is one way of solving the problem, but again not an entirely acceptance one. Optimization algorithms are powerful tools and should be utilized to the maximum of their potential.

Finally there remains the subject of scaling which was extensively discussed in Chapter 5. It is quite clear to the author, and it is anticipated that it will be equally clear to the reader by now, that scaling is a critical factor on the presentation of the physical problem to the numerical optimization algorithm. Numerical decisions are not based on engineering judgement and what is required is the engineer's adaptation to the numerical thinking of an optimization routine. Acquisition of theoretical background on basic numerical optimization literature is necessary but not sufficient at all times. Most of the author's time was spen~~d~~ on relating the acquired t theoretical background to the behaviour of the selected routine and redesigning the presentation of the problem for numerical stability. It is hoped that the discussion on the numerical aspect of the optimization problem will provide future investigators with useful guidelines.

# REFERENCES


1. Crede, C.E.
   Vibration and Shock Isolation, John Wiley and Sons, New York (1951).

2. Horovitz, M.
   "Suspension of Internal-combustion Engines in Vehicles", Proc. IMechE (AD), No. 1 (1957-58) pp 17-35.

3. Wilson, W.K.
   Vibration Engineering - a Practical Treatise on the Balancing of Engines, Mechanical Vibration and Vibration Isolation.

4. Bolton-Knight, B.L.
   "Engine Mounts: Analytical Methods to Reduce Noise and Vibration", IMechE (1971).

5. Lee, M.K.
   "An Analytical Study of the Vibration Isolation of a Reciprocating Engine from a Rigid Foundation", MSc Thesis, Loughborough University of Technology, England (1977).

6. Zibelo, D. and Thompson, F.M.
   "POEM - A Computer-Assisted Procedure for Optimizing Elastomeric Mountings", SAE Paper No. 710057 (1970).

7. Johnson, R.S.
   "Computer Optimization of Engine Mounting Systems", SAE Paper No. 790974 (1979).

8. Starkey, John Mark.
   "Redesign Techniques for Improved Structural Dynamics", PhD Thesis, Michigan State University USA (1982).

9. Geck, P.E. and Patton, R.D.
"Front Wheel Drive Engine Mount Optimization", SAE Paper 800432 (1984).

10. Spencer, P.A., Phillips, A.V. and Bharj, T.
Ford Motor Company, Private communications.

11. Greenwood, D.T.
Principles of Dynamics, Prentice-Hall Inc., Eaglewood Cliffs, New Jersey (1965).

12. Smollen, E.L.
"Generalized Matrix Methods for the Design and Analysis of Vibration-Isolation Systems", The Journal of the Acoustical Society of America, 40, pp 195-204 (1966).

13. Synge, J.L. and Griffith,. B.A.
Principles of Mechanics, McGraw-Hill (1970).

14. Biezeno, C.B. and Grammel, R.
Engineering Dynamics, Volume IV, Blackie and Son Ltd., London (1954).

15. Taylor, C.F.
The Internal Combustion Engine in Theory and Practice, Volume II, the MIT Press (1968).

16. Shigley, J.E. and Vicker, J.J.
Theory of Machines and Mechanisms, McGraw Hill (1980).

17. Bishop, R.E.D., Gladwell, G.M.L. and Michaelson, S.
The Matrix Analysis of Vibration,. Cambridge (1965).

18. Johnson, S.R. and Subhedar, J.W.
"Computer Optimization of Engine Mounting Systems", SAE Paper No. 790974 (1979).

19. Ragsdell, K.M.
"Optimization as a Tool for Automotive Design", SAE Paper 800432 (1980).

20. Lev, Ovadia E.
Structural Optimization: Recent Developments and Applications, The American Society of Civil Engineers (1981).

21. Gill, E.P., Murray, W. and Wright, M.H.
Practical Optimization, Academic Press (1981).

22. Luenberger, D.G.
Linear and Nonlinear Programming, Addison-Wesley Publishing Company (1984).

23. Numerical Algorithms Group
FORTRAN Library Manual, Mark 8, Volume 3, E04 (1981).

24. Milne, E.A.
Vectorial Mechanics, Methuen and Co. Ltd., London (1948).

# APPENDIX A

## INTERNALLY GENERATED FORCES IN MULTI-CYLINDER ENGINES

For the purpose of calculating inertia forces it is generally accepted that the distributed mass of the crank mechanism of Figure A.1 can be approximated by two concentrated masses, namely a reciprocating mass ($m_{rec}$) at the gudgeon pin and a rotating mass ($m_{rot}$) at the crank pin. Using a two mass-element approximation for the con-rod and the crank, based on the assumption that the sum of the masses of the elements equals the distributed mass of the link and that there is zero moment about the mass centre of the link, it can be shown that:

$$m_{rec} = m_p + \frac{l_1}{l} m_r \tag{A.1}$$

$$m_{rot} = m_c \frac{r_1}{r} + \frac{l_1}{l} m_r \tag{A.2}$$

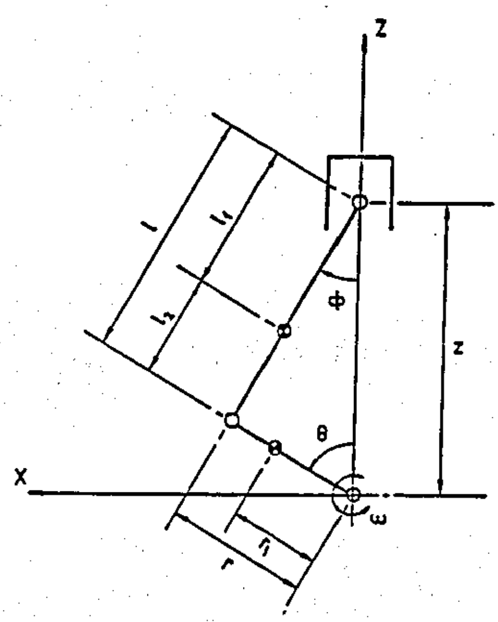


FIGURE A.1: SINGLE CYLINDER CRANK-MECHANISM where $m_p$, $m_r$, $m_c$ denote the mass of the piston, connecting rod and crank respectively.

Kinematic analysis of the mechanism shows that the piston displacement can be expressed as an infinite series in terms of the crank rotation ($\theta$) and the ratio of the crank radius to the con-rod length $\lambda$ (= r/L). Usually this ratio falls in the range 0.17 to 0.4 and the common practice is to ignore second order terms in $\lambda$ from the kinematic expressions. The complete expression for the piston displacement is given in reference [14] as

$$\frac{Z}{r} = A_o + \cos\theta + \sum_{j=1}^{\infty} (-1)^{j-1} \frac{A_{2j}}{4j^2} \cos 2j\theta$$

where (A.3)

$$A_{2j} = 4j^2 \sum_{k=j}^{\infty} (-1)^{k-1} [\frac{\frac{1}{2}}{k}] [\frac{2k}{k-j}] (\frac{\lambda}{2})^{2k-1}, \quad j = 1,2,\ldots$$

However, for the purpose of this work a sufficiently accurate expression is given in reference [16] as

$$\frac{Z}{r} = (\frac{1}{\lambda} - \frac{\lambda}{4}) + \cos\theta + \frac{\lambda}{4} \cos 2\theta \qquad (A.4)$$

Differentiating equation (A.4) twice will give the acceleration of the reciprocating mass while the acceleration of the rotating mass is simply $r\omega^2$ assuming constant engine speed. For the single cylinder engine the reciprocating mass will generate a vertical force on the frame and a torque about the crankshaft while the rotating mass will generate a vertical and a lateral force on the engine frame.

The cylinder gas pressure due to combustion generates a torque about the crankshaft which can be expressed as a Fourier series in the crank angle by

$$T_c = b_o + \sum_i a_i \sin(i\theta) + \sum_i b_i \cos(i\theta) \qquad (A.5)$$

For four-cycle engines where a cycle is completed in two revolutions of the crank, half as well as integer orders appear in the Fourier series and hence $i = \frac{1}{2}, 1, 1\frac{1}{2}, \ldots$

For a single cylinder engine the forces and moments exerted on the frame due to both inertia and combustion forces are given by equations (A.6) to (A.11)

$$F_x = m_{rot}\, r\omega^2 \sin\theta \qquad (A.6)$$

$$F_y = 0 \qquad (A.7)$$

$$F_z = r\omega^2 [m_{rot} \cos\theta + m_{rec} (\cos\theta + \lambda\cos 2\theta)] \qquad (A.8)$$

$$M_x = 0 \qquad (A.9)$$

$$M_y = 0 \qquad (A.10)$$

$$M_z = -m_{rec}\, r^2\omega^2 \left[\frac{\lambda}{4} \sin\theta - \frac{1}{2} \sin 2\theta - \frac{3\lambda}{4} \sin 3\theta\right] - - \sum_i a_i \sin(i\theta) - \sum_i b_i \cos(i\theta) \qquad (A.11)$$

The coefficient $b_o$ has been ignored in equation (A.11) for the reason that it represents the mean static torque and hence does not affect the dynamnic response of the engine.

The multicylinder crank arrangement is illustrated in Figure A.2. A set of axes is fixed at the crankshaft centre with the Z axis along the cylinder centre line, the Y axis along the crankshaft centre line and the X axis in the fore/aft direction to form a right hand system.

The forces and moments defined by equations (A.6) to (A.11) are applied to each cylinber, taking into account the crank-angle spacing and the firing order, and the individual cylinder forces are then added algebraically to give the individual resultants at the crank centre.

If the crank angle of the $i^{th}$ cylinder is $\omega t + \theta_i$ and the cylinder spacing is $d_i$, then with reference to Figure A.2 the forces at the crank centre for the n-cylinder engine can be expressed as follows:

$$F_x = m_{rot}\, r\omega^2 \, \mathrm{Im}\, [\sum_{i=1}^{n} e^{i(\omega t+\theta_i)}] \quad (A.12)$$

$$F_y = 0 \quad (A.13)$$

$$F_z = (m_{rot} + m_{rec})\, r\omega^2 \, \mathrm{Re}[\sum_{i=1}^{n} e^{j(\omega t+\theta_i)}] + \\ + m_{rec}\, r\omega^2 \, \mathrm{Re}\, [\lambda \sum_{i=1}^{n} e^{j2(\omega t+\theta_i)}] \quad (A.14)$$

$$M_x = -(m_{rot} + m_{rec})\, r\omega^2 \, \mathrm{Re}\, [\sum_{i=1}^{n} d_i\, e^{j(\omega t+\theta_i)}] - \\ - m_{rec}\, r\omega^2 \, \mathrm{Re}\, [\lambda \sum_{i=1}^{n} d_i\, e^{j2(\omega t+\theta_i)}] \quad (A.15)$$

$$M_y = m_{rot}\, r\omega^2 \, \mathrm{Im}\, [\sum_{i=1}^{n} d_i\, e^{j(\omega t+\theta_i)}] \quad (A.16)$$

$$M_z = -m_{rec}\, r^2\omega^2 \, \mathrm{Im}\, [\frac{\lambda}{4} \sum_{i=1}^{n} e^{j(\omega t+\theta_i)} - \frac{1}{2} \sum_{i=1}^{n} e^{j2(\omega t+\theta_i)} - \\ - \frac{3\lambda}{4} \sum_{i=1}^{n} e^{j3(\omega t+\theta_i)}] - \{\sum_{k} a_k \, \mathrm{Im}\, [\sum_{i=1}^{n} e^{jk(\omega t+\theta_i)}] + \\ + \sum_{k} b_k \, \mathrm{Re}\, [\sum_{i=1}^{n} e^{jk(\omega t+\theta_i)}]\} \quad (A.17)$$

The terms in { } represent the gas pressure torque and are formulated under the assumption that the Fourier coefficients are obtained from gas pressure data measured at one cylinder only and that cylinder-to-cylinder pressures are identical. For real engines cylinder-to-cylinder pressure variations do exist and a better representation of the torque spectrum is obtained by flywheel torque measurements. Should such a torque spectrum be available then it could be used in place of the calculated values of equation (A.17).

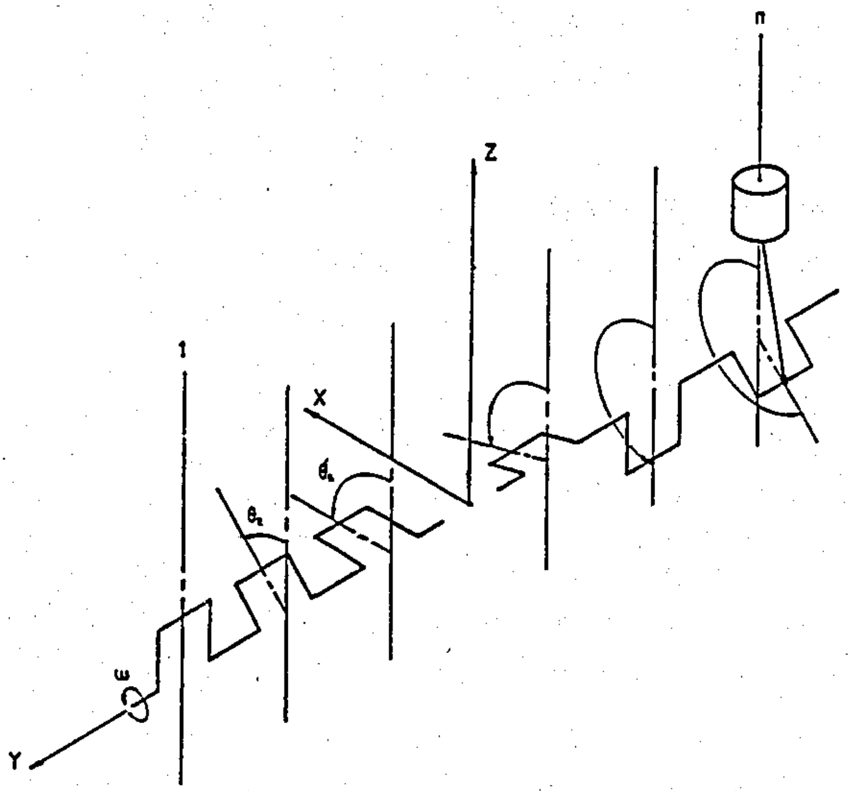


FIGURE A.2: MULTICYLINDER CRANK ARRANGEMENT

# APPENDIX B

## PICTORIAL REPRESENTATION OF MODE SHAPES

The problem of visualising a mode shape, of a dynamic system of both rotational and translational freedom, arises from the difficulty of relating rotations and translations on a common scale. This difficulty can be overcome if the body modal general displacement, described by the modal vector, is reduced to a screw displacement i.e. resembled to the motion of a nut on a screw.

The general displacement of a rigid body can be described by a translation vector $\delta \mathbf{s}$ and a rotation vector $\delta \mathbf{n}$ (assuming small displacement) about some fixed point O. The displacement of some other point on the body located by a position vector $\mathbf{r}$ relative to O is given by:

$$\delta \mathbf{s}' = \delta \mathbf{s} + \delta \mathbf{n} \times \mathbf{r} \tag{B.1}$$

$$\delta \mathbf{n}' = \delta \mathbf{n} \tag{B.2}$$

Milne [24], for example, shows that this displacement can also be described by a screw displacement about an axis located at $\mathbf{r}_1$ with respect to O, if a vector $\mathbf{r}_1$ can be found so that for all $\mathbf{r}$

$$\delta \mathbf{s}' = p\, \delta \mathbf{n}' + \delta \mathbf{n}' \times (\mathbf{r} - \mathbf{r}_1) \tag{B.3}$$

Substituting for $\delta \mathbf{s}'$ and $\delta \mathbf{n}'$ into equation (B.3) yields

$$\delta \mathbf{s} + \delta \mathbf{n} \times \mathbf{r} = p\, \delta \mathbf{n} + \delta \mathbf{n} \times (\mathbf{r} - \mathbf{r}_1)$$

$$\delta \mathbf{s} + \delta \mathbf{n} \times \mathbf{r}_1 = p\, \delta \mathbf{n} \tag{B.4}$$

Equation (B.4) is solved for p and $\mathbf{r}_1$ by taking the dot product first and the cross product in turn of $\delta$n with equation (A.4) and assuming that $\delta \mathbf{n}.\mathbf{r}_1 = 0$ giving the location of the screw axis as

$$\mathbf{r}_1 = \frac{\delta s \times \delta n}{|\delta n|^2} \tag{B.5}$$

and the pitch of the screw as

$$p = \frac{\delta s . \delta n}{|\delta n|^2} \tag{B.6}$$

The equation of the screw axes is then given by the locus of $\mathbf{r}_1$, i.e. by

$$\mathbf{r}_1 = \frac{\delta s \times \delta n}{|\delta n|^2} + \lambda \delta n \tag{B.7}$$

Using the modal vector as a general displacement vector for the body and assigning its translational part to $\delta$s and its rotational part to $\delta$n, as is illustrated in the example which follows, the location and pitch of the "modal screw axis" can be obtained from equations (B.5) and (B.7). Rotating the body about this axis through an arbitrary angle $\phi$ and translating the body along the axes by $p\phi/2\pi$ the mode shape of the body can be obtained. It will now be shown how this method can be implemented into a computer to use three-dimensional graphics for pictorial representation of the mode shapes.

Figure B.1 shows the screw axis in relation to the original body axes. A screw axes system can be formed from $r_1$, $\delta n$ and the cross product of $r_1$ and $\delta n$. The location of O, after the screw displacement, with respect to the screw axes system is first computed and then transformed to the X, Y, Z axes. The new orientation of the X, Y, Z axes after the screw rotation can be found and the resulting direction cosine matrix can be reduced to three Euler angles. If the body is drawn in its original position using a 3D graphics routine and then the drawing axes are shifted according to the computed translation of the point O and rotated by the three Euler angles, the body mode shape is obtained by simply redrawing the body with respect to the new axis.

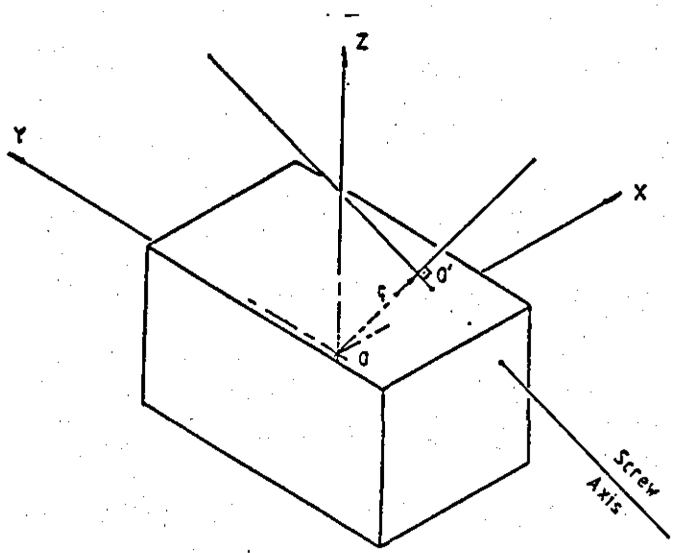


FIGURE B.1: SCREW AXIS POSITION RELATIVE TO BODY AXES

The procedure is summarised by the following set of matrix equations. The position of 0 with respect to the screw axes is:

$$x_{os} = - C\ R_1 \tag{B.8}$$

where $R_1$ is the position matrix of 0'.
The position of 0 with respect to the screw axes after the screw rotation $\phi$ is:

$$x'_{os} = x_{os} + R_1^T\ \phi \tag{B.9}$$

and after the screw translation it becomes

$$x''_{os} = x'_{os} + p\,\phi \tag{B.10}$$

If C is the direction cosine matrix so that

$$x_s = C\ x \tag{B.11}$$

then the position of 0 with respect to the X, Y, Z axes after the screw displacement is given by

$$x_o = C^T\ x''_{os} \tag{B.12}$$

The orientation of the body axes after the screw displacement is shown in Figure B.2.

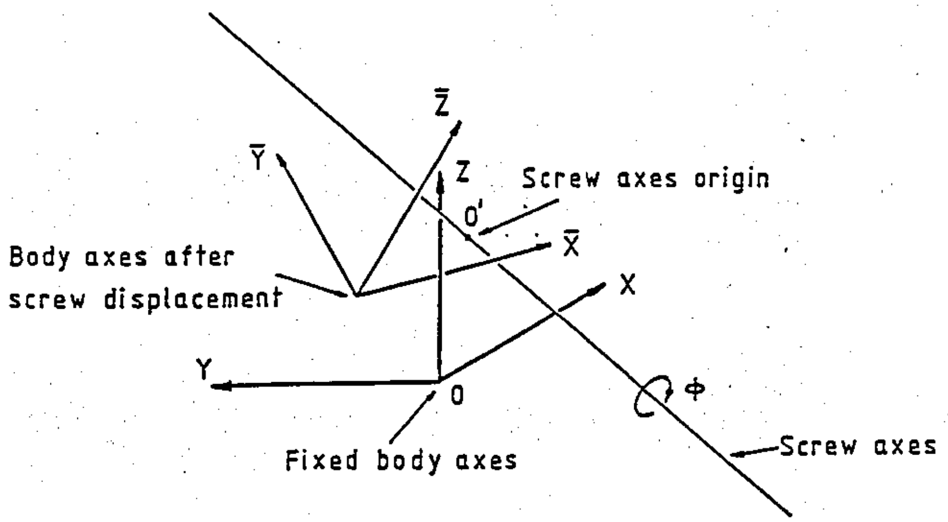


FIGURE B.2: ORIENTATION AND POSITION OF BODY AXES AFTER SCREW DISPLACEMENT

Let $X^S$, $Y^S$,$Z^S$ denote the screw axis and $X^{S'}$, $Y^{S'}$, $Z^{S'}$ denote the screw axes after the screw rotation and $\mathbf{C'}$ the direction cosine matrix so that

$$\mathbf{x}^S = \mathbf{C'}\ \mathbf{x}^{S'} \qquad \text{(B.13)}$$

From equation (B.11)

$$\mathbf{x}^{S'} = \mathbf{C}\ \mathbf{x} \qquad \text{(B.14)}$$

and

$$\mathbf{x}^S = \mathbf{C}\ \mathbf{x} \qquad \text{(B.15)}$$

Combining equations (B.13), (B.14) and (B.15) yields:

$$x = C^T C' C \bar{x} \tag{B.16}$$

giving the transformation between the original and the rotated body axes as

$$T = C^T C' C \tag{B.17}$$

from which the three Euler angles can be obtained.

Example:

Consider the modal vector v where

$$v = \begin{bmatrix} -0.001071 \\ 0.005738 \\ -0.002695 \\ -0.007879 \\ -0.008955 \\ -0.006839 \end{bmatrix} \begin{matrix} \left.\begin{matrix} \\ \\ \\ \end{matrix}\right\} \text{translational part (i.e. } \delta s) \\ \left.\begin{matrix} \\ \\ \\ \end{matrix}\right\} \text{rotational part (i.e. } \delta n) \end{matrix}$$

From equation (B.7) the screw axis will pass from the point $r_1$ given by equation (B.5) as:

$$r_1 = -0.3352\, i + 0.07358\, j + 0.2899\, k$$

and its direction cosines will be those of $\delta n$ i.e.

$$[-0.57305, \quad -0.65131, \quad -0.49741]$$

The screw pitch is computed from equation (B.6) and

$$p = -0.129676$$

Having located the screw axis, we can proceed to define the screw axes system noting that the vector $\mathbf{r}_1$ is perpendicular to the screw axis and hence it can be used as the second axis of the system, the direction cosines of which are those of $\mathbf{r}_1$ i.e.

$$[-0.74621,\ \ 0.163774,\ \ 0.645245]$$

Comparing the direction cosines of the screw axis with those of $\mathbf{r}_1$ we can adopt the convention that the screw axis is the $Y^S$ axis of the new system and the axis along $\mathbf{r}_1$ is the $X^S$ axis. The direction cosines of the $Z^S$ axis are then computed by taking the cross-product $\mathbf{r}_1 \times \delta\mathbf{n}$ and calculating the direction cosines of the resulting vector.

If $\mathbf{r}_2 = \mathbf{r}_1 \times \delta\mathbf{n}$ then

$$\mathbf{r}_2 = 0.0209272\ \mathbf{i} - 0.045767\ \mathbf{j} + 0.035818\ \mathbf{k}$$

giving the direction cosines for the $Z^S$ axis as

$$[0.33879,\ \ -0.740929,\ \ 0.579866]$$

and hence the direction cosine matrix $\mathbf{C}$ in (B.11) is assembled as

$$C = \begin{bmatrix} -0.746215 & 0.163774 & 0.645244 \\ -0.57305 & -0.651307 & -0.497408 \\ 0.33879 & -0.740929 & 0.579866 \end{bmatrix}$$

Assembling the position matrix for O' from the vector $\mathbf{r}_1$

$$R_1 = \begin{bmatrix} 0 & -0.2899 & 0.07358 \\ 0.2899 & 0 & 0.3352 \\ -0.07358 & -0.3352 & 0 \end{bmatrix}$$

Then the position of O with respect to the screw axes system is computed from equation (A.8) and

$$\mathbf{x}_{os} = -0.44926\ \mathbf{i}_s$$

Assuming a $10^o$ (0.174533 rad) screw rotation, the rotation vector $\phi$ is set as

$$\phi^T = [0,\ 0.174533,\ 0]$$

and hence the position of O after the screw displacement is computed from equations (B.9) and (B.10) as

$$x''_{os} = -0.449263\ \mathbf{i}^s + 0.078411\ \mathbf{k}^s$$

and from equation (B.12) the position vector of O with respect to the X, Y, Z axes is found as

$$\mathbf{x}_o = 0.039534\ \mathbf{i} - 0.043356\ \mathbf{j} + 0.056726\ \mathbf{k}$$

The direction cosine matrix **C'** which relates the original screw axes system with the screw axes system after the screw rotation (equation B.13) is assembled using the "Yaw-Pitch_Roll" Euler angle rotation discussed in Chapter 2.

For the screw rotation: Rotate about $Z_s$ by $\Phi = 0$
Rotate about $X^s$ by $\Theta = 0$
Rotate about $Y^s$ by $\Psi = 0.174533$.

Giving the direction cosine matrix **C'** as

$$\mathbf{C}' = \begin{bmatrix} 0.98481 & 0 & 0.173648 \\ 0 & 1 & 0 \\ -0.17365 & 0 & 0.98481 \end{bmatrix}$$

and hence from equation (B.17) the transformation matrix **T** is computed as

$$T = \begin{bmatrix} 0.9897 & 0.0920 & -0.1088 \\ -0.0807 & 0.9912 & 0.1044 \\ 0.1174 & -0.0946 & 0.9884 \end{bmatrix}$$

This transformation matrix can be solved for a new set of Euler angles $\phi'$, $\Theta'$, $\Psi'$ which together with the vector $\mathbf{x}_o$ will define the coordinate transformation required for the computer graphics. The angles $\Phi'$, $\Theta'$, $\Psi'$ are computed from **T** as

$$\Phi' = -5.31^{\circ}, \quad ' = -5.43^{\circ}, \quad = -6.77^{\circ}$$

The computer program, included in this Appendix, is the program written by the author to utilize three dimensional computer graphics, supported by GINO-F routines, for pictorial representation of mode shapes.

# APPENDIX C

## THE FORD 1.6 LITRE ENGINE AND ISOLATION SYSTEM

The power train-isolator arrangement described below is that of a standard production car. All the data presented here have been kindly supplied by the Dunton Research and Engineering Centre of the Ford Motor Company [10].

Power Train

| | |
|---|---|
| Type | In line four cylinder diesel |
| Capacity | 1608 cc |
| Maximum power | 40 kW at 4800 rev/min |
| Maximum torque | 95 Nm at 3000 rev/min |
| Firing order | 1 3 4 2 |
| Bore | 80 mm |
| Stroke | 80 mm |
| Piston mass | 0.6989 kg |
| Con rod mass | 0.7494 kg |
| Fraction of con rod acting at small end | 0.287 kg |
| Effective mass of piston | 0.9139 kg |
| Con-rod length | 130 mm |
| Crank radius | 40 mm |
| Crank radius/con-rod length [λ] | 0.3076 |
| Distance between cylinder centre lines | 96 mm |
| Power train mass | 197 kg |
| Principal moments of inertia | $I_{xx}$ = 13.58 kg.m2 |
| | $I_{yy}$ = 5.89 kg.$m^2$ |
| | $I_{zz}$ = 11.66 kg.$m^2$ |

Direction cosine matrix for principal axes

$$\begin{bmatrix} 0.9660 & 0.2317 & -0.0754 \\ 0.1848 & -0.9026 & -0.3814 \\ -0.1558 & 0.3583 & -0.9156 \end{bmatrix}$$

| | |
|---|---|
| Location of power train mass centre from vehicle mass centre | $X = -0.414m$ |
| | $Y = 0.094m$ |
| | $Z = 0.199m$ |

| | |
|---|---|
| Location of centre of crankshaft from vehicle mass centre | $X_c = -0.418m$ |
| | $Y_c = 0.140m$ |
| | $Z_c = 0.097m$ |

Zero load torque spectrum at 800 rpm engine speed.

| | | Fourier Coefficients | | |
|---|---|---|---|---|
| Harmonic No. | Frequency (Hz) | Real | Imaginary | Phase Angle |
| 0.5 | 6.9794 | -0.31676 | -0.36043 | 0.47984 |
| 1.0 | 13.959 | 5.14327 | -7.88074 | 9.41060 |
| 2.0 | 27.918 | -48.65539 | -168.34996 | 175.2400 |
| 3.0 | 41.876 | -3.47907 | -3.5206 | 4.9496 |
| 4.0 | 55.835 | -64.61180 | -76.07989 | 99.814 |
| 5.0 | 69.794 | -2.95054 | 0.19391 | 2.9569 |
| 6.0 | 83.753 | -45.45762 | -21.06217 | 50.10 |
| 7.0 | 97.712 | -1.22193 | 1.11813 | 1.6563 |
| 8.0 | 111.67 | -22.79407 | 1.26241 | 22.829 |
| 9.0 | 125.63 | 0.43749 | 0.83497 | 0.94264 |
| 10.0 | 139.59 | -7.28576 | 6.04232 | 9.4653 |

Maximum speed reduction of final drive: 12.827:1.

Isolation System:

Number of isolators: 3

Isolator positions (see also Figure 2.7) and stiffness rates:

First isolator (RH mount):

| | | | |
|---|---|---|---|
| Position: | $X_1 = -0.290$m | Stiffnesses: | $k_{x1} = 418$ N/mm |
| | $Y_1 = 0.386$m | | $k_{y2} = 132$ N/mm |
| | $Z_1 = 0.280$m | | $k_{z3} = 165$ N/mm |

Second isolator (LH mount):

| | | | |
|---|---|---|---|
| Position: | $X_2 = -0.106$m | Stiffnesses: | $k_{x2} = 288$ N/mm |
| | $Y_2 = -0.185$m | | $k_{y2} = 77$ N/mm |
| | $Z_2 = -0.093$m | | $k_{z2} = 226$ N/mm |

Third isolator (LH mount):

| | | | |
|---|---|---|---|
| Position: | $X_3 = -0.595$m | Stiffnesses: | $k_{x3} = 288$ N/mm |
| | $Y_3 = -0.209$m | | $k_{y3} = 77$ N/mm |
| | $Z_3 = -0.073$m | | $k_{z3} = 226$ N/mm |

Space Constraints:

These define the free space in the engine compartment relative to the vehicle mass centre.

1. $-0.500 \leqslant X_1 \leqslant -0.250$ metres
2. $0.350 \leqslant Y_1 \leqslant 0.500$
3. $0.180 \leqslant Z_1 \leqslant 0.370$

4. $-0.400 \leqslant X_2 \leqslant -0.050$
5. $-0.420 \leqslant Y_2 \leqslant -0.150$
6. $-0.050 \leqslant Z_2 \leqslant 0.410$

7. $-0.650 \leqslant X_3 \leqslant -0.300$
8. $-0.360 \leqslant Y_3 \leqslant -0.150$
9. $-0.200 \leqslant Z_3 \leqslant 0.050$

Stiffness Constraints:

These define a practical range of isolators as follows:

10. $100 \leqslant k_{x1} \leqslant 750$ kN/m
11. $100 \leqslant k_{y1} \leqslant 500$
12. $100 \leqslant k_{z1} \leqslant 400$

13. $100 \leqslant k_{x2} \leqslant 500$
14. $100 \leqslant k_{y2} \leqslant 400$
15. $100 \leqslant k_{z2} \leqslant 400$

16. $100 \leqslant k_{x3} \leqslant 500$
17. $100 \leqslant k_{y3} \leqslant 400$
18. $100 \leqslant k_{z3} \leqslant 400$

# APPENDIX D

## COMPUTER PROGRAM AND DATA

### D.1 THE ENGVIB COMPUTER PROGRAM

The program is not of the interactive type. All data are read from a data file and all output is similarly diverted into an output file. It has been written for a FORTRAN 77 compiler and consists of the main segment ENGVIB and fourteen subroutines, three of which are called directly from the optimization routine. The flowchart of each of these three routines as well as that of the main segment are shown in Figures D.1 to D.4. The function of the remaining eleven subroutines is as follows. (The numbers in the boxes correspond to those on the flowcharts and indicate where each subroutine is called):

DIRCOS: Computes the direction cosine matrix from a given set of Euler angles (Yaw-Pitch-Roll convention). Called at $\boxed{7}$

EULER: Computes the Euler angles from a given direction cosine matrix. Called at $\boxed{1}$

FORCE: Calculates the force vector generated by the engine inertias at the centre of the crankshaft. Called at $\boxed{3}$

LOCAL: Computes the static deflections of the isolators caused by a displacement of the power train. This subroutine is called by CON1

MATD: Called at $\boxed{8}$ for printing of intermediate results

PCHANGE: Print the percentage change of the optimization variables on exit from E04UAF. Called at $\boxed{5}$

REPORT: Prints out final and original values of the optimization function and the percentage change. Called at $\boxed{5}$

SCALE: Scales all the optimization variables so that they lie in the range (-1, +1) before entry to the optimization routine $\boxed{2}$ and scales them back to their physical units when control is passed from the optimization routine to FUNCT1 $\boxed{6}$

STRAIN: Computes the strain energy at the end of each cycle of subroutine FUNCT1 and returns the value of the optimization functions on the last call. Called at $\boxed{11}$

TRANSFORM: Computes the transformation matrix which is required to transform the crankshaft forces to an equivalent set of forces applied at the power train mass centre. Called at $\boxed{9}$

VLCHECK: Checks that the cosines and the sines of the Euler angles, computed from the elements of the direction cosine matrix do not exceed unity. Called from subroutine EULER.

Apart from the optimization routine E04UAF two more routines are used from the NAG-Library. These are F02AEF, which is called to solve the eigenvalue problem of equation (2.13) and F01ADF, which is called to estimate the inverse of the stiffness matrix.

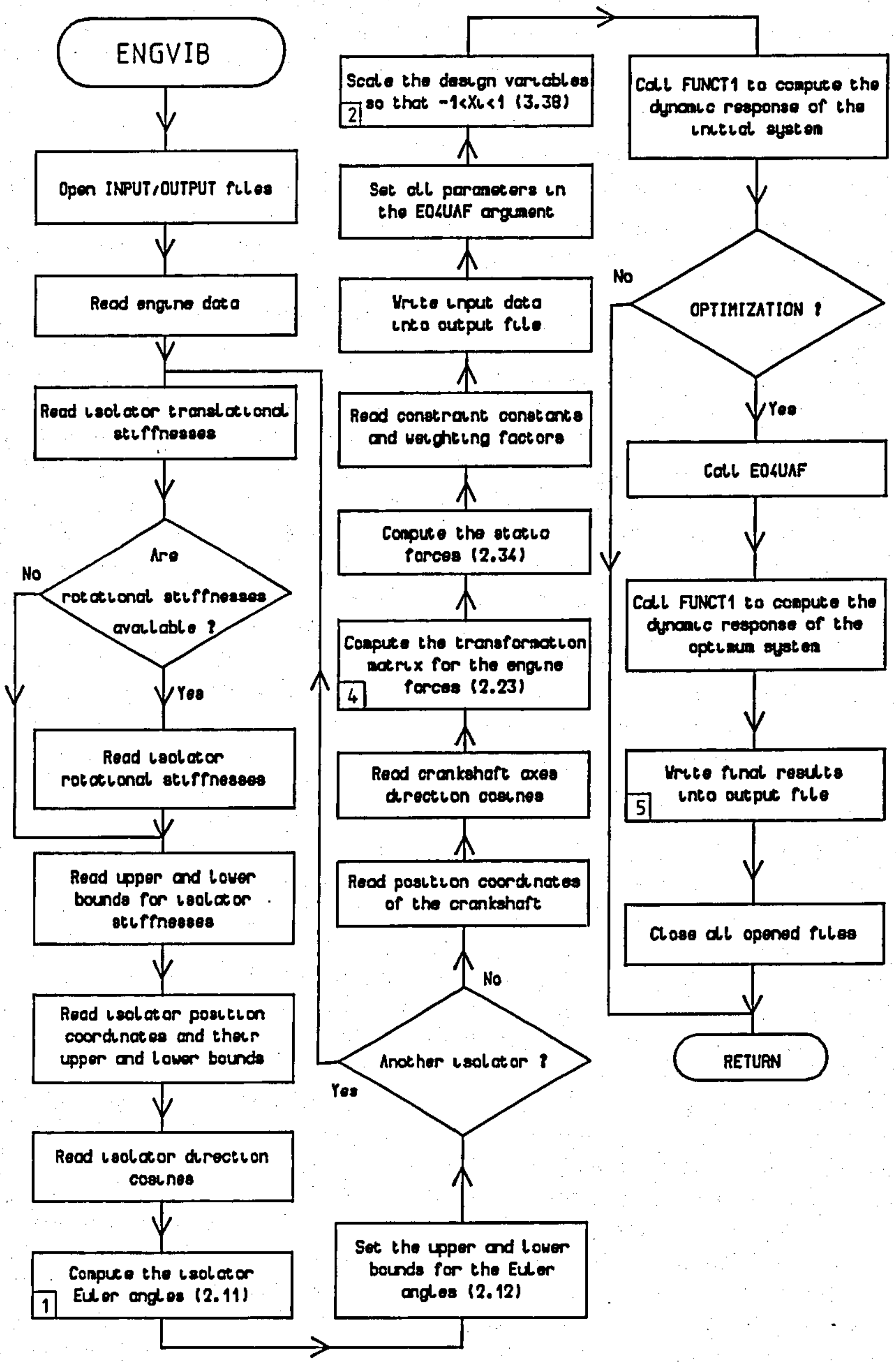


FIGURE D.1: FLOWCHART OF MAIN PROGRAM

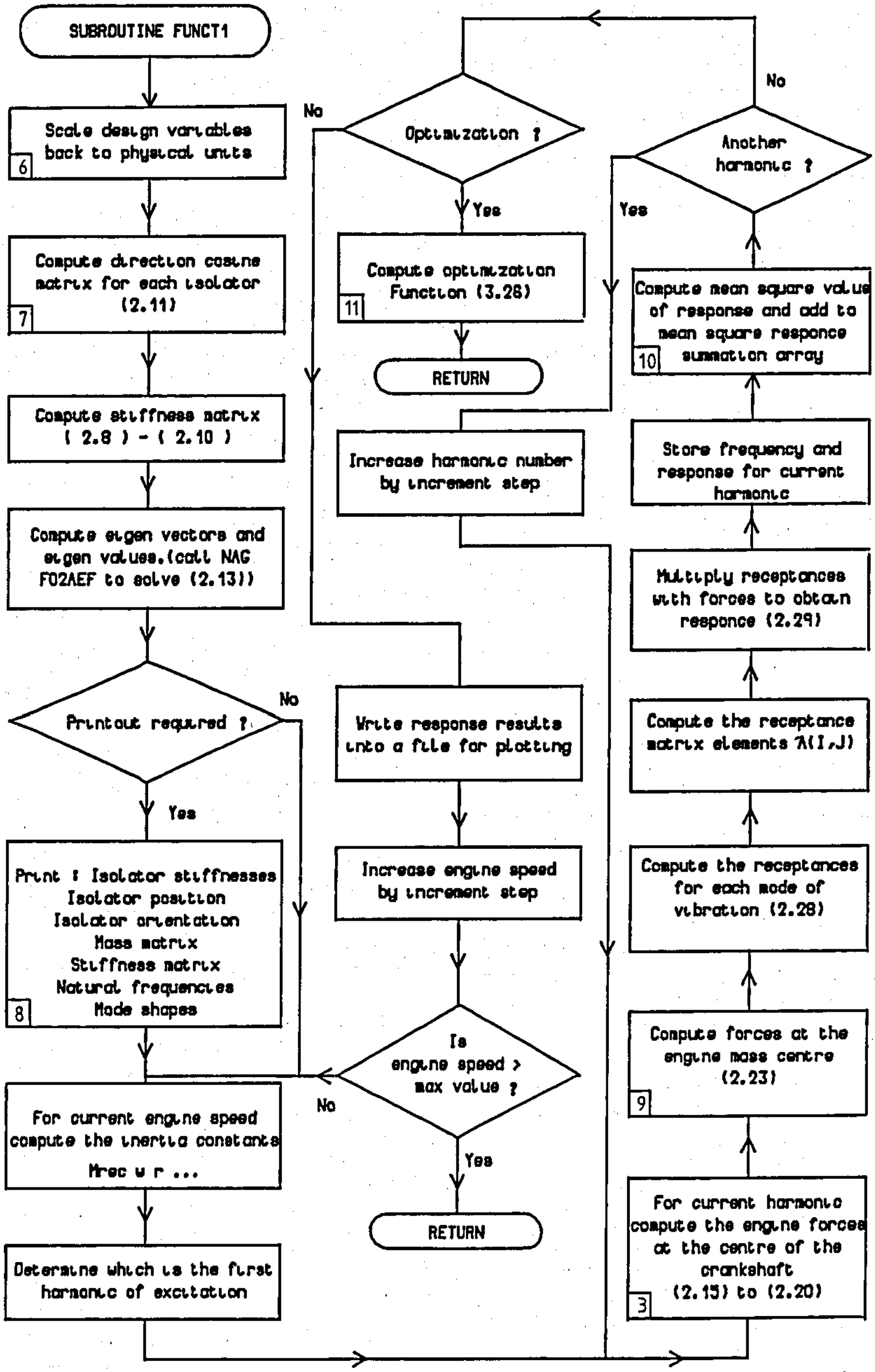


Fig. D-2 Flow chart for subroutine FUNCT1

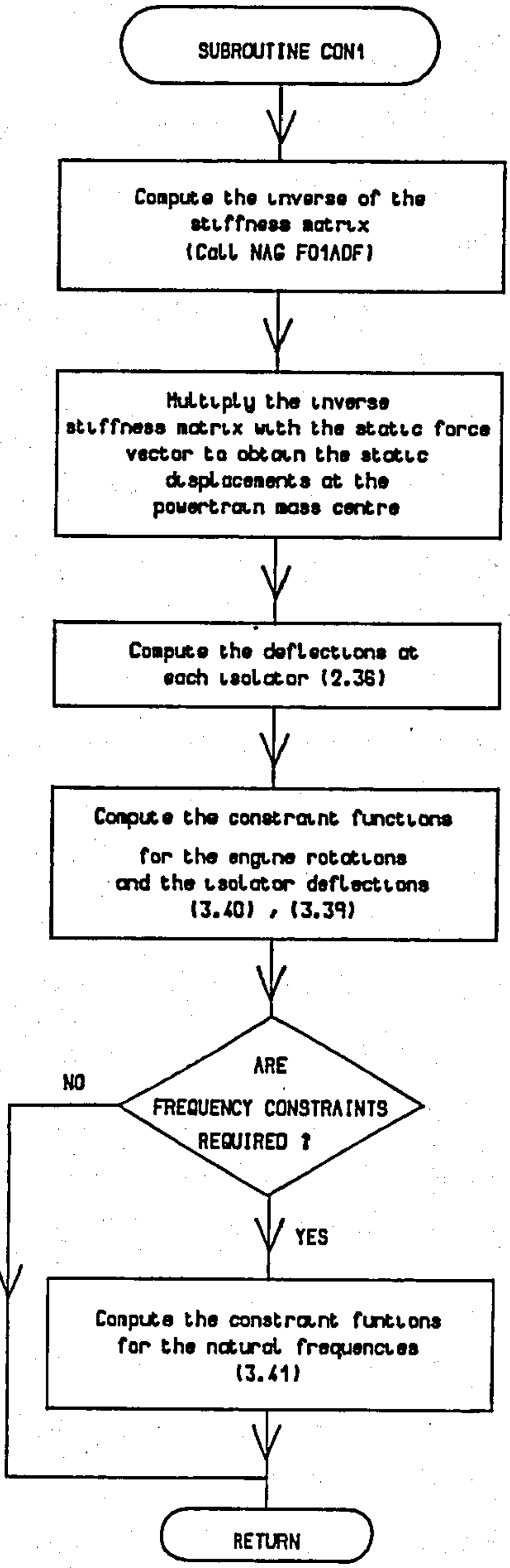


Fig. D·3 Flow chart for subroutine CON1

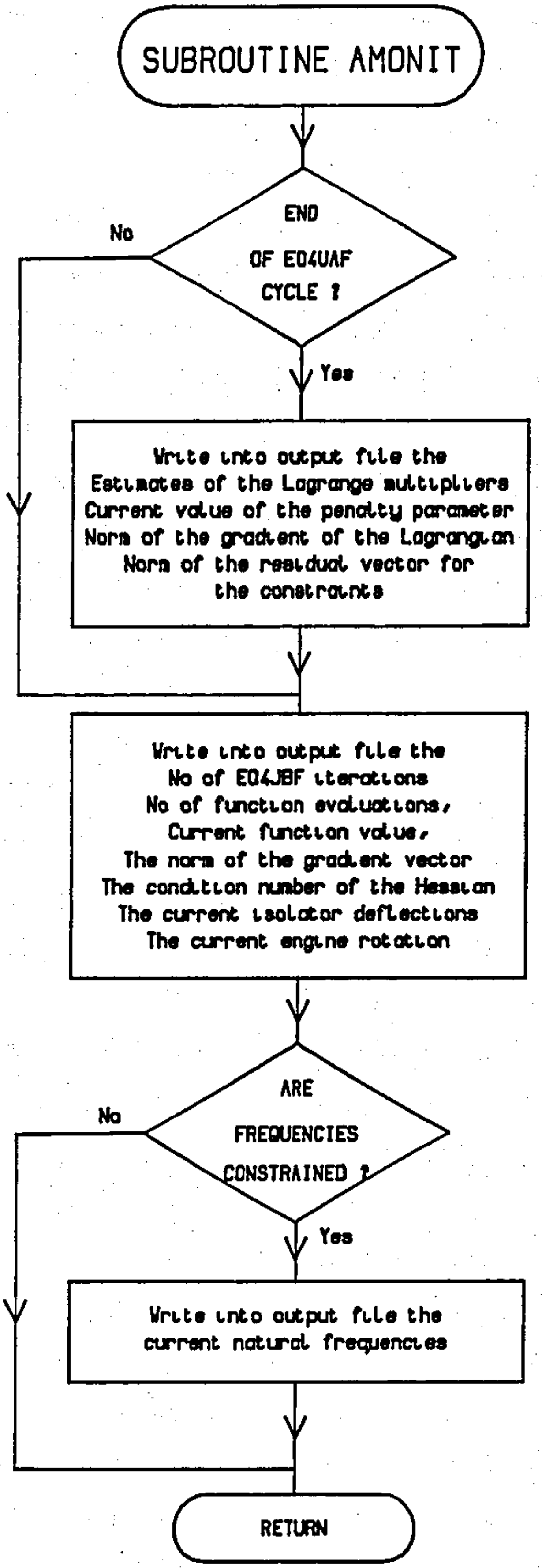


FIGURE D.4: FLOWCHART OF MONITORING SUBROUTINE AMONIT

## D.2 DATA FILE STRUCTURE

All the read statements in the program are in free format and hence the only requirement in constructing the data file is that the data should be separated by a space and that they should be assembled in the right order. A typical data file is listed below with a line-by-line explanation following.

```
'FORD DIESEL ENGINE 1.6 LITRE - ZERO LOAD'. FALSE.                 (1)
3 0 4 3 2 1.0 1 1000 20 1 10.0 0.5                                 (2)
0.0 10.0 -10.0 10.0 0.0 10.0                                       (3)
197.0 13.1564 7.0244 10.7088 1.4062 0.25904 -2.03478               (4)

0.418E6 0.132E6 0.165E6                                            (5)
1.05E  1.0E5  1.0E5                                                (6)
7.5E5  5.0E5  4.0E5                                                (7)
0.124  0.292  0.081                                                (8)
-86.0E-3 256.0E-3 -19.0E-3 164.0E-3 406.0E-3 171.0E-3              (9)
1.0 0.0 0.0 0.0 1.0 0.0 0.0 0.0 1.0                                (10)

0.288E6 0.077E6 0.22E6                                             (11)
1.05E  0.7E5  1.0E5                                                (12)
5.0E5  4.0E5  4.0E5                                                (13)
0.308 -0.279 -0.292                                                (14)
14.03-3 -514.0E-3 -295.0E-3 364.0E-3 -244.0E-3 211.0E-3            (15)
1.0 0.0 0.0 0.0 1.0 0.0 0.0 0.0 1.0                                (16)

0.288E6 0.077E6 0.226E6                                            (17)
1.0E5  0.07E6  1.05E6                                              (18)
5.0E5  4.0E5   40E5                                                (19)
-0.181 -0.303 -0.272                                               (20)
-236.0E-3 -444.0E-3 -399.0E-3 114.0E-3 -244.0E-3 -149.0E-3         (21)
1.0 0.0 0.0 0.0 1.0 0.0 0.0 0.0 1.0                                (22)

1 3 4 2 0.0 180.0 540.0 360.0                                      (23)
0.5 1.0 1.0 0.04 0.0 0.9139 0.096 0.3077 -609.28915                (24)
6 800.0 0.05                                                       (25)
```

```
-0.36043 -0.31676                 (26)
-7.88074 -5.14327                 (27)
-168.349 -48.6554                 (28)
-3.5206 -3.47907                  (29)
-76.079  -64.612                  (30)
0.19391  -2.95054                 (31)
-21.0622 -45.4576                 (32)
1.11813  -1.22193                 (33)

1.0 0.0 0.0                       (34)
0.0 1.0 0.0                       (35)
0.0 0.0 1.0                       (36)
-4.0E-3 46.0E-3 -102.0E-3         (37)

5.0E-3 5.0E-3                     (38)
10.0 10.0                         (39)
15.0E-3 -15.0E-3 10.0             (40)
5.0E-3 5.0E-3                     (41)
10.0 10.0                         (42)
15.0E-3 -15.0E-3 10.0             (43)
5.0E-3 5.0E-3                     (44)
10.0 10.0                         (45)
15.0E-3 -15.0E-3 10.0             (46)
0.1745 0.01                       (47)
0.1745 0.01                       (48)
0.1745 0.01                       (49)
5.0 0.1                           (50)
5.0 0.1                           (51)
5.0 0.1                           (52)
5.0 0.1                           (53)
5.0 0.1                           (54)
5.0 0.1                           (55)
```

The interpretation of the data is as follows:

Lines:

| | |
|---|---|
| 1 | Title for current computer run (character variable) |
| | Switch for optimization/dynamic response (logical variable) |
| 2 | Number of isolators (integer) |
| | Number of additional points on the power train, the static displacements of which are critical and should be constrained (integer) |
| | Number of engine cylinders (integer) |
| | Number of available stiffness rates/isolator 3 or 6 (integer) |
| | Optimization switch IPAR. If IPAR=2 then the objective function, F(X), is defined as the maximum strain energy of the system. If IPAR=1 then F(X) is defined as the sum of the mean square displacements at the power train mass centre |
| | Scaling factor for the objective function |
| | Count down parameter for complete output of results during optimization |
| | Optimization parameter which defines the frequency of monitoring intermediate optimization results |
| | Optimization switch, which declares whether frequency constraints will be applied |
| | Initial value of penalty parameter RHO |
| | Optimization parameter which defines the accuracy of each linear search |
| 3 | Upper and lower bounds for the Euler angles |
| 4 | Power train mass and inertias |
| 5 | Stiffness rates for first isolator |
| 6 | Lower bounds of stiffness rates |
| 7 | Upper bounds of stiffness rates |
| 8 | Isolator position coordinates |
| 9 | Lower and upper bounds of position coordinates |
| 10 | Isolator direction cosines (orientation) |
| 11-16 & 17-22 | Same as 5-10 for second and third isolator |

| | |
|---|---|
| 23 | Engine firing sequence |
| | Crank arrangement |
| 24 | First excitation harmonic to be considered |
| | Second excitation harmonic to be considered |
| | Harmonic number increment |
| | Crank radius |
| | Rotating mass |
| | Reciprocating mass |
| | Distance between cylinder centre lines |
| | Ratio of crank radius/conrod length |
| | Maximum static torque/ number of engine cylinders |
| 25 | Number of excitation forces |
| | Engine speed |
| | Modal loss factor |
| 26-33 | Combustion Fourier coefficients (imaginary-real) |
| 34-36 | Direction cosines for crankshaft axes |
| 37 | Position coordinates for crankshaft centre |
| 38-55 | Constraint constants and weighting factors |

```
      CHARACTER*12 OLD
      REAL MOD2,MOD,MODR2,MODR,MODP2,MODP
      DIMENSION TR(3),V(6,6),RO(3),R(3),DC(3),DC1(3,3),P(3)
     *,DC2(3,3),XF(3),R1(3),XT(3),W(6),ITITLE(80),XF1(3),DC3(3,
      PI2=8.0*ATAN(1.0)
      RAD=PI2/360.0
C
C
      WRITE(0,110)
  110 FORMAT(T5,'Enter data file name ...')
      READ(0,*)OLD
      OPEN(5,FILE=OLD)
      READ(5,1)ITITLE
    1 FORMAT(80A1)
      READ(5,*)IPLOT
      READ(5,*)(W(I),I=1,6)
      READ(5,*)((V(I,J),J=1,6),I=1,6)
      CLOSE(5)
C
      WRITE(0,100)
  100 FORMAT(T5,'Enter screw axis rotation (Degrees)'//
     *T5,'and translation scale factor'//)
      READ(0,*)FSCR,TSCL
C
      IF(IPLOT.EQ.1)THEN
      L=-1
      CALL DEVICE(L)
      CALL PICCLE
      END IF
      DO 10 J=1,6
      IF(J.LE.3)THEN
      IVAL=J-1
      ELSE
      IVAL=J-4
      END IF
      YSHIFT=50.0
      IF(J.GT.3)YSHIFT=150.0
      MOD2=0.0
      DOT=0.0
      DO 20 I=1,3
      TR(I)=V(I,J)
      RO(I)=V(I+3,J)
C
C     FORM THE DOT PRODUCT  DS . DN  AND CALCULATE  |DN|**2
C
      DOT=DOT+TR(I)*RO(I)
      MOD2=MOD2+RO(I)*RO(I)
   20 CONTINUE
C
C     CALCULATE THE PITCH OF THE SCREW
C
      PITCH=DOT/MOD2
      MOD=SQRT(MOD2)
C
C     FORM THE VECTOR PRODUCT  DS X DN
C
      CALL CROSS(TR,RO,R)
      MODR2=0.0
      DO 30 I=1,3
C
```

```
C     FIND THE LOCATION VECTOR OF THE SCREW AXIS  R
C
      R(I)=R(I)/MODD
      MODR2=MODR2+R(I)*R(I)
   30 CONTINUE
      MODR=SQRT(MODR2)
      KP=1
C
C     CALCULATE THE DIRECTION COSINES OF THE SCREW AXIS
C
      CALL DCOS1(RO,MOD,DC)
      CALL MAXV(DC,KP)
      KS=KP
      CALL DCOS2(KP,DC,DC1)
      KP=1
C
C     CALCULATE THE DIRECTION COSINES OF THE POSITION VECTOR
C
      CALL DCOS1(R,MODR,DC)
      CALL MAXV(DC,KP)
      IF(KP.EQ.KS)THEN
      DUMMY= DC(KP)
      DC(KP)=0.0
      CALL MAXV(DC,KP)
      DC(KS)=DUMMY
      END IF
      KS2=KP
      CALL DCOS2(KP,DC,DC1)
      IF(KP.LT.KS.AND.KP*KS.NE.3)THEN
      CALL CROSS(R,RO,P)
      ELSE
      CALL CROSS(RO,R,P)
      END IF
      MODP2=0.0
      DO 40 I=1,3
      MODP2=MODP2+P(I)*P(I)
   40 CONTINUE
      MODP=SQRT(MODP2)
      KS3=KS+KS2
C
C     CALCULATE THE DIRECTION COSINES OF THE THIRD SCREW AXIS  R X
C
      CALL DCOS1(P,MODP,DC)
      IF(KS3.EQ.6)KP=1
      IF(KS3.EQ.3)KP=2
      IF(KS3.EQ.2)KP=3
      KS3=KP
      CALL DCOS2(KP,DC,DC1)
      IF(IPLOT.EQ.0)THEN
      WRITE(0,200)J,W(J)
      WRITE(0,120)KS,KS2,KS3,PITCH,(R(I),I=1,3),(DC1(KS,K),K=1,3)
      END IF
  200 FORMAT(T5,'MODE  ',I2,T20,'MODAL FREQUENCY ',F7.2,
     +' (RADS/SEC)')
  120 FORMAT(T5,'KSCREW = ',I2,T25,'KS1 = ',I2,T45,'KS2 = ',I2//
     +T5,'PITCH OF SCREW = ',E10.4//T5,'LOCATED AT   ( ',3(E10.4,2

     +,'//T5,'WITH DIRECTION COSINES '//T18,'( ',3(E10.4,2X),' )'/
      FRAD=FSCR*RAD
C
C     Calculate coordinates of C.G  w.r.t the screw axes
```

```
C
      DO 60 I=1,3
      XF(I)=0.0
      R1(I)=0.0
      DO 60 K=1,3
      R1(I)=R1(I)+DC1(I,K)*R(K)
   60 CONTINUE
C
C     Set screw rotation vector and calculate displacement of C.
C                                 to screw rotation
C
      XF(KS)=FRAD
      CALL CROSS(R1,XF,XF1)
C
C     Calculate new coordinates of C.G  w.r.t the screw axes af
C              screw rotation and screw translation
C
      DO 90 I=1,3
      XF(I)=XF1(I)-R1(I)
   90 XF1(I)=XF(I)
      XF(KS)=XF(KS)+PITCH*FRAD
C
C     Transform final coordinates of C.G to engine axes system
C
      DO 70 I=1,3
      XT(I)=R(I)
      DO 70 K=1,3
      XT(I)=XT(I)+DC1(K,I)*XF(K)
   70 CONTINUE
C
C             Calculate new oriantation of engine axes after
C                          screw displacement
C
      FI=0.0
      THE=0.0
      PSI=0.0
      IF(KS.EQ.1)THE=FRAD
      IF(KS.EQ.2)PSI=FRAD
      IF(KS.EQ.3)FI=FRAD
      CALL DIRCOS(DC2,FI,THE,PSI)
      DO 50 I=1,3
      DO 50 IJ=1,3
      DC3(I,IJ)=0.0
      DO 50 K=1,3
      DC3(I,IJ)=DC3(I,IJ)+DC2(I,K)*DC1(K,IJ)
   50 CONTINUE
      DO 30 I=1,3
      DO 30 IJ=1,3
      DC2(I,IJ)=0.0
      DO 30 K=1,3
      DC2(I,IJ)=DC2(I,IJ)+DC1(K,I)*DC3(K,IJ)
   30 CONTINUE
      CALL EULER(DC2,FI,THE,PSI,PI2)
      FI=FI/RAD
      THE=THE/RAD
      PSI=PSI/RAD
      IF(IPLOT.EQ.0)WRITE(0,130)(XT(I),I=1,3),FI,THE,PSI
  130 FORMAT(T5,'MOVE ORIGIN TO ( ',3(E10.4,2X),' )'//
     +T5,'ROTATE ABOUT Z-AXIS ',F7.2,' (Degrees)'//
     +T5,'ROTATE ABOUT X-AXIS ',F7.2,' (Degrees)'//
```

```
     -T5,'ROTATE ABOUT Y-AXIS ',F7.2,' (Degrees)'//)
      IF(IPLOT.EQ.1)THEN
C
C     DRAW MODE SHAPE
      CALL TRANSF(-1)
      CALL WINDOW(3)
      CALL VIEWSE(2,3)
      ZSHIFT=230.0-IVAL*75.0
      CALL SHIFT3(0.0,YSHIFT,ZSHIFT)
      CALL SCALE(.5)
      CALL LINCOL(1)
      CALL ROTAT3(3,-30.0)
      CALL ROTAT3(2,30.0)
      CALL BOX(50.0,100.0,60.0)
      CALL AXES(50.0,100.0,60.0)
      DX=TSCL*XT(1)
      DY=TSCL*XT(2)
      DZ=TSCL*XT(3)
      CALL SHIFT3(DX,DY,DZ)
      CALL ROTAT3(3,FI)
      CALL ROTAT3(1,THE)
      CALL ROTAT3(2,PSI)
      CALL LINCOL(3)
      CALL BOX(50.0,100.0,60.0)
      END IF
   10 CONTINUE
      IF(IPLOT.EQ.1)THEN
      CALL TITLE(ITITLE,W)
      CALL DEVEND
      END IF
      END
C
C
      SUBROUTINE CROSS(V1,V2,VV)
      DIMENSION V1(3),V2(3),VV(3),PM(3,3)
      DO 10 I=1,3
      VV(I)=0.0
      PM(I,I)=0.0
   10 CONTINUE
      PM(2,1)=V1(3)
      PM(3,2)=V1(1)
      PM(1,3)=V1(2)
      PM(1,2)=-PM(2,1)
      PM(2,3)=-PM(3,2)
      PM(3,1)=-PM(1,3)
      DO 20 I=1,3
      DO 20 J=1,3
      VV(I)=VV(I)+PM(I,J)*V2(J)
   20 CONTINUE
      RETURN
      END
C
C
      SUBROUTINE DCOS1(X,MD,DC)
      REAL MD,X(3),DC(3)
      DO 10 I=1,3
      DC(I)=X(I)/MD
   10 CONTINUE
      RETURN
      END
C
```

```
C
      SUBROUTINE MAXV(DC,KP)
      DIMENSION DC(3)
      DMAX=ABS(DC(1))
      DO 10 I=1,3
      IF(ABS(DC(I)).GT.DMAX)THEN
      DMAX=ABS(DC(I))
      KP=I
      END IF
   10 CONTINUE
      RETURN
      END
C
C
      SUBROUTINE DCOS2(KP,DC,DC1)
      DIMENSION DC1(3,3),DC(3)
      DO 10 I=1,3
      DC1(KP,I)=DC(I)
   10 CONTINUE
      RETURN
      END
C
C
      SUBROUTINE EULER(D,FI,THE,PSI,PI2)
      DIMENSION D(3,3)
C
C     =========================================================
\c===
C
C             Calculate the angle  THETA   ( -PI/2 <= THETA <= PI
C
C     =========================================================
\c===
C
      CTHE=SQRT(1.0-D(3,2)*D(3,2))
      THE=ATAN2(D(3,2),CTHE)
C
C     =========================================================
\c===
C
C             Calculate the angles  PSI  and  FI  ( 0 <= FI,PSI
\c
C
C     =========================================================
\c===
C
      SFI=-D(1,2)/CTHE
      CFI=D(2,2)/CTHE
      SPSI=-D(3,1)/CTHE
      CPSI=D(3,3)/CTHE
C
C     ---------------------------------------------------------
\c---
C
C     Check that the absolute values of Sine and Cosine do not
1.0
C
C     ---------------------------------------------------------
\c---
C
      CALL VLCHECK(CFI,SFI)
      CALL VLCHECK(SFI,CFI)
```

```
      CALL VLCHECK(CPSI,SPSI)
      CALL VLCHECK(SPSI,CPSI)
C
C     -----------------------------------------------------------
\c---
C
      FI=ATAN2(SFI,CFI)
      PSI=ATAN2(SPSI,CPSI)
C      IF(FI.LT.0.0)FI=PI2+FI
C      IF(PSI.LT.0.0)PSI=PI2+PSI
      RETURN
      END
C
C
      SUBROUTINE VLCHECK(X,Y)
      IF(ABS(X).GT.1.0)THEN
      X=X/ABS(X)
      Y=0.0
      END IF
      RETURN
      END
C
      SUBROUTINE BOX(XBOX,YBOX,ZBOX)
C DRAW A BOX OF DIMENSIONS XBOX,YBOX,ZBOX IN XYZ
      CALL MOVTO3(XBOX/2.0,YBOX/2.0,ZBOX/2.0)
      CALL BROKEN(0)
C FRONT EDGES
      CALL LINBY3(0.0,-YBOX,0.0)
      CALL LINBY3(0.0,0.0,-ZBOX)
      CALL LINBY3(0.0,YBOX,0.0)
      CALL LINBY3(0.0,0.0,ZBOX)
C SIDE EDGES
      CALL LINBY3(-XBOX,0.0,0.0)
      CALL LINBY3(0.0,0.0,-ZBOX)
      CALL LINBY3(XBOX,0.0,0.0)
C TOP EDGES
      CALL MOVTO3(XBOX/2.0,-YBOX/2.0,ZBOX/2.0)
      CALL LINBY3(-XBOX,0.0,0.0)
      CALL LINBY3(0.0,YBOX,0.0)
C DASHED REAR EDGES
C      CALL BROKEN(1)
C      CALL MOVBY3(0.0,-YBOX,0.0)
C      CALL LINBY3(0.0,0.0,-ZBOX)
C      CALL LINBY3(XBOX,0.0,0.0)
C      CALL MOVBY3(-XBOX,0.0,0.0)
C      CALL LINBY3(0.0,YBOX,0.0)
      RETURN
      END
C
C
      SUBROUTINE DEVICE(L)
      IF(L.EQ.-1)THEN
      WRITE(0,100)
  100 FORMAT(T5,'Enter device no i.e.'//T10,
     +'1.  TEKTRONICS , CALCOMP'//T10,
     +'2.  WESTWARD 2019'//T10,
     +'3.  SERVOGOR'//T10,
     +'4.  SIGMA '//)
      READ(0,*)L
      END IF
      IF(L.EQ.1)CALL T4010
```

```
      IF(L.EQ.2)CALL T4014
      IF(L.EQ.3)CALL SE281
      IF(L.EQ.4)CALL 35664
      RETURN
      END
C
C
      SUBROUTINE TITLE(ITITLE,W)
      DIMENSION ITITLE(80),W(6),IAR(10),IAR1(5)
      DATA IAR/77,79,68,69,32,0,32.32,45,32/,
     *     IAR1/32,40,72,122,41/
      CALL TRANSF(-1)
      CALL WINDOW(3)
      CALL VIEWSE(2,3)
      CALL LINCOL(1)
      CALL MOVTO3(0.0,20.0.25.0)
      CALL CHAA1(ITITLE,80)
      DO 10 I=1.6
      IAR(6)=48+I
      FR=W(I)
      IF(I.LE.3)THEN
      IVAL=I-1
      ELSE
      IVAL=I-4
      END IF
      YMOD=25.0
      IF(I.GT.3)YMOD=125.0
      ZMOD=230.0-IVAL*75.0-30.0
      CALL MOVTO3(0.0,YMOD,ZMOD)
      CALL ASCII(IAR,10)
      CALL CHAFIX(FR,7,2)
      CALL ASCII(IAR1,5)
   10 CONTINUE
      RETURN
      END
C
C
      SUBROUTINE AXES(XBOX.YBOX,ZBOX)
      CALL MOVTO3(0.0.0.0,0.0)
      CALL BROKEN(1)
      CALL LINBY3(XBOX/2.0.0.0,0.0)
      CALL BROKEN(0)
      CALL LINBY3(30.0,0.0,0.0)
      CALL MOVTO3(0.0,0.0,0.0)
      CALL BROKEN(1)
      CALL LINBY3(0.0.YBOX/2.0,0.0)
      CALL BROKEN(0)
      CALL LINBY3(0.0.30.0,0.0)
      [illegible].0,0.0)
      CALL BROKEN(1)
      CALL LINBY3(0.0,0.0.ZBOX/2.0)
      CALL BROKEN(0)
      CALL LINBY3(0.0,0.0,30.0)
      CALL MOVTO3(XBOX/2.0-30.0,0.0,-7.0)
      CALL CHAHOL(4H X+.)
      CALL MOVTO3(0.0,YBOX/2.0+30.0,0.0)
      CALL CHAHOL(4H Y+.)
      CALL MOVTO3(0.0,0.0.ZBOX/2.0-30.0)
      CALL CHAHOL(4H Z+.)
      RETURN
      END
C
```

```
C
      SUBROUTINE DIRCOS(D,FI,THE,PSI)
      DIMENSION D(3,3)
C
C     -------------------------------------------------------------
C -
C
C        Get Euler angles from array of optimization variables &
C                    calculate their sines and cosines
C
C     -------------------------------------------------------------
C -
C
      CFI=COS(FI)
      SFI=SIN(FI)
      CTHE=COS(THE)
      STHE=SIN(THE)
      CPSI=COS(PSI)
      SPSI=SIN(PSI)
C
C     -------------------------------------------------------------
C -
C
C               Calculate direction cosines from Euler angles
C
C     -------------------------------------------------------------
C -
C
      D(1,1)=CPSI*CFI-SPSI*STHE*SFI
      D(1,2)=-CTHE*SFI
      D(1,3)=SPSI*CFI+CPSI*STHE*SFI
      D(2,1)=CPSI*SFI+SPSI*STHE*CFI
      D(2,2)=CTHE*CFI
      D(2,3)=SPSI*SFI-CPSI*STHE*CFI
      D(3,1)=-SPSI*CTHE
      D(3,2)=STHE
      D(3,3)=CPSI*CTHE
      RETURN
      END
15:37 4.461 19
```